Summer 8-15-2019

Diverse Far-Red Light Utilization Strategies in Cyanobacteria and Algae

Benjamin Martin Wolf
Washington University in St. Louis

WASHINGTON UNIVERSITY IN ST. LOUIS

Division of Biology and Biomedical Sciences
Plant and Microbial Biosciences

Dissertation Examination Committee:
Robert E. Blankenship, Chair
Michael Gross
Joseph Jez
Robert Kranz
Himadri Pakrasi

Diverse Far-Red Light Utilization Strategies in Cyanobacteria and Algae

by
Benjamin M. Wolf

A dissertation presented to
The Graduate School
of Washington University in
partial fulfillment of the
requirements for the degree
of Doctor of Philosophy

August 2019
St. Louis, Missouri

Table of Contents

List of Figures

Acknowledgments

I would like to thank all the people who made this work possible, not only through their scientific contributions, but also their encouragement and support throughout my time in graduate school, including the important contributors recognized here.

Firstly, I'd like to thank my advisor Prof. Robert E. Blankenship for his continuous support, advice, mentorship, and for providing an excellent environment for me to work and grow as a student and as a scientist. I'd also like to thank all the members of the lab, both past and present, for all their help and for creating a supportive and enjoyable lab environment. I'd also like to thank the members of my thesis committee, and Prof. Ursula Goodenough, who was a great help to me as I got started and began working on the Eustigmatophyte FP5.

The original impetus behind the environmental sampling and far-red light isolation came from Jeremy King, a previous graduate student in the lab. He also obtained our Chlorophyll *b*-containing strain of *Acaryochloris*. The project would not be where it is today if it hadn't been for his interests in far-red chlorophylls and teaching undergraduate students about microbiology and photosynthesis through his PARC outreach campaign, which provided the original need for specialty LEDs when I joined.

On three occasions during my time in graduate school, I was fortunate enough to be able to visit collaborator's labs, who of which were located internationally. Two of these trips were funded through the Photosynthetic Antenna Research Center (PARC) Scientific Exchange program. The first was to the University of Sydney in Sydney, New South Wales, Australia, where I visited the lab of Prof. Min Chen to perform molecular biology experiments in search of the Chl *d* synthase gene. While I ended up pivoting the direction of my thesis to characterization of novel

environmental isolates, this experience was important to me in terms of learning new skills and gaining additional molecular biology experience. The second such trip was to Sandia National Labs in Albuquerque, NM, USA, where I visited the lab of Dr. Jerilyn Timlin and worked with her postdoc Dr. Meghan Barnhart-Dailey. During this trip, we imaged FP5 and LSP65 using the hyperspectral confocal fluorescence microscope (HCFM), which led to the submission of a manuscript. I also appreciated the opportunity to learn about HCFM. Finally, I traveled to Třeboň, Czech Republic to perform some experiments on my Eustigmatophyte culture FP5 in the lab of Prof. Ondřej Prášil. I would like to thank everyone who made these experiences possible, especially the host PIs and the people in the lab who made the work possible and made each of these experiences memorable and scientifically productive.

Outside the lab, I'd like to thank everyone else who provided their support and encouragement throughout my time at Washington University, including my parents, Cindy and Mark Wolfe, and my girlfriend Zuzana Kocsisová. One of my great passions in life is growing plants, both ornamental and edible, a hobby I learned from my mom and have continued to enjoy here in St. Louis with Zuzana as we have built up our collection of over 100 ornamental plants and a garden that provides us fresh produce all year around via its indoor and outdoor components. In addition to encouragement, Zuzana has also provided me help with my scientific questions at times, teaching me how to use ImageJ and do statistical analyses, as well as being an indispensable member of my Sling Health team and the WashU BioEntrepreneurship Core (BEC).

Finally, I want to thank everyone who has helped me to get involved in the St. Louis entrepreneurial community, including Jeff Melly, Nick Turk, the entire Sling Health organization (especially my team members, Zuzana and Rafael Saer), and all the members of the BEC. I've learned a lot from all of them and look forward to our future endeavors together.

This work was supported by PARC, an Energy Frontier Research Center funded by the U.S. Department of Energy, Office of Science, Office of Basic Energy Sciences under Award Number DE-SC 0001035. I would like to thank everyone involved in PARC for their continued support and help, as well as all the teaching and outreach opportunities they have provided me.

I'd also like to thank my fellowship funding that has paid my stipend for the past four years, the William H. Danforth Plant Sciences Fellowship of Washington University in St. Louis.

Benjamin M. Wolf

Washington University in St. Louis

August 2019

ABSTRACT OF THE DISSERTATION

Diverse Far-Red Light Utilization Strategies in Cyanobacteria and Algae

by

Benjamin M. Wolf

Doctor of Philosophy in Biology and Biomedical Sciences

Plant and Microbial Biosciences

Washington University in St. Louis, 2019

Robert E. Blankenship, Chair

In their natural environments, photosynthetic organisms are often exposed to widely varied light environments. Species adapted to shade light, often found growing in lower layers of photosynthetic biofilms, must survive on filtered light alone. Filtered light is highly enriched in far-red wavelengths, which are normally unavailable for photosynthetic energy production in most oxygenic phototrophs. To overcome light limitations in filtered light environments, some species of algae and cyanobacteria utilize specialized photosynthetic pigments and antenna systems to harvest these far-red wavelengths. By sampling the natural environment and using custom-built far-red light growth chambers, I have isolated several species of oxygenic phototrophs that are capable of utilizing far-red light, and have characterized their photosynthetic antenna systems. The Eustigmatophyte alga I isolated from Forest Park, St. Louis, MO uses a red-shifted light-harvesting complex that contains Chlorophyll *a* as its only chlorophyll. The filamentous cyanobacterium LSP65 isolated from the underside of a lily pad in Ludington, MI, contains far-red-absorbing Chlorophyll *f*, with which it harvests far-red wavelengths. These far-red light-harvesting systems may play an important role in the improvement of photosynthetic light utilization in crop plants in the future.

Chapter 1: Introduction[1]

Oxygenic photosynthesis begins with the capture of light energy by pigment-protein antenna complexes (Blankenship 2014; Saer and Blankenship 2017). The spectrum of light absorbed by these complexes is controlled by the properties of the pigments and the interactions of the pigments with one another and with the protein environment in which they are located. In plants and most algae and cyanobacteria, the spectral range that can be utilized effectively for photosynthesis is primarily limited to the visible range, approximately 400 to 700 nm, which makes up only about half of the incident solar spectrum (Fig. 1A) (Zhu et al. 2010). However, specialized pigments or pigment-proteins are utilized in some species of algae and cyanobacteria to expand this spectral range into the far-red region, about 700-750 nm for these species (Fig. 1B-C) (Chen and Blankenship 2011; Blankenship and Chen 2013). This spectral expansion allows these specialized organisms to thrive in niches otherwise unavailable to their spectrally limited neighbors (Swingley et al. 2008; Duxbury et al. 2009; Mohr et al. 2010).

Far-red light is particularly enriched in shaded conditions. When a stratification exists in a forest canopy, water column, microbial mat, or other biological community, far-red light tends to penetrate the first few layers of phototrophs (Kasperbauer 1987; Gilbert et al. 2001). The top layers generally absorb most of the visible wavelengths of light. This leaves an enrichment of far-red light that passes through the canopy or upper layer and reaches lower strata. In a forest or crop canopy, this far-red light serves as a trigger for phytochromes in the leaves of shaded plants,

[1] This chapter was originally published as: Wolf, B.M & Blankenship, R.E. (2019) Far-Red Light Acclimation in Diverse Oxygenic Photosynthetic Organisms. *Photosynthesis Research.* 10.1007/s11120-019-00653-6

causing them to initiate a shade-avoidance response that leads to stem stretching and leaning to escape the shade (Kasperbauer 1987). Additionally, Photosystem I (PSI) antennas in higher plants have been shown to utilize some far-red wavelengths, and this can be important to photosynthetic output in shaded leaves (Rivadossi et al. 1999).

In some specialized algae and cyanobacteria, these far-red wavelengths can be put to much more use for the organism (Chen and Blankenship 2011). To do this, several adaptations have been discovered. Chlorophylls may be modified, such that they can absorb far-red wavelengths. These pigments include Chlorophylls *d* and *f* (Chl *d* and *f*) (Fig. 2), and have so far only been discovered in cyanobacteria (Miyashita et al. 1996; Chen et al. 2010). Cyanobacteria may also modify their phycobilisome antennas to absorb far-red light when exposed to far-red conditions, and this is typically observed in conjunction with Chl *f* production (Ho et al. 2016b; Li et al. 2016). Finally, many algae, including many diatoms and some Eustigmatophytes, can absorb far-red light by shifting the absorption spectrum of Chl *a* in their LHC-type antennas (Koehne et al. 1999; Kotabová et al. 2014; Wolf et al. 2018). Evidence suggests that this may be due to an aggregation phenomenon in the antenna systems (Bína et al. 2014).

By using one or more of these adaptations, these organisms are specifically evolved to effectively utilize wasted far-red light while living in the lower layers of photosynthetic strata. Many of these organisms are capable of turning their far-red light utilization system on and off as needed through complex regulatory mechanisms (Kotabová et al. 2014; Zhao et al. 2015). This allows them to survive highly varied light conditions.

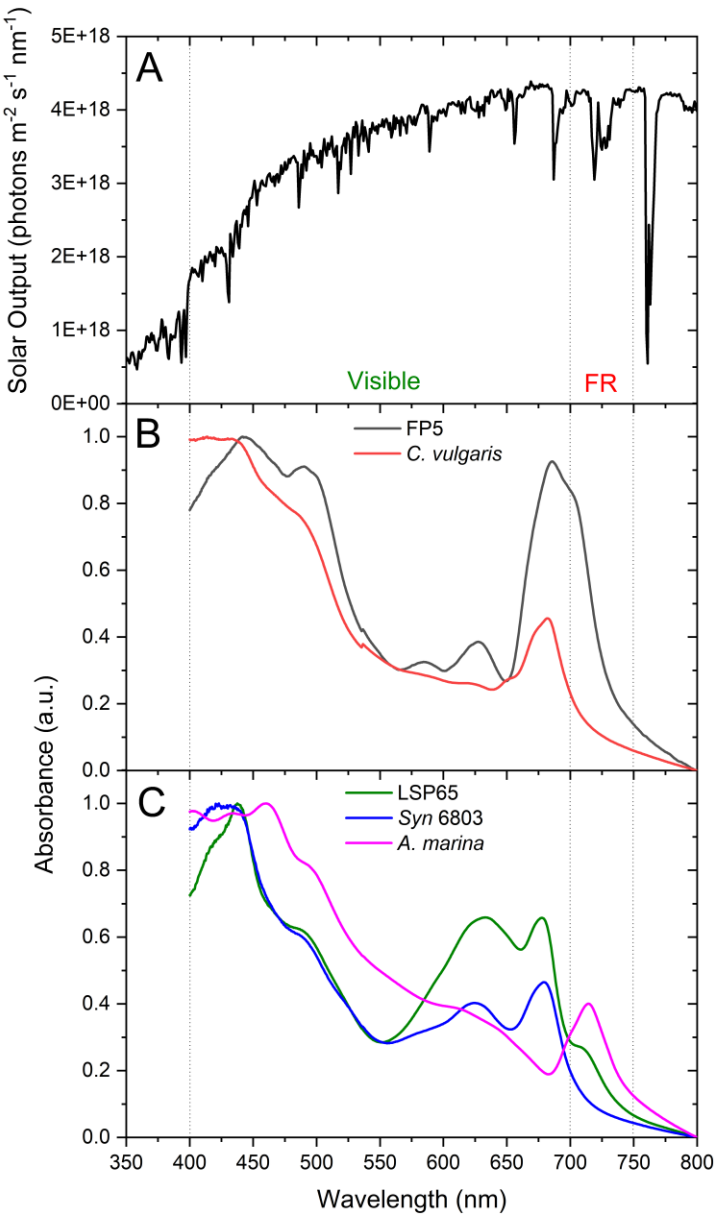

Figure 1.1: Solar spectrum at ground level and several examples of far-red antennas and systems. A) Quantum solar output spectrum. Data derived from ASTM 1.5. B) An example of far-red adaptation in Eukaryotes, showing whole cells of the far-red adapted Eustigmatophyte alga FP5 (black line) and the green alga *Chlorella vulgaris* grown under white light (red line). C) Several examples of far-red absorption in prokaryotes, showing whole cells of Chl *f*-containing far-red adapted filamentous environmental isolate LSP65 (green line), the white-light-grown *Synechocystis* sp. PCC 6803 (blue line), and Chl *d*-containing *Acaryochloris marina*, grown under white light (magenta line). On both panels, vertical lines indicate boundaries of visible (400 and 700 nm) and the far-red region primarily used by shade-adapted oxygenic phototrophs (700 and

750 nm). Scattering in absorbance spectra of whole cells has not been corrected, and these spectra are normalized to unity.

Although these specific far-red adaptations have not been observed in plants, they could potentially play an important role in crop improvements. Heavily-shaded lower leaves in dense crop canopies could be made more productive by utilizing the transmitted far-red wavelengths that make it through the canopy leaves. In an idealized situation in which all photons of wavelengths between 700 and 750 nm could be utilized in a crop field, a 19% increase in absorbable photons could be realized (Chen and Blankenship 2011). In the field, this ideal situation is unlikely to be achieved, but even an increase of a few percent could have a significant impact.

1.1 Far-Red Light Utilization in Plants

In crop and forest canopies, light is filtered by the upper canopy leaves, which tend to preferentially absorb blue and red wavelengths of sunlight while transmitting or reflecting much of the far-red and a small fraction of the green (Kasperbauer 1987; Ort et al. 2015). Plants are much more effective at absorbing and utilizing visible light than far-red, which is a notable feature of any photosynthetic action spectrum. The perception that leaves are green is the result of a slightly lower absorption of green light than red and blue, although this difference is still much less significant than the difference of far-red versus visible light. Plants primarily use this differential absorption as a shade-sensing mechanism. Under shaded conditions, the spectrum of light is enriched in far-red wavelengths, and the ratio of red to far-red light is sensed by phytochromes (Gilbert et al. 2001; Ort et al. 2015).

Phytochromes are photosensors involved in various aspects of plant development, including germination, hypocotyl elongation, gene expression, and flowering, just to name a few (Reed et

al. 1994; Furuya and Schäfer 1996; Nagy and Schäfer 2002). Light absorbed by phytochromes serves a purely signaling function and does not directly drive photosynthesis. The reversible phytochromes can be switched from the far-red-absorbing to the red-absorbing form by a short pulse of far-red light (Furuya and Schäfer 1996). Phytochromes are used to sense photoperiod in many flowering plants, switching to the far-red absorbing form as the day goes on (Reed et al. 1994). During the night, the far-red form will slowly revert if kept in darkness (Searle 1965). A short pulse of far-red light at the end of the day can have a strong effect on plants, as this will rapidly reset the photosensor back to its red-absorbing form (Kasperbauer 1987; Furuya and Schäfer 1996). This effect can be utilized in greenhouse and indoor growth situations of short-day plants. To promote flowering even when the day length is long, a relatively short pulse of far-red light can be applied at the end of the light period. This serves to reset the phytochrome rapidly, a process that would normally occur slowly in darkness, leading to a short-day response in a long-day environment.

In crop canopies, the ratio of far-red to red light is an important determinant of plant morphology, with closer plant spacing leading to higher ratios of far-red to red and shade avoidance responses (Kasperbauer 1987). Shade-avoidance responses include stem stretching, internode length, and branching patterns. The response to far-red light, therefore, of crop plants can be an important factor in determining minimum row spacing.

Despite the low absorption cross section beyond 700 nm, plants can effectively intercept and use a limited fraction of far-red light. Light as far to the red as 780 nm was able to drive some oxygen evolution as seen in one report (Pettai et al. 2005a). This PSII activity was suggested to be the result of possible low-energy chlorophyll *a* dimers that might be present in LHCII.

Photosystem I antennas have been shown to utilize far-red light much more effectively owing to their efficient far-red antennas. In the lower leaves of forest canopies, far-red light may make up 40% of the total photon capture and usage (Rivadossi et al. 1999). In the antennas of PSI, far-red absorbing Chl *a* molecules, and some of the ligands interacting with them, were identified (Morosinotto et al. 2003, 2005; Wientjes and Croce 2011; Wientjes et al. 2012). The protein environment surrounding these pigments is essential to their red-shifted absorption, and specific ligand-pigment interactions and Chl *a* dimerization are responsible for the red-shifting of the absorption spectra of these antennas (Rivadossi et al. 1999; Morosinotto et al. 2003, 2005). In plants, these red-shifted forms of Chl *a* found within the light-harvesting antennas of PSI absorb light at wavelengths up to 738 nm, up to 6kT lower than P700 (Croce et al. 1996). This indicates a necessity for thermally-activated uphill energy transfer between low-energy antenna pigments and P700 (Jennings et al. 2003).

This efficient utilization of far-red wavelengths preferentially by PSI also presents a particular problem for plant leaves utilizing shade light. Under shaded conditions, a significant increase in LHCII is required to match the activities of PSI and PSII under shaded conditions (Rivadossi et al. 1999). Given the relatively low absorption cross sections under far-red conditions, to improve the utilization efficiency of PSII, particular modifications found in algae and cyanobacteria can be employed. These natural adaptations to deep shade light conditions will be discussed in more detail below.

1.2 Far-Red Chlorophyll *d*

A far-red light niche adaptation of particular interest is Chlorophyll *d* (Chl *d*), a chlorophyll with a Q_y absorption maximum of 696 nm in methanol (Fig. 2C) and significantly longer *in vivo* (Fig. 1C). Chl *d* was discovered by Manning and Strain in 1943 in pigment extractions from red

macroalgae growing along the Northern California intertidal zones (Manning and Strain 1943). At the time, they logically attributed their newly discovered pigment to the macroalgae themselves, and they called this new pigment Chlorophyll *d*. However, as time went on, it was realized that the red macroalgae do not in fact contain any Chl *d*, and for some time it was considered that Chl *d* was merely an artifact of Manning and Strain's chlorophyll extraction procedure, given the observation that Chl *a* could be converted to Chl *d* in solvent (Holt and Morley 1959). However, in 1996, Miyashita *et al.* isolated from extracts of ascidia and cultured an oxygenic photosynthetic prokaryote that contained Chl *d* as its primary photopigment (Miyashita et al. 1996, 1997). Amazingly, the prokaryote they cultured contained only a few percent Chl *a*. This unique prokaryote was named *Acaryochloris marina* (Miyashita et al. 2003). The finding led to further research suggesting that the Chl *d* isolated by Manning and Strain probably came from epiphytes living on the surface of the red macroalgae, not an artifact of extraction (Murakami et al. 2004a; Larkum and Kühl 2005).

Since this discovery, several other *Acaryochloris* strains were identified. *Acaryochloris* is the only known genus containing Chl *d* as a primary photopigment, though many other far-red adapted prokaryotes contain traces of the pigment. In such cases, Chl *d* was found in very low levels in PSII of these Chl *f* containing species when grown under far-red light (Airs et al. 2014). However, in *Acaryochloris*, Chl *d* makes up to 95% of the total chlorophylls found in the organism, implicating the pigment as a near-complete replacement for Chl *a*.

In Photosystem II of Chl *d*-containing *Acaryochloris marina*, Photosystem II contains primarily Chl *d*, as well as two Pheophytin *a* molecules and a very small amount of Chl *a* (Chen et al. 2005; Tomo et al. 2007). Chl *d* is found to be the primary donor of PSII, and in *Acaryochloris*, P680 is replaced by P725 (Itoh et al. 2007), although P713 has also been suggested (Tomo et al. 2007).

This represents a significant red-shift compared to the typical P680 found in Chl *a*-containing phototrophs. The Chl *a* that is found in each PSII reaction center (RC) is also of notable importance (Schlodder et al. 2007; Tomo et al. 2007; Ohashi et al. 2008; Renger and Schlodder 2008). However, some debate still exists as to its exact function and location in PSII. The special pair of PSII is often considered to be composed entirely of Chl *d* molecules (Tomo et al. 2007), although some have suggested that a Chl *a* molecule is also part of the special pair based on spectroscopic evidence (Renger and Schlodder 2008). Whereas some argument still exists regarding the exact location and function of the Chl *a* in PSII, it is understood that Pheophytin *a* (Pheo a) serves as the primary electron acceptor (Chen et al. 2005). The redox potential of the Pheo *a* was shown to be lower in Chl *d*-containing organisms than in Chl *a*-containing ones (Allakhverdiev et al. 2010).

In *Acaryochloris marina,* photochemistry of Photosystem I is also driven by Chl *d* (Hu et al. 1998). The primary donor of PSI in *Acaryochloris* is P740, significantly red-shifted compared to P700 in Chl *a*-containing species, and is made up of a special pair of Chl *d* molecules (Hu et al. 1998). Despite absorbing at a lower energy than P700, excited P740 (P740*) is still capable of generating a reducing power that is roughly equivalent to that of P700 (Hu et al. 1998).

Chl *d* differs from Chl *a* only in the addition of a formyl group in the place of a vinyl in the C3 position of the chlorin ring (Fig. 2A). The biosynthetic enzyme responsible for the formation of Chl *d in vivo* still has not been identified, although experiments in *A. marina* have provided clues to its origins. ^{18}O labeling experiments have shown that Chl *a* and molecular oxygen serve as precursors in the synthesis of Chl *d* in *Acaryochloris* (Schliep et al. 2010; Chen 2014).

Given the precursors to Chl *d*, the multifunction oxidases known as Cytochrome P450s have been implicated as possible Chl *d* synthase candidates (Chen and Blankenship 2011; Blankenship et al.

2013; Chen 2014). P450s are particularly strong candidates because of their ability to use molecular oxygen to oxidize various compounds. However, to date, no cytochrome P450 has been shown to catalyze the catalysis of Chl *d* production *in vivo.* Another hypothesis would assume that Chlorophyllide *a* (Chlide *a*) serves as a precursor, and would draw parallels between the synthesis of Chl *d* and a very common Chl molecule in plants, Chl *b.* The addition of a formyl at the C7 site instead of C3 would generate Chl *b.* The precursor to Chl *b*, Chlide *b* is synthesized from Chlide *a* by using the enzyme Chlorophyllide *a* Oxidoreductase (CAO) (Oster et al. 2000). The oxygen atom in the formyl group is derived from molecular oxygen (O_2) (Porra et al. 1994). This seeming similarity suggests the possibility that CAO could be implicated in the biosynthesis of Chl *d.* However, the chemistry performed by CAO is to oxidize a methyl group to a formyl, whereas in the case of Chl *d*, a vinyl must be oxidized and a C=C double bond broken, so the chemistry is significantly different. In both of these cases, the need for molecular oxygen was suggested to provide evidence to put the evolutionary origin of Chl *d* after the origin of oxygenic photosynthesis (Chen and Blankenship 2011).

A potential opportunity to investigate the synthesis process of Chl *d* has recently arisen with the discovery of a very unusual *Acaryochloris* (RCC1774) that does not produce any Chl *d*, but rather produces Chl *b* as do the somewhat-related prochlorophytes (Partensky et al. 2018, unpublished observations, J.D. King, B.M. Wolf, R.E. Blankenship). Given the unusual pigmentation in these otherwise very similar species, this may suggest that the biosynthetic processes of Chl *d* and *b* are evolutionarily related. Significantly, it may be possible to compare the new genome sequencing data for both Chl *d* and Chl *b*-containing *Acaryochloris* to gain insights into the identity of the Chl *d* synthase.

1.3 Far-Red Chlorophyll *f*

Whereas Chl *d* alone holds the position of the far-red pigment that can replace nearly every function of Chl *a* in the reaction center, another modified chlorophyll takes the prize the for longest wavelength absorption. Chlorophyll *f* (Chl *f*) was discovered in 2010 in cyanobacterial isolates from stromatolites in Shark Bay, Australia (Chen et al. 2010). Chl *f* has the longest wavelength absorption of any known chlorophyll at 707 nm in methanol (Fig. 2C) and longer *in vivo* (Fig. 1C). The red-shift is the result of a formyl group in the C2 position on the chlorin ring instead of a methyl as in Chl *a* (Chen et al. 2010; Li et al. 2013). The first cyanobacterium discovered containing Chl *f* was the filamentous cyanobacterium *Halomicronema hongdechloris,* which contains less than 10% Chl *f* when grown under far-red light, but no Chl *f* at all under white light (Chen et al. 2012; Li et al. 2014b). When grown under far-red light conditions, *H. hongdechloris* responds by altering the localization of the phycobilisomes and Chl *f* (Majumder et al. 2017). *H. hongdechloris* does not limit its light-harvesting system alterations under various light conditions to chlorophyll pigmentation, and has been shown to alter its phycobilisome antennas dramatically in response to far-red light (Li et al. 2016). When grown under far-red light, isolated phycobilisomes not only exhibit a marked decrease in overall size and structure but also an absorption shift to 712 nm, nearly 100 nm to the red of the absorption maximum of white light grown cells (Li et al. 2016).

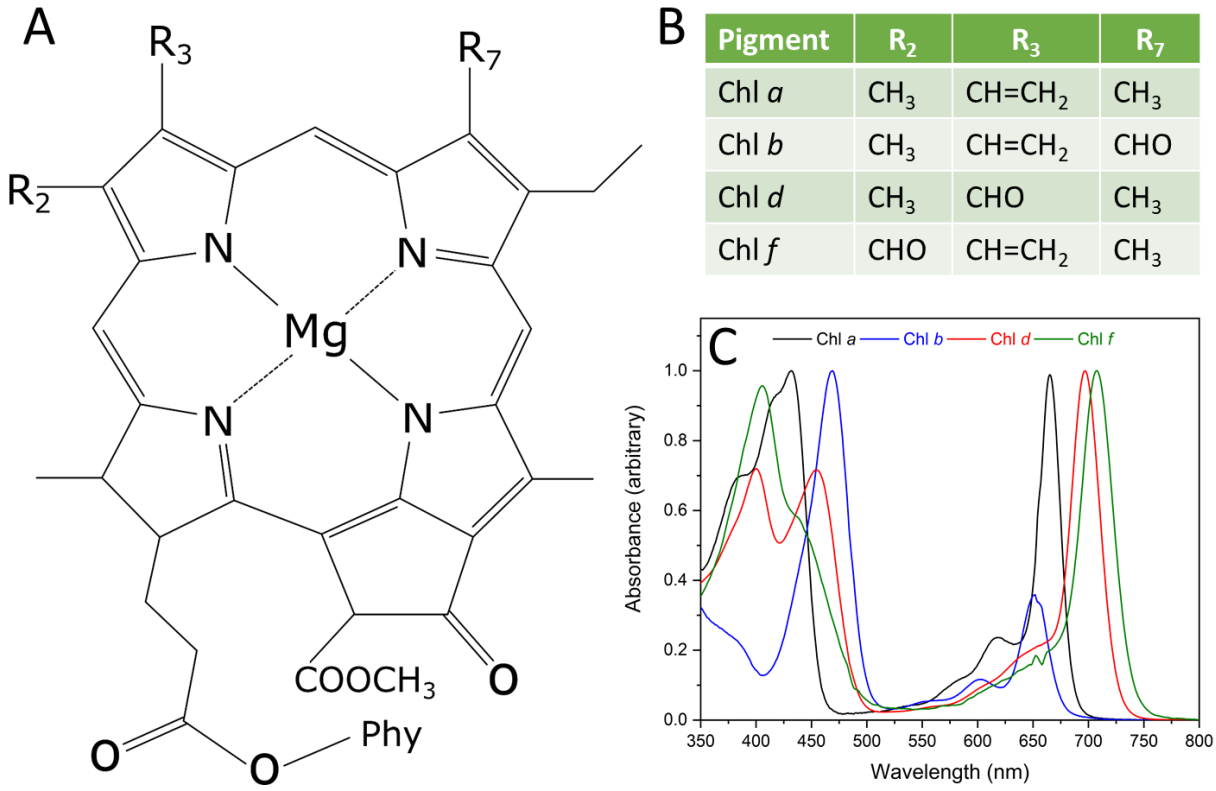

Pigment	R_2	R_3	R_7
Chl *a*	CH_3	$CH=CH_2$	CH_3
Chl *b*	CH_3	$CH=CH_2$	CHO
Chl *d*	CH_3	CHO	CH_3
Chl *f*	CHO	$CH=CH_2$	CH_3

Figure 1.2: Several chlorophyll structures and their absorption spectra. A) A chlorophyll macrocycle is shown, with labeled R groups substituted in various chlorophylls. B) Identification of the various R groups in each of four chlorophylls. C) Spectra of each of these chlorophylls in pure methanol that were purified using HPLC.

Following the discovery of Chl *f* in *H. hongdechloris*, a proverbial floodgate was opened and it was quickly discovered that Chl *f*-containing cyanobacteria are widely dispersed and quite common throughout the natural environment. When grown under far-red light, these cyanobacteria photoacclimate through a process termed FaRLiP (Far-Red Light Photoacclimation) (Gan et al. 2014a). FaRLiP involves significant changes to the organisms capable of it, including the production of Chl *f*, as well as a small amount of Chl *d*, and alterations to PSI, PSII, phycobilisomes, and several light receptors, all of which are encoded on a common 21-gene cluster (Gan et al. 2014a, b; Gan and Bryant 2015; Zhao et al. 2015; Ho et al. 2016b, c).

Under far-red light, FaRLiP-capable cyanobacteria make significant changes to their entire photosynthetic apparatus, but Chl *f* does not fully replace Chl *a* in the way that Chl *d* does. Although its low abundance even in far-red light-adapted cells might suggest that it serves only as an accessory pigment, this turns out not to be the case. Chl *f* plays a role in photochemistry in cyanobacteria when FaRLiP responses are activated. In the Chl *f*-containing cyanobacterium *Chroococcidiopsis thermalis*, Chl *f* has been identified in PSI and PSII when the cells were grown under far-red light, where it participates in charge separation (Nürnberg et al. 2018). When grown under far-red light, P700 is replaced by P745, and P680 is replaced by P727, and both contain Chl *f* while P727 also contains a single molecule of Chl *d* (Nürnberg et al. 2018). Similar to the case with Chl *d*, these red-shifted primary donors are still capable of driving oxygenic photosynthesis, indicating that the red limit is further into the far-red region than originally thought.

The biosynthetic process of Chl *f* has been determined to involve a light-dependent "super-rogue" D1 protein, called ChlF or PsbA4 (Ho et al. 2016a). Using either Chl *a* or Chlide *a* as a precursor, the enzyme uses catalytically active chlorophylls and an absorbed photon to oxidize the C2 methyl to a formyl group. It is, however, unknown what the oxygen source is for the oxidation. Ho *et al.* suggest a possible implication of the Chl *f* synthase as a precursor to the D1 protein in the early evolution of photosynthesis, rather than the opposite interpretation. This hypothesis would suggest that Chl *f* preceded oxygenic photosynthesis, and that the Mn_4CaO_5 cluster, essential to water oxidation in PSII, came later. The limited distribution of Chl *f*-containing species and the possibility of evolutionary tree reconstruction artifacts make this conclusion uncertain, however.

Because of the pervasiveness of Chl *f* in nature, it is likely to be found in additional genera of cyanobacteria. The ability to photoacclimate to far-red enriched conditions allows cyanobacteria with the FaRLiP adaptations to survive in stratified or otherwise shaded growing conditions. Given

the effects of such adaptations, the FaRLiP gene cluster could potentially be transformed into plants to improve their shade light utilization.

1.4 Algal Light-Harvesting Complexes that Red-Shift the Absorption of Chlorophyll *a*

Like plants, algae take a very different approach to far-red utilization than cyanobacteria. Some species of algae are very adept at far-red adaptation, but they do not produce specialized forms of chlorophyll for the purpose like cyanobacteria do. Instead, algae use a much more poorly-understood system of light-harvesting complex modifications that serve to shift the absorption spectrum of Chl *a*. Less is known about how algae utilize far-red light than cyanobacteria, possibly owing to their large genomes and the fact that the phenotypes are often not as clear-cut as the production of a novel chlorophyll. Here, we describe several systems that have been characterized to date, such as that of Eustigmatophytes and *Chromera velia*, as well as some of the studies that serve as foundations to understand how these processes work.

Algal light harvesting begins with the absorption of light in a system of integral trans-membrane light-harvesting complexes (LHCs) (Blankenship 2014). For PSII, these antennas are mostly trimeric in structure, being composed of three units, which each contain three transmembrane helices. The pigment composition of these pigment-proteins varies by species. Green algae (and land plants) contain Chl *a* and *b*, as well as several carotenoids including xanthophyll. These antenna complexes are designated LHCII, and they were characterized in some detail, including through crystallography (Liu et al. 2004). A notable feature of LHCII antennas is their lateral mobility in the membrane. Through the process of state transitions, LHCII antennas can move through the thylakoid membrane to interact with PSI or PSII, helping to balance the excitation of

the two types of reaction center (Rochaix 2014). Also, a great diversity exists in LHCIIs expressed in plants and algae.

In stramenopile algae, formerly called heterokonts, a different type of LHC is present, though it is related to the LHCII found in plants and green algae. Stramenopiles include brown algae, diatoms, eustigmatophytes, and others, and make up an important part of the plankton in the oceans. In diatoms, the antenna is a Fucoxanthin-Chlorophyll Protein, or FCP, and it contains Chl *a*, Chl *c*, and the carotenoid fucoxanthin (Gundermann and Büchel 2014; Büchel 2015). FCPs are found in trimeric form, like LHCIIs, but have not been characterized in the same level of detail. Recently, however, an FCP from the diatom *Phaeodactylum tricornutum* was crystallized, leading to the identification of important pigment-pigment and pigment-protein interactions that are important for energy transfer (Wang et al. 2019). There are separate FCP organizations and types for PSI and PSII (Gundermann and Büchel 2014). The antenna system is similar in Eustigmatophytes, which are free-living coccoid secondary endosymbiont algae of about 10 μm in size with a characteristic red lipidic body of unknown function (Eliáš et al. 2017). Eustigmatophyte antennas are Violaxanthin Chlorophyll Proteins, or VCPs. VCPs contain only Chl *a* and carotenoid, principally violaxanthin and vaucheriaxanthin (Sukenik et al. 2000; Litvín et al. 2016; Eliáš et al. 2017).

In diatoms and eustigmatophytes, a high level of gene diversity is present. In the eustigmatophyte *Nannochloropsis oceanica*, for instance, 17 different gene products associated with LHC-type proteins were identified (Litvín et al. 2016). In both *N. oceanica* and the close relative *N. gaditana*, large PSII-LHC complexes were not observed owing to its weak interaction, though PSI-LHC complexes were, and it is apparent that there are separate LHC pools for both PSI and PSII (Basso et al. 2014; Litvín et al. 2016). However, several LHC-type antennas did have some interaction with PSII even after purification (Litvín et al. 2016). It can, therefore, be concluded that the

interaction of LHC antennas to PSI is stronger than to PSII in *Nannochloropsis*, though separate pools do exist for each reaction center.

Although *Nannochloropsis* has not been shown to utilize far-red light effectively, several Eustigmatophyte algae have been shown to possess LHCs capable of absorbing far-red light to promote oxygenic photosynthesis (Wolf et al. 2018; Bína et al. 2019; Niedzwiedzki et al. 2019). One of these species, the eustigmatophyte alga FP5, survives entirely on far-red wavelengths of light by using an antenna system that contains only Chl *a* and carotenoids (Fig. 1B) (Wolf et al. 2018). In FP5, the LHC appears to rely on an aggregation-based mechanism to red-shift its Chl *a* to an absorption component of approximately 705 nm. This is sufficient to allow survival using light from a 740 nm LED or filtered shade light.

The green alga *Ostreobium* is a coral symbiont capable of growing in highly shaded and far-red light enriched environments. This alga has a notable far-red fluorescence peak at 719 nm at 77 K in whole cells, and fluorescence excitation shows a strong contribution to the far-red fluorescence from a pigment absorbing at 702 nm, indicating the presence of low-energy pigments even when grown under white light (Fork and Larkum 1989). *Ostreobium* sp. was also shown to possess a significant far-red absorption shoulder in whole cells. When compared with another species of *Ostreobium* lacking the far-red spectral features, a denaturing electrophoretic analysis identified a unique Lhca1 polypeptide, which was confirmed by N-terminal amino acid sequencing (Koehne et al. 1999). This same study showed evidence for up to three far-red pigments within whole membranes, but concluded that these are more likely caused by protein-pigment interactions than excitonic interactions between pigments. This hypothesis, combined with the fact that the system is not conserved amongst all species of *Ostreobium*, is also interesting, and provides a possible means for future comparative biochemical studies.

The finding that the far-red spectral forms of chlorophyll in *Ostreobium* sp. are primarily associated with a PSI antenna provides a basis for some interesting biological questions. In a later study, it was shown that the far-red antenna system in *Ostreobium* sp. is capable of driving PSII under far-red illumination (Wilhelm and Jakob 2006a). In this study, when *Ostreobium* sp. was grown under far-red light, it was capable of growth, and a photosynthetic action spectrum of oxygen evolution confirmed an extension of the red drop and PSII activity under wavelengths out to 740 nm. Whether this might represent a mobile Lhca protein or some sort of physical interaction in the form of a supercomplex of both RCs and the far-red antenna remains an open question.

A more recently characterized eukaryotic far-red antenna is that of the alveolate *Chromera velia.* The discovery of the coral reef symbiont was published in 2008, and was shown to be a close relative of apicomplexan parasites, which contain a non-photosynthetic plastid (Moore et al. 2008). The light-harvesting systems of this unusual alga are of particular interest due to their evolutionary history. Although their plastid is indeed photosynthetic, phylogenetically, they are more closely related to parasitic, non-photosynthetic apicomplexans than to the photosynthetic alveolates, the dinoflagellates (Moore et al. 2008; Weatherby and Carter 2013). The plastid is clearly divergent from that of the dinoflagellates, in that it lacks the peridinin and Chl *c* that they contain, but rather contains Chl *a*, violaxanthin, isofucoxanthin, and β,β-carotene (Moore et al. 2008; Quigg et al. 2012).

The retained photosynthetic plastid of *Chromera* has some interesting features, including an unusual antenna composition. While the photosynthetic apparatus of *C. velia* appears to be rather primitive, its efficiency is still high, and the ability to respond to various light intensities is still adequate (Quigg et al. 2012). The plastid of the apicomplexans and *Chromera* seems to have arisen from the endosymbiosis of a red alga (secondary endosymbiosis), and the plastid appears to be

closely related to that of heterokonts (stramenopiles) (Janouškovec et al. 2010). In a separate study, the 23 nuclear-encoded LHC genes were found to have varied evolutionary histories, including 17 related to the FCPs in diatoms and dinoflagellate PCP, but only three of red algal origin (Pan et al. 2012). This is interesting given that the *Chromera* light-harvesting proteins lack Chl *c*, and given the red algal lineage of the plastid. Biochemical characterization of the antenna complexes in *Chromera velia* revealed the anticipated FCP-like LHCs, which were named *Chromera* Light Harvesting (CLH), and also PSI-LHCr complexes, which were red algal in origin (Tichy et al. 2013).

When grown under long wavelength light, this coral symbiont, like the *Ostreobium* sp. described above, is capable of producing a far-red antenna system. When grown under red light, a notable 710 nm room temperature fluorescence was observed, which was accompanied by a red shoulder on the absorption spectrum (Kotabová et al. 2014). This was not observed under blue light, and was reversible. The LHC-type proteins responsible for this shift were named Red-CLH complexes, and were functionally linked to PSII (Kotabová et al. 2014). When the Red-CLH proteins were purified, it was found that they were made up of antenna multimers or aggregates that could be easily disrupted, leading to a complete loss of their far-red absorption and fluorescence properties (Bína et al. 2014). Given that this property has also been observed in a Eustigmatophyte alga (Wolf et al. 2018), which shares an ancestor with *Chromera* through the secondary endosymbiotic event (Janouškovec et al. 2010), it appears that such a multimerization red-shifting effect may be a widespread adaptation among secondary endosymbionts.

1.5 Relevance

In nature, surviving the common niche of deep shade is a driving factor for far-red light adaptations. Whether the case of a shaded coral symbiont alga (Fork and Larkum 1989),

cyanobacteria forming shaded layers within a stromatolite (Chen et al. 2010), or a shaded lifestyle on the bottom of an ascidian (Miyashita et al. 1996) or brown macroalgal frond (Murakami et al. 2004a), organisms throughout the tree of life have evolved mechanisms to use the dim transmitted wavelengths of marginal quality far-red light. In land plants, these adaptations do not seem to represent a large portion of the absorption spectrum, even under light-limited conditions, though far-red light is still an important signal. This has led to a great deal of speculation regarding the potential gains that could be realized in agriculture if such systems could be transformed into plants.

Because photosynthesis is a quantum process, it is not a significant disadvantage to use far-red light, as long as the energy of the absorbed photons is high enough to support photochemistry. The champions of this expansion are currently the Chl *f*-related adaptations, which were shown to shift the primary donor of PSI all the way out to 745 nm and PSII to 727 nm (Nürnberg et al. 2018). If all of the photons between 700-750 nm could be used by crop plants, a 19% increase in the number of absorbable photons could be realized (Chen and Blankenship 2011). Of course, this provides an upper limit, but nevertheless, it serves to demonstrate the fact that a far-red utilizing crop plant could be of value in terms of yield enhancement. Control of such a system would rely on phytochromes, similar to the smart canopies that were suggested previously by using non-far-red adaptations (Ort et al. 2015). This would allow light-starved lower leaves to capture unused far-red light, which saturated upper leaves would not intercept.

Several approaches can be taken to engineering a far-red utilizing crop plant. One would be to use the genes from the 21-gene FaRLiP cluster (Gan et al. 2014a) to produce Chl *f* in a plant, along with all of the modified reaction center proteins. However, this presents several serious challenges, including differences in eukaryotic and prokaryotic reaction centers and the presence of LHC

proteins in plants that may or may not properly incorporate Chl *f in vivo*. To circumvent some of these challenges, it might instead be possible to engineer plants with some of the eukaryotic far-red LHC proteins we have described, such as the Red-CLH proteins (Bína et al. 2014; Kotabová et al. 2014) or the red Lhca1-type light harvesting complex from *Ostreobium* sp. (Koehne et al. 1999). While these do not possess as significant a reach into the far-red as the modified pigments, this might be balanced by the potentially simpler and less costly path to engineering and subsequent commercialization. Far-red-utilizing oxygenic phototrophs offer a potential method to increase photosynthetic yields in crop plants worldwide. Continued research will be needed to discover new systems and engineer those already present in plants.

Chapter 2: Environmental Sampling

Environmental sampling was used to collect novel far-red light utilizing species. Once samples were taken from the environment, they were grown under several far-red light chambers, which were specifically constructed for the purposes of this research project. Using these chambers, we found that isolation efficiencies were high. Not all enriched organisms were studied in more detail other than spectral capture and preliminary microscopy and 16S or 18S sequence analysis. Of the isolated species, the eustigmatophyte alga FP5 and the filamentous cyanobacterium LSP65 were scaled up and studied in more detail. These chambers were also efficient in growing large volumes of culture for the in-depth analysis of the antenna systems within these species.

2.1 Culture Collection and Isolation

Isolation of far-red light utilizing strains of algae and cyanobacteria involves sample collection, far-red enrichment and selection, growth on solid medium, and several colony restreaks. Once a culture is made unialgal through restreaking procedures, it can be scaled for investigation of its photosynthetic apparatus. The entire process takes several months at minimum but has a surprisingly high rate of success. Most far-red cultures collected were not analyzed further; however, several of interest were cleaned of contaminating species, scaled up for culturing, and maintained. These included prominently the Eustigmatophyte alga FP5 and the filamentous chlorophyll *f* cyanobacterium LSP65.

Collection of samples can be accomplished in any location: soil, water, scrapings of other plants, or other biofilms. For this purpose, it is important to start with clean sampling equipment to prevent any cross contamination that would result in incorrect identification of sampling location. For this purpose, sterile, factory-packaged plastic sealable culture tubes were used. For aquatic sampling,

clean, factory-packaged disposable pipettes were used to obtain water samples before placing them into collection tubes. Tubes either had BG-11 growth medium already in them (which would be slightly diluted by the sample), or samples were soon after injected into a separate culture tube containing BG-11. For biofilms, clean, factory-packaged cotton swabs were used to collect biofilm material. Depending on the tenacity of the material, cotton swabs were either swirled in a sterile solution BG-11 growth medium already within the tube, or the ends were broken and placed into the medium. Generally, the later produced poorer results as mold and heterotrophic bacteria tended to form on the cotton swab end after a time.

For muck samples and for some of the earlier water samples (including the Forest Park sample from which FP5 was collected), the samples were injected into sterile BG-11 following collection. For muck samples, care was taken to add only a small amount of organic matter so as not to provide excessive carbon sources for heterotrophic contaminants. Once diluted with BG-11, samples were immediately placed under 740 nm LED lights (described below). Once green growth was detected in a sample, some of this growth was removed, sonicated for 10 seconds with a micro probe, and absorption and fluorescence spectra were taken using a Shimadzu UV-1800 or UV-2401 and a Cary Varian Fluorometer, respectively. Fluorescence measurements were taken using an excitation wavelength of 435 nm and default settings.

Isolates with significantly red-shifted absorption and fluorescence spectra were used to inoculate additional tubes of BG-11, as well as shaken flasks, and placed back under far-red light. In addition, aliquots of these stable enrichment cultures were used to inoculate BG-11 agarose plates. Pure agarose must be used, as the contaminants normally found in typical agar can lead to mold growth and algal-cell death. These plates were also placed under far-red LED light. When colonies formed, they were picked with a sterile loop or pipette tip and transferred to a new plate by

streaking, and the process was repeated until a unialgal culture was obtained. The status of the culture was determined by light microscopy of large swaths of culture as well as 18S or 16S sequencing (Sanger) for algae and cyanobacteria, respectively.

Not all bacterial symbionts are necessarily removed by this technique. In fact, it was shown that in some cases these symbionts are necessary for growth of certain algae and are found to directly interact with cells. Normally, it was not required that all heterotrophic symbionts be eliminated for the purposes of the studies detailed in this document. A unialgal culture is sufficient for isolation of light-harvesting complexes, found only in phototrophs.

2.2 Far-Red Growth Chambers

Two far-red growth chambers, in addition to several ancillary growth systems, were constructed as an integral part of this work. For all, far-red LEDs were used as a strong selection source to allow growth of only the desired far-red utilizing algae and cyanobacteria. For this purpose, 740 nm far-red LEDs were obtained from Amazon.com from the seller LED World. Although these LEDs do not come with much characterization, such as datasheets, they provide a significant photon flux at a reasonable price and are easy to work with. Spectral measurements using an Ocean Optics spectrometer confirmed the 740 nm emission peak, and a calibrated ThorLabs laser energy meter was used to accurately measure light intensity. The 740 nm LEDs are of the near-monochromatic type and as such have no phosphor emission bands and thus bear very little evidence of peak trailing. This leads to a spectrum with nearly no emission in the range of classically-defined photosynthetically active radiation (PAR). Thus, these inexpensive and simple 1 amp 2.1 volt star-board-mounted LEDs provide an optimal spectrum for delivering a strong selective pressure for far-red utilizing oxygenic phototrophs.

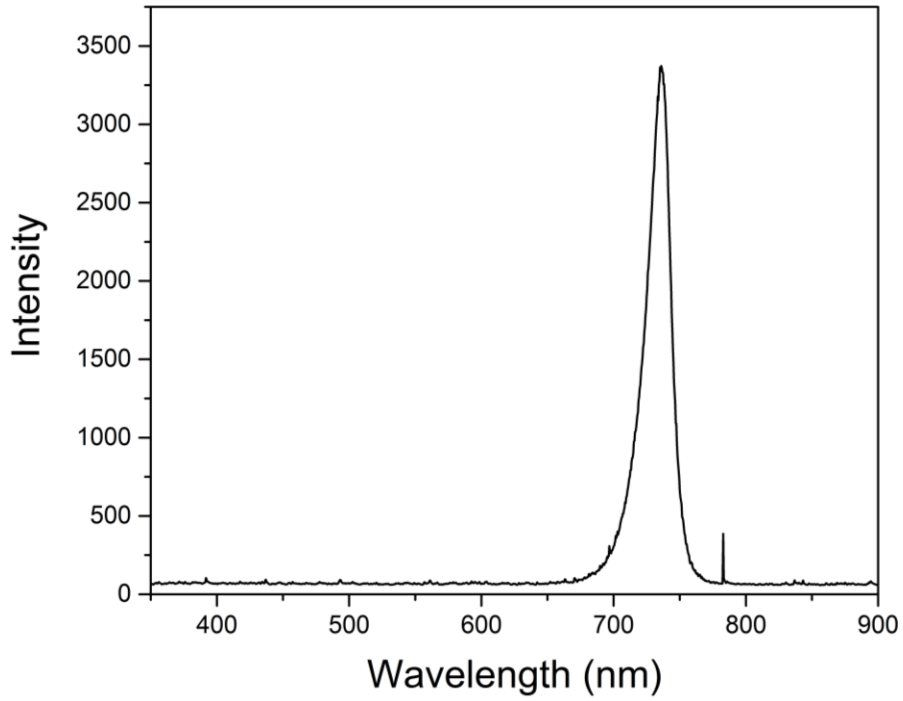

Figure 2.1: Emission spectrum of the 740 nm far-red LEDs referenced throughout this dissertation.

Each chamber uses a different cooling approach. LEDs are highly efficient light sources, but cooling is still essential as they are very sensitive to what heat they do produce. Horticultural LED lighting solutions are normally air-cooled, either by forced air (i.e. fans, blowers) or passive air-cooling (i.e. radiation and convection). Lower temperature luminaires tend to last longer than higher temperature luminaires, and higher temperatures also tend to lead to inefficiencies in LEDs, which leads to increased heating (a condition that can lead to thermal runaway, where an electronic component is destroyed by a positive feedback loop of heating and decreased forward voltage). LEDs must be controlled using constant current or constant power to reduce the chances of a thermal runaway event and to allow more precise control. For all LED systems designed for this project, constant current sources were used. These were either of a switched-mode topology or a linear topology.

2.2.1 Liquid-Cooled Chamber

Given the rarity for fully far-red growth chambers, it was necessary to construct my own to isolate far-red light-utilizing species. The first of these chambers constructed, which was used for the vast majority of the isolation experiments used to obtain the FP5 and LSP65 cultures, is a converted wooden laboratory cabinet with 60 liquid cooled 740 nm LEDs. The cabinet itself was obtained from the Michigan State University Surplus Store in East Lansing, Michigan, USA. To transport the cabinet to St. Louis, Missouri, it was required that the cabinet be cut in half. To reattach the halves and to affix the center shelf firmly, the cabinet was then attached back together using 8 metal L-brackets, as well as a liberal coating of wood glue on the interfacing surface. The inside was painted white to increase light reflection.

For cooling, liquid cooling channels were constructed by brazing an aluminum flat bar to a ½ inch ID copper pipe. Brazing rods were obtained from Harbor Freight Tools and a natural gas Bunsen burner was used as a heat source for brazing. Copper fittings were soldered to the pipes as appropriate to create a snaking path for cooling water through the entire chamber. Three rails per shelf were positively affixed by using standard pipe clamps. Using a drill press, I bored 20 holes into each copper flat bar. I then tapped threads into each hole using a 6-32 NC hand tap. I wired ten LEDs in series for each rail before affixing them to allow solder to flow easily without the heat sinking effect of the rails. I then affixed these wiring harnesses to the rails by using #6-32 screws obtained from McMaster-Carr (www.mcmaster.com) with a small amount of a thermally-conductive non-adhesive grease, branded Coca and obtained from www.amazon.com.

Thus, each of six rails had ten LEDs wired in series, which at their rated power could operate at over 120 watts of power. However, this high power was not required for operation. A 24 volt DC power supply was attached to the underside void of the cabinet, but because LEDs require a

constant current source owing to very high forward voltage sensitivity to temperature, each shelf was fitted with a constant current buck converter driver. These drivers were of a generic type with a voltage and current readout. These units were purchased from Amazon.com. The three rails on each shelf were wired in parallel so that they could be connected to the driver outputs. Current was set based on the specific need for the experiment to be completed.

A thermal cutout switch was affixed to a separate small aluminum strip brazed to a copper connector pipe. This switch was wired in series with the AC power to the main power supply, such that an over-temperature condition would result in the shutdown of power to the DC bus.

The system was at times cooled in four different ways: 1) water was chilled and pumped by a precision refrigerated water bath, 2) water was pumped from a flask with a drain side-arm using an inline DC pump and through a heat sink with water channels cut out, and a DC fan affixed, 3) water was flowed from a sink supply directly to waste (emergency cooling), and 4) water was pumped from a large bucket using a submersible pump without a dedicated water to air heat exchanger. Several significant problems were discovered with all four options, so a fifth option was proposed, detailed below.

Figure 2.2: Liquid-cooled far-red light chamber interior, showing far-red LEDs, built-in power outlets, shaker, and custom tube rack.

Option 1 worked well as long as the temperature was set above the dew point of the room air. It was discovered that, while cooling to a lower temperature could also be used to control the air temperature within the chamber, this led to condensation on the rails. The condensation led to galvanic corrosion between the copper pipe and the electrically connected aluminum rail. In addition, this caused damage to several LEDs. The water bath was later needed for other uses, and its high energy usage made it unsuitable as a sustainable long-term solution.

Option 2 worked well for some time but was eventually abandoned for several reasons. The brass fittings used to affix the hosing to the aluminum heat sink underwent galvanic corrosion, which in time led to the clogging of the narrow cooling channels. The resulting resistance to flow eventually caused the failure of the inline DC water pump, which was attributed to the disintegration of a plastic bushing under load. For these reasons, this system was abandoned, and Option 3 was used

as an interim measure until Option 4 was set up. Option 3 was clearly unsustainable, as it involved the discharge of large amounts of clean water to the sewer system.

Option 4 eliminated the clog-prone air to water heat exchanger, and instead relied on a large bucket with a large thermal mass and surface area for heat transfer. A submersible pump was used to circulate the water. The primary disadvantages of this system are the large amount of water, which tends to evaporate, leaving the pump dry. Otherwise, this system was entirely workable.

This system, though it worked well for many experiments, could easily be improved in future iterations of the design. Further experimentation identified copper flat bar as a better option than aluminum, primarily because it could be soldered directly to the cooling tube without the need for high-temperature brazing. Additionally, this union will not lead to galvanic corrosion. Copper is expensive, so care should be taken to minimize the size of the bar. It is also difficult to machine, so it is advisable to attach LEDs using a permanent adhesive rather than screws. Optimally, LEDs would be mounted to long aluminum-backed circuit boards that could be mounted using a dielectric adhesive strip. To improve the design further, or if a larger budget is available, the copper flat and pipe should be replaced with a dedicated aluminum extrusion. This will allow for simple construction and high reliability of operation.

Water delivery can also be optimized. An inline pump is still recommended, although one of a higher reliability than was originally used. Design iteration on other systems has shown that the combination of a closed PVC reservoir with an air expansion vent, an inline pump running at a low or variable voltage, and a CPU cooler radiator with a fan combined make an excellent pump/heat exchanger combination. Such a system was used in further iterations.

2.2.2 Air-Cooled Chamber

A second chamber was also built from scratch. A wooden flat-pack storage cabinet was purchased from Menards and converted into an air-cooled chamber. The inside of the chamber was painted white for reflection. It consisted of four shelves, and each was lamped with twenty of the same far-red LEDs as above. However, instead of being connected to a liquid cooling system, they were connected using #6-32 screws to square aluminum tubes, which were used to carry cooling air. Along the left side of the chamber, two 2-inch PVC pipes were connected and small square holes were cut from them using a rotary tool to admit the aluminum tubes. At the bottom of each pipe, a blower fan was mounted to suck air from the pipes. The open end of the aluminum tubes opened into the chamber itself, allowing chamber air to be exchanged.

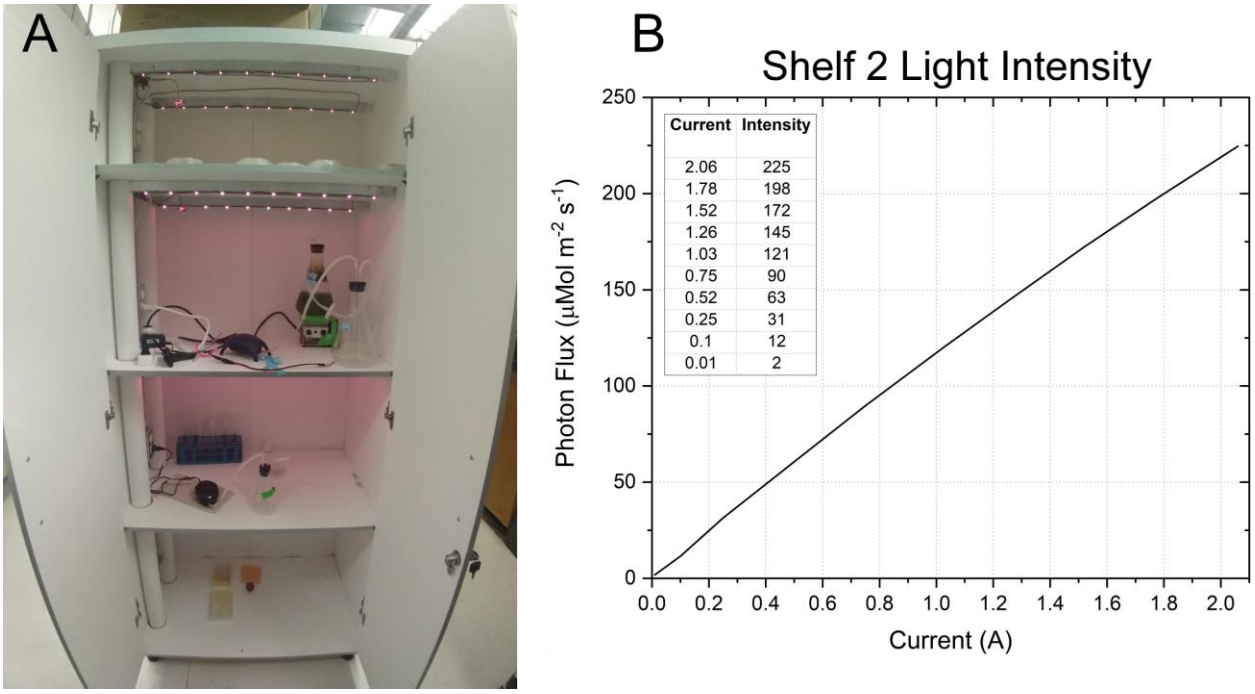

Figure 2.3: Four-shelf air-cooled far-red growth chamber. A) The growth chamber itself with several cultures in it. B) Photon flux vs current curve for the second shelf from the top.

The LEDs were mounted in the same way as above. However, the power supply was different. Instead of using a switched-mode buck converter, linear regulators were constructed by using an operational amplifier (op-amp), measuring the voltage drop across a current sense resistor and a bipolar junction transistor (BJT), thermally connected to the aluminum tube. A potentiometer was used to control the reference voltage to the op-amp, allowing for current adjustment. Each of two rails in each shelf had its own current source, but they were controlled by a unified reference voltage. A voltmeter was permanently connected across a separate 1 ohm sense resistor, which provided a readout of current. Using the same ThorLabs energy meter and the known spectrum, I generated a curve of LED current vs photon flux (Figure 2.3B).

2.3 Isolation Results

Over the course of the original isolation experiments, a large collection of enrichment cultures was established. These cultures included eukaryotes and prokaryotes. The majority of these cultures were analyzed broadly, including absorption spectra of the whole cells when grown under far red light and the extracted pigments. Some isolates were also placed into families based on 18S or 16S rRNA sequences. Although it was not practical to analyze all of these cultures in a high level of depth or to purify them all, several of the most interesting cultures were maintained, cleaned, and scaled up.

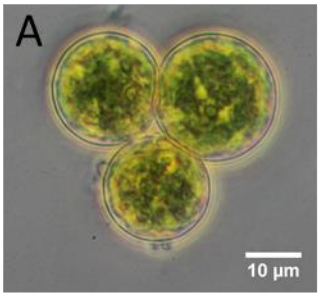
A
10 µm

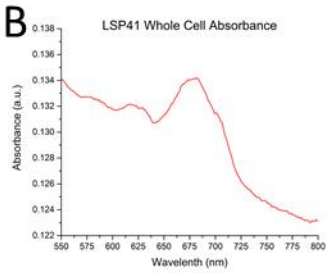
B
LSP41 Whole Cell Absorbance
Absorbance (a.u.)
Wavelenth (nm)

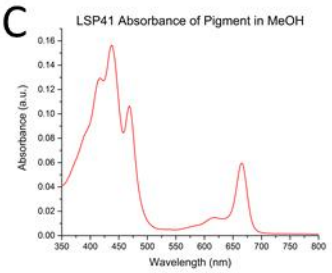
C
LSP41 Absorbance of Pigment in MeOH
Absorbance (a.u.)
Wavelength (nm)

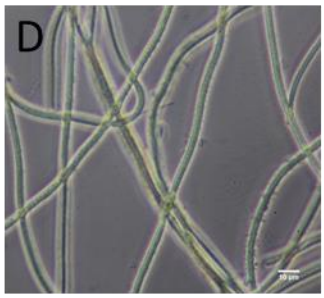
D

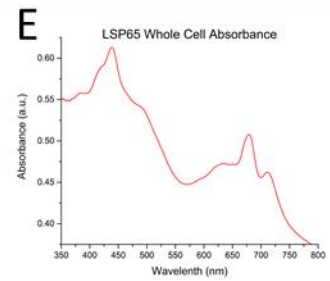
E
LSP65 Whole Cell Absorbance
Absorbance (a.u.)
Wavelenth (nm)

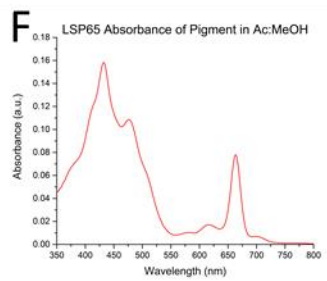
F
LSP65 Absorbance of Pigment in Ac:MeOH
Absorbance (a.u.)
Wavelength (nm)

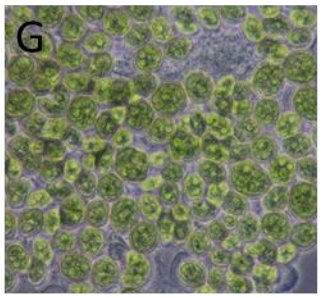
G

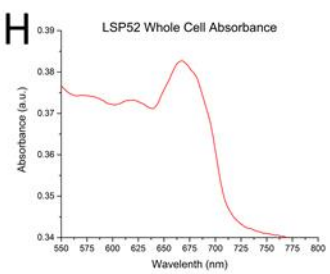
H
LSP52 Whole Cell Absorbance
Absorbance (a.u.)
Wavelenth (nm)

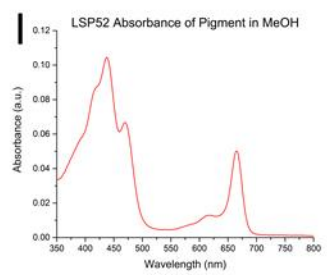
I
LSP52 Absorbance of Pigment in MeOH
Absorbance (a.u.)
Wavelength (nm)

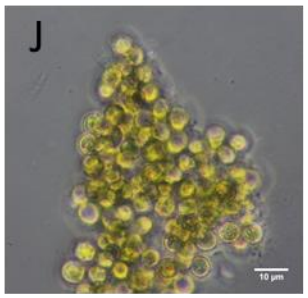
J

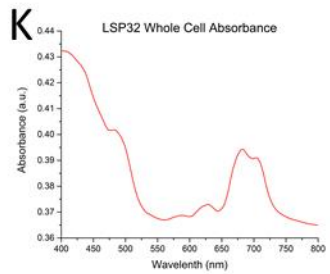
K
LSP32 Whole Cell Absorbance
Absorbance (a.u.)
Wavelenth (nm)

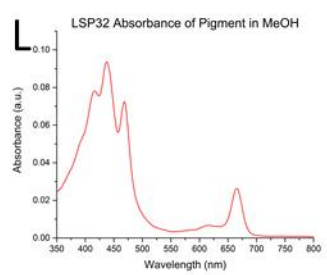
L
LSP32 Absorbance of Pigment in MeOH
Absorbance (a.u.)
Wavelength (nm)

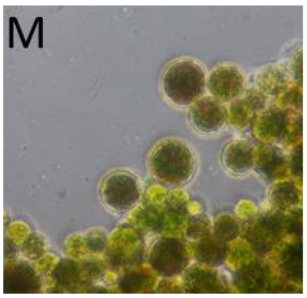
M

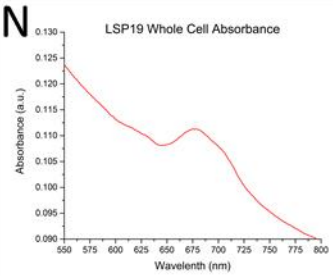
N
LSP19 Whole Cell Absorbance
Absorbance (a.u.)
Wavelenth (nm)

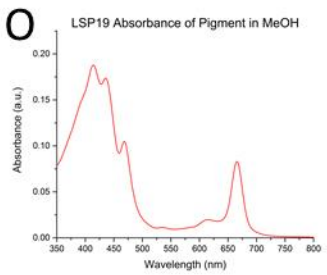
O
LSP19 Absorbance of Pigment in MeOH
Absorbance (a.u.)
Wavelength (nm)

Figure 2.4: Examples of five enrichment cultures obtained from Ludington State Park in Ludington, Michigan. LSP41 A) microscope image, B) whole cell absorption spectrum, C) absorbance of pigment in methanol. LSP65 D) microscope image, E) whole cell absorption spectrum, F) absorbance of pigment in methanol. LSP52 G) microscope image, H) whole cell absorption spectrum, I) absorbance of pigment in methanol. LSP32 J) microscope image, K) whole cell absorption spectrum, L) absorbance of pigment in methanol. LSP19 M) microscope image, N) whole cell absorption spectrum, O) absorbance of pigment in methanol.

A sampling campaign in Ludington State Park in Ludington, Michigan was particularly successful. Summaries of several of the isolates are shown in Figure 2.4. Isolates were collected from varied environments. LSP41 (Figure 2.4A-C) was collected from pond water in the park. LSP65 (Figure 2.4D-F) was collected as a scraping of a biofilm from the bottom of a lily pad. It will be discussed in more detail in Chapter 6. LSP52 (Figure 2.4G-I) was collected from a warm, shallow, red-colored dune pond with abundant pond grass and sunlight. 18S rRNA sequences indicate that this is a type of green alga called Scenedesmus. It does not bear a strong far-red absorption feature (Figure 2.4H), but it is still capable of growth under far-red light by using what far-red feature it does have. LSP32 (Figure 2.4J-L) was collected from a pond in a forested sand dune environment. It has a significant far-red absorption shoulder (Figure 2.4K) but no far-red chlorophylls (Figure 2.4L). LSP19 (Figure 2.4M-O) was collected from pond water in the park.

Chapter 3: Characterization of the Eustigmatophyte alga FP5[2]

Oxygenic phototrophs typically utilize visible light (400–700 nm) to drive photosynthesis. However, a large fraction of the energy in sunlight is contained in the far-red region, which encompasses light beyond 700 nm. In nature, certain niche environments contain high levels of this far-red light owing to filtering by other phototrophs, and in these environments, organisms with photosynthetic antenna systems adapted to absorbing far-red light are able to thrive. We used selective far-red light conditions to isolate such organisms in environmental samples. One cultured organism, the Eustigmatophyte alga Forest Park Isolate 5 (FP5), is able to absorb far-red light by using a chlorophyll (Chl) *a*-containing antenna complex, and it is able to grow under solely far-red light. Here we characterize the antenna system from this organism, which is able to shift the absorption of Chl *a* to > 705 nm.

3.1 Background

The spectral range that can be utilized to drive oxygenic photosynthesis in most plants, algae, and cyanobacteria is usually limited to the visible range, 400–700 nm (Chen and Blankenship 2011). Although light in the visible region is abundant in unfiltered sunlight and is thus an efficient way to drive photosynthesis for most species, those organisms growing under filtered light tend to experience illumination enriched in the transmitted far-red wavelengths (beyond 700 nm). A well-

[2] A version of the following chapter was published originally as: Wolf, B. M., Niedzwiedzki, D. M., Magdaong, N. C. M., Roth, R., Goodenough, U., & Blankenship, R. E. (2018). Characterization of a newly isolated freshwater Eustigmatophyte alga capable of utilizing far-red light as its sole light source. *Photosynthesis Research, 135*(1–3), 177–189. https://doi.org/10.1007/s11120-017-0401-z

characterized example of this sort of light filtering is found in ascidians that inhabit coral reefs, where their symbionts such as *Prochloron*, containing chlorophylls (Chls) *a* and *b*, absorb most of the incoming visible light, transmitting far-red light (FRL) (Kühl et al. 2005; Behrendt et al. 2011). In addition to marine coral reefs, such environments also exist in terrestrial and freshwater systems. Some organisms adapted to growth under these conditions possess specialized antenna systems able to absorb light in the far-red range (Kühl et al. 2005; Behrendt et al. 2011; Chen and Blankenship 2011; Kotabová et al. 2014).

Multiple strategies have been discovered by which specialized organisms can perform oxygenic photosynthesis using FRL. These include expression of antennas containing the red-shifted Chls *d* and *f* (Miyashita et al. 1996; Miyashita et al. 1997; Kühl et al. 2005; Behrendt et al. 2011; Chen et al. 2012), red-shifted phycobilisomes (Gan et al. 2014; Li et al. 2016), or transmembrane light-harvesting complexes (LHCs) that utilize the protein environment to red-shift the absorption spectrum of Chl *a* (Bína et al. 2014; Kotabová et al. 2014; Pazdernik 2015). Such organisms tend to be found in habitats enriched in FRL, such as would be found located below a layer of other phototrophs that absorb visible light but transmit FRL. For example, the Chl-d-containing cyanobacterium *Acaryochloris marina* was originally isolated from extracts of colonial ascidians (Miyashita et al. 1996; Miyashita et al. 2003). The Alveolate *Chromera velia*, which contains a FRL-absorbing LHC-like protein (Bína et al. 2014; Kotabová et al. 2014), was isolated as a coral symbiont off the coast of Australia (Moore et al. 2008; Tichy et al. 2013). Although many of the described FRL-utilizing species are marine (Miyashita et al. 2003; Chen et al. 2012; Tichy et al. 2013), there have been several descriptions of freshwater organisms containing FRL-absorbing antennas (Pazdernik 2015).

In some marine and freshwater algae, these far-red-adapted antennas do not contain specialized pigments, but rather use the protein environment to shift the absorption properties of Chl a. For example, in *Chromera velia*, multimerization of the antenna complex results in the observed red-shift in absorption and fluorescence (Bína et al. 2014; Kotabová et al. 2014). Several species of the Chlorophyte algal genus *Ostreobium* contain significantly red-shifted antennas, which were shown to perform thermally activated uphill energy transfer to drive charge separation in the special pair of photosystem (PS) II (P680) (Wilhelm and Jakob 2006). Unlike higher plants and most algae that exhibit a so-called "red drop," where oxygen evolution falls sharply beyond a certain wavelength, this is not observed in *Ostreobium*; it continues its photosynthetic productivity even in the far-red range (Wilhelm and Jakob 2006).

In both higher plants and algae, integral membrane protein-pigment complexes known as LHCs capture solar energy and transfer the resulting excitation to the reaction center, with which they form a supercomplex wherein photochemistry is performed (Kühlbrandt 1994; Wientjes and Croce 2011; Wei et al. 2016). Whereas plants do not grow under far-red illumination, their PSI antennas have some red-shifted Chl *a*, which is accomplished by tuning the protein-pigment interaction (Morosinotto et al. 2003). The observed red-shift can be significant, with the fluorescence of these red-shifted chlorophylls at 77 K peaking at 730 nm, but the absorption, at 700 nm, is not significantly shifted to the far-red (Morosinotto et al. 2003). It has also been demonstrated that heterodimerization of several Lhca polypeptides is responsible for the red-shifted characteristic of Chl *a* in these antennas (Wientjes and Croce 2011). Many niche-adapted photosynthetic microbes have absorption bands shifted much farther to the red (Wilhelm and Jakob 2006; Mohr et al. 2010; Chen et al. 2012; Bína et al. 2014; Kotabová et al. 2014; Pazdernik 2015). Although far-red absorbing chlorophylls like Chls *d* and *f* can extend in vivo absorption out to nearly 750 nm (Chen

and Blankenship 2011), some LHC systems that contain only Chl *a* are able to absorb well beyond 700 nm (Wilhelm and Jakob 2006; Bína et al. 2014; Kotabová et al. 2014; Pazdernik 2015).

Besides *Ostreobium* and *Chromera*, FRL-absorbing antennas have been found in some Stramenopiles, including diatoms (Herbstová et al. 2015) and a Eustigmatophyte (Pazdernik 2015). Eustigmatophytes are Stramenopiles that lack Chl *c*, containing only Chl *a* as well as carotenoids including violaxanthin and vaucheriaxanthin (Litvín et al. 2016). Eustigmatophytes are of particular interest to the biofuel industry because of their ability to produce large amounts of triacylglycerol (Iliev et al. 2010; Li et al. 2014). The LHCs of Eustigmatophytes are known as Viola-/Vaucheriaxanthin Chlorophyll Proteins (VCPs), as contrasted with the typical Fucoxanthin Chlorophyll Protein (FCPs) found in most Stramenopiles (Sukenik et al. 2000; Litvín et al. 2016).

The substantial diversity of these long-wavelength adaptations suggests that there are likely additional adaptations of this sort yet to be discovered. Because they are found in so many radiations of both prokaryotes and eukaryotes, we posited that they may be found in any shaded location with filtered light. We, therefore, adopted a broad approach to obtain as many different species as possible. By collecting samples from varied environments and growing the samples by using far-red light as the sole light source, these organisms were enriched. To accomplish such selection, we constructed FRL LED growth chambers and isolated several algae and cyanobacteria capable of utilizing FRL by using these selective conditions.

One particularly well-adapted isolate has been identified as a previously uncharacterized Eustigmatophyte, which we have provisionally named Eustigmatophyceae sp. FP5. To understand better how this specialized alga captures far-red light and uses it to support its growth and survival,

we characterized its antenna system spectroscopically as well as through imaging and protein analysis.

3.2 Results

3.2.1 Isolation and Identification of Eustigmatophyceae sp. FP5

Environmental isolates were left in the FRL chamber for several months and periodically checked. Culture Forest Park #5 (FP5) was found to contain an antenna system with substantial FRL absorption, peaking at 705 nm (Fig 3.1) as measured by fluorescence and absorption spectroscopy. Because the only chlorophyll present is Chl *a* (see below), this additional peak cannot be explained by the presence of any far-red chlorophyll such as Chls *d* or *f*. Room temperature fluorescence spectroscopy of whole cells indicated that a single fluorescence maximum is present at 709 nm (Fig 3.1B), which represents emission from the red-shifted antenna. At 77 K, this maximum shifts to 718 nm in whole cells (Fig 3.1B).

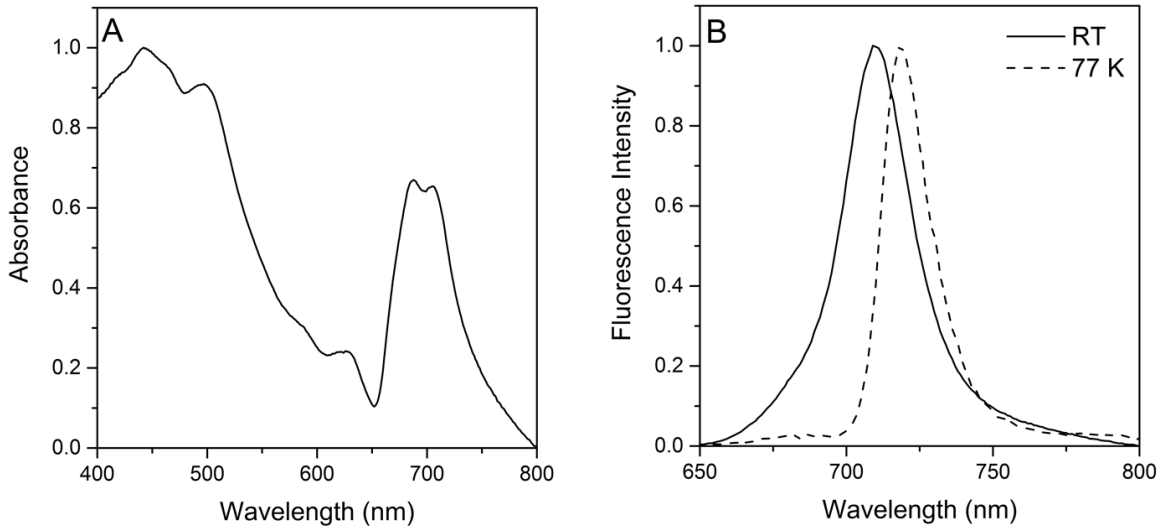

Figure 3.1: Whole-cell absorption (A) and fluorescence (B) measurements of FP5 in liquid suspension when grown under 740 nm LEDs. For fluorescence, the excitation wavelength was 435 nm. Spectra were normalized to unity at their maxima.

Phase-contrast light microscopy revealed spherical non-motile cells with a morphology similar to the Eustigmatophyte *Vischeria* (Gartner et al. 2012) (Fig 3.2A–B), ranging in size from 5 µm to (rarely) greater than 20 µm. A thick cell wall is visible. The cells appear to be primarily occupied by green photosynthetic material, but in many cells, a punctate red organelle is present (Fig 3.2A and 2B arrows), also seen in other Eustigmatophytes and considered a hallmark trait of the class (Hibberd and Leedale 1972; Gartner et al. 2012).

Fluorescence confocal microscopy (Fig 3.2C–D) revealed that most of the cell volume is taken up by a large, irregular chloroplast that fluoresces in the far-red region of the spectrum (shown red in these false-color images). A small point of red fluorescence was observed in the middle of each cell (shown green in these false-color images) when a green excitation light was used, presumably corresponding to the red punctae observed by phase microscopy.

Quick-freeze deep-etch electron microscopy (Fig 3.1E–G) revealed a massive chloroplast that comprised a large portion of the cell's volume. The tightly appressed thylakoids form laterally stacked groups, also observed in other Eustigmatophytes such as several *Vischeria* species (Santos 1996; Gartner et al. 2012). The cells also contain a central organelle containing a stack of plates (Fig 3.2E), which we propose corresponds to the red/fluorescent body seen in the phase/confocal images.

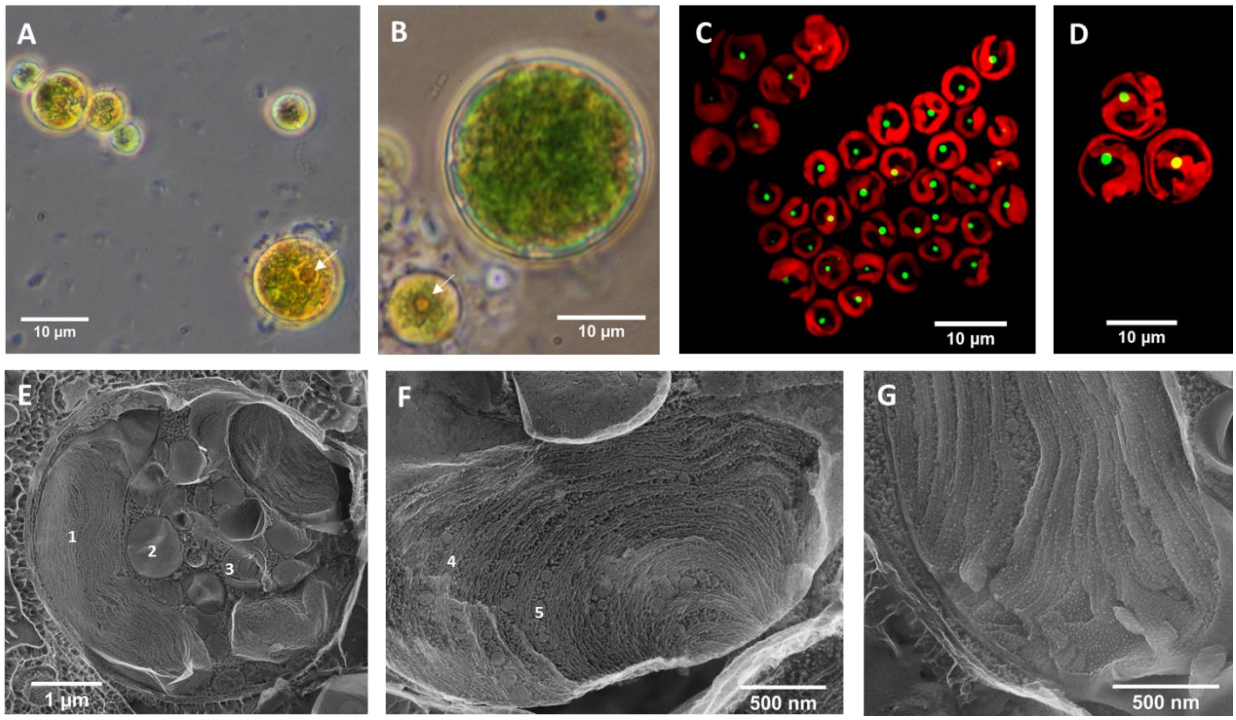

Figure 3.2: Images of *Eustigmatophyceae* sp. FP5 cells. (A) Phase contrast light microscopy of typical FP5 cells grown under FRL. (B) Phase contrast light microscopy showing one of the largest cells present in the FP5 enrichment culture, possibly representing a spore. (C–D) Confocal fluorescence microscopy of FP5 cells. Red indicates excitation with a 405 nm laser and a 485 nm (W60) and 705 nm (W90) band-pass emission filter. Green indicates excitation with a 561 nm laser and emission at 615 nm (W70). (E–G) Quick-freeze deep-etch EM of FP5 cells. (E) Cross-fracture through a whole cell, showing the large chloroplast (1), lipid droplets (2), and the plate-containing organelle (enlarged in Fig S3) (3). (F) Portion of the chloroplast showing tightly appressed thylakoids (4) and plastoglobules (5). (G) Fractured thylakoid membrane faces showing intramembranous particles that correspond to transmembrane proteins.

18S rDNA amplification produced a usable sequence of 1008 base pairs. When these same primers were compared *in silico* to the 18S ribosomal RNA gene of a model Eustigmatophyte, *Nannochloropsis gaditana* strain CCMP526, the sequence length was 1075 base pairs of the total 1796 base pairs in the gene for a coverage of 60% of the total sequence. Phylogenetic analysis revealed that Isolate FP5 is a Eustigmatophyte alga, in the Stramenopile radiation, most closely related to several other cultured species in the *Eustigmatophyceae* genus. Using this analysis, we provisionally placed FP5 into this genus (Fig 3.3).

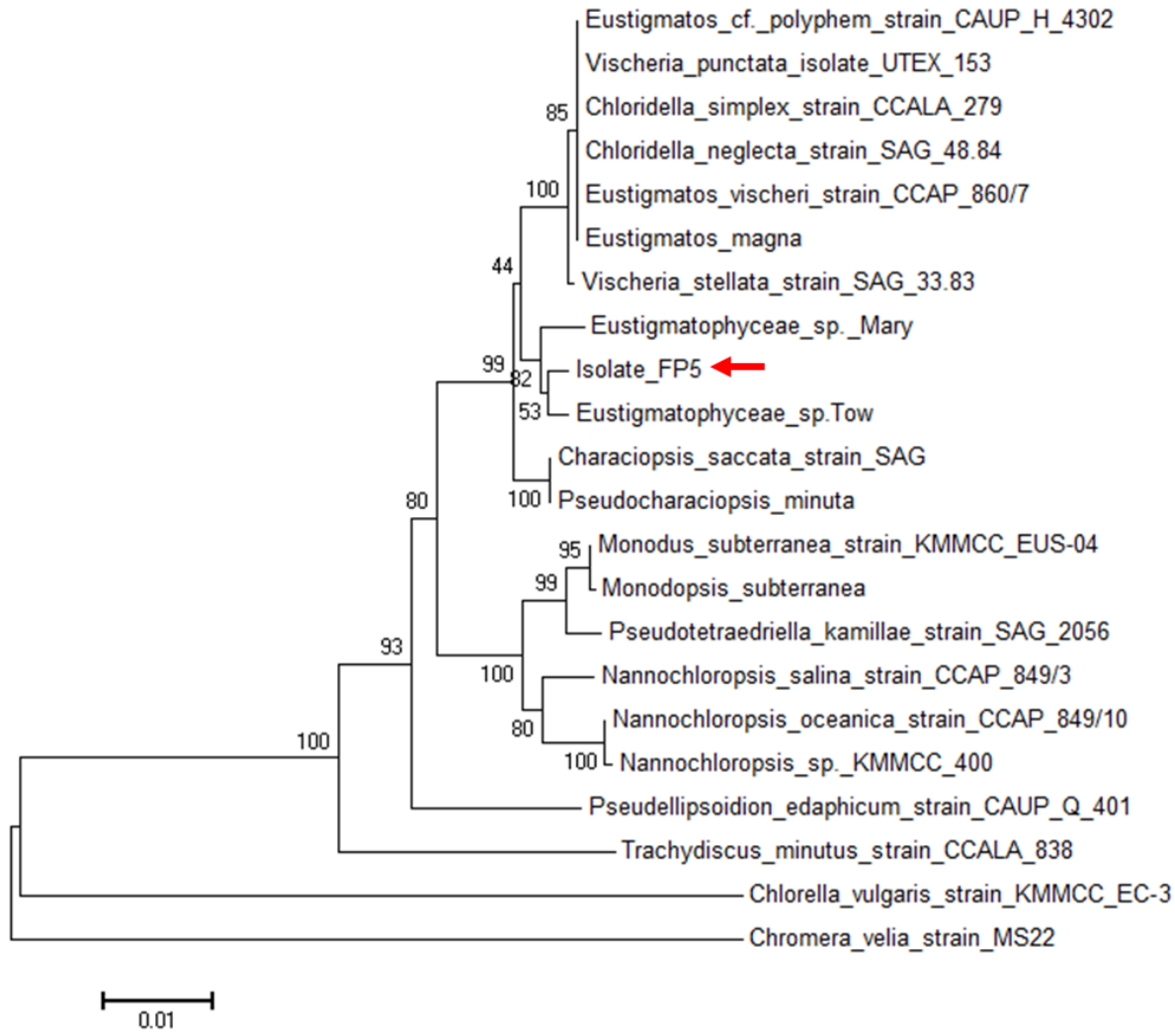

Figure 3.3: Neighbor-joining phylogenetic tree of 18S ribosomal RNA gene sequences showing the relationship of FP5, indicated by the red arrow, to several other algae, primarily the Eustigmatophytes. Isolate FP5 was found to be within the *Eustigmatophyceae* branch. The length of the FP5 18S rDNA sequence was 1008 base pairs. Bootstrap values are shown at each branch point, showing the percentage of replicate trees that showed the same branch point using 500 bootstrap replicates. Branch length indicates evolutionary distance.

3.3.2 Pigment Composition

Although FP5 is capable of growing under FRL by using wavelengths typically not absorbed by Chl *a*, reversed phase HPLC of extracted FP5 pigments revealed that the organism contains only Chl *a* and various unidentified carotenoids (Fig 3.4A-B), implicating pigment-protein interactions

as the primary cause of the red shift observed in the absorption of the light-harvesting complexes of FP5. Four carotenoid peaks were observed on the HPLC chromatogram and only a single chlorophyll peak with a spectrum corresponding to Chl *a* (Fig 3.4A,C). The time range shown encompasses all peaks observed, and extension of the run to one hour did not reveal any additional carotenoid peaks.

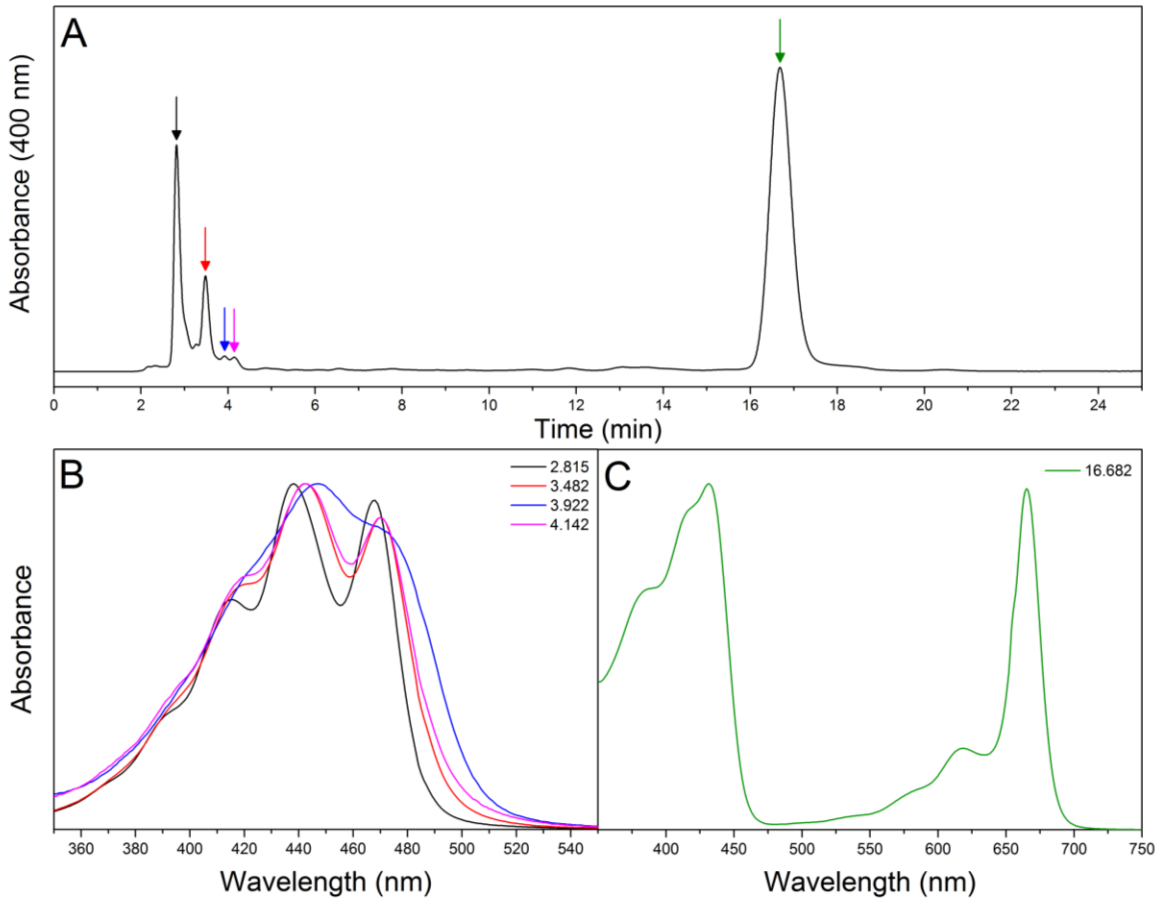

Figure 3.4: HPLC of pigments extracted from whole cells of FP5. (A) Chromatogram at 400 nm. Arrows indicate peaks. (B) Absorption spectra of carotenoids. Line colors match arrows in A. All spectra were normalized to unity at their maxima. (C) Chl *a* absorption spectrum. Line color matches arrow in A.

3.2.3 Gel Filtration Chromatography

Gel filtration chromatography of solubilized membrane material generated a profile of protein complexes, and these were monitored by fluorescence excitation. Highly separated bands do not form, but several distinct zones were detected. The longest wavelength portions elute from the column first and the shorter wavelength portions elute last (Fig 3.5). The FR-LHC purified by gel filtration fluoresces at approximately 705 nm at room temperature when excited at 435 nm (Fig 3.5D). The pigment-protein complex is unstable and breaks down over time, and when breakdown occurred, the fluorescence emission was blue-shifted to 697 nm.

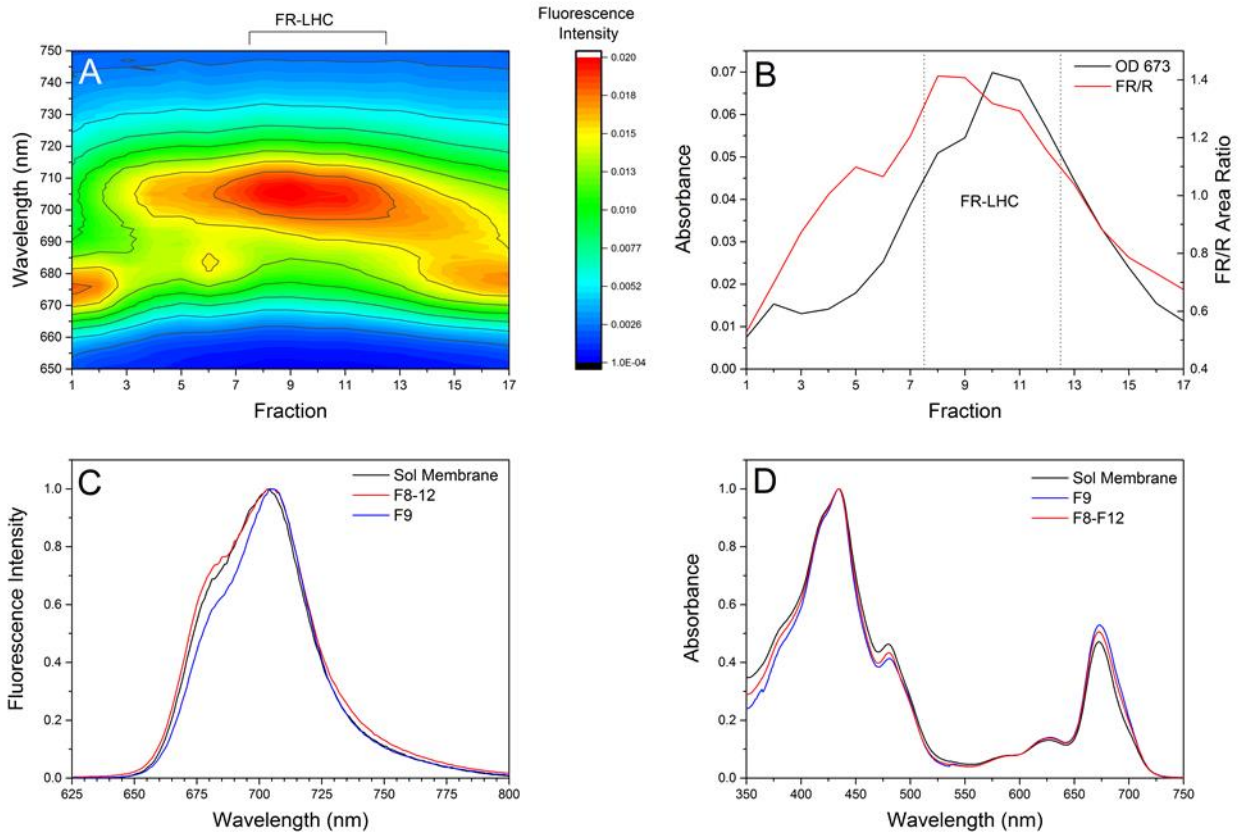

Figure 3.5: Gel filtration purification of the FR-LHC. (a) 3D pseudo-color plot of fluorescence of each fraction collected from the gel filtration purification process with excitation at 435 nm. The

fluorescence emission traces were normalized to integrated area. (b) Plot showing the far-red to red ratio (defined as the area between 600 and 699 nm for red and the area under the 700 to 800 nm portion for far-red) and the OD of the Q_y region. Samples were diluted 40X before measurements. Dotted lines show the FR-LHC portion. (c) Fluorescence emission when excited at 435 nm of total solubilized membrane material, fraction #9, and the pooled fractions used to load a gel, normalized to unity at their maxima. (d) Absorption of total solubilized membrane material, fraction #9, and the pooled fractions used to load a gel, normalized to unity at their maxima.

3.2.4 Clear Native Polyacrylamide Gel Electrophoresis

FR-LHC fractions from gel filtration were subjected to clear native gel electrophoresis (native PAGE). Five bands, B1-B5, were visible and well separated, with two, B2 and B3, representing the most far-red fluorescing complexes (Fig 3.6A). When stained with Coomassie and compared with a native protein mass standard, approximate molecular weights were: B1: 300 kDa, B2: 200 kDa, B3: 120 kDa, B4: 110 kDa, and B5: 50 kDa (Fig 3.6A). Two additional low molecular weight bands were also stained, but they were not observed on the visible or fluorescence images. These bands, at approximately 20 kDa, are putatively considered to be antenna monomers. Fluorescence and absorption spectra of the native PAGE bands showed that the FR-LHC complex contains two forms: one with primarily red-shifted pigments and a second with less red-shifted forms. B2 and B3 exhibit more far-red absorption than B4 and B5, shown by the difference spectrum between B3 and B5 (Fig 3.6C), and increases in their red-shifted fluorescence emission characteristics (Fig 3.6E).

Comparing the second derivative of absorbance for B3 and B5, we find that the positions of the negative peaks are significantly different (Fig 3.6D). Negative second derivative peaks indicate positions of individual absorbing components within a complex spectrum. In B3, a significant negative peak is observed at 703 nm, compared to the 693 nm negative peak of B5. This indicates the presence of a species absorbing at 703 nm in B3. Three components were visible in the

absorption spectrum at room temperature (Fig 3.6B–C). The absorption difference spectrum showed that the difference between the larger far-red absorbing complex and the smaller red-absorbing bands is a sharp peak at 706 nm, representing the FR-LHC (Fig 3.6C). This was seen as a far-red shoulder on the second peak of the Q_y band of the absorption spectra (Fig 3.6C).

A 683 nm component in the fluorescence emission spectra of B1 was observed in addition to a far-red peak, whereas B2 and B3 contain only a single emission peak at 709 nm, which is consistent with the fluorescence emission of whole cells. B4 and B5 had fluorescence maxima near 700 nm (Fig 3.6E).

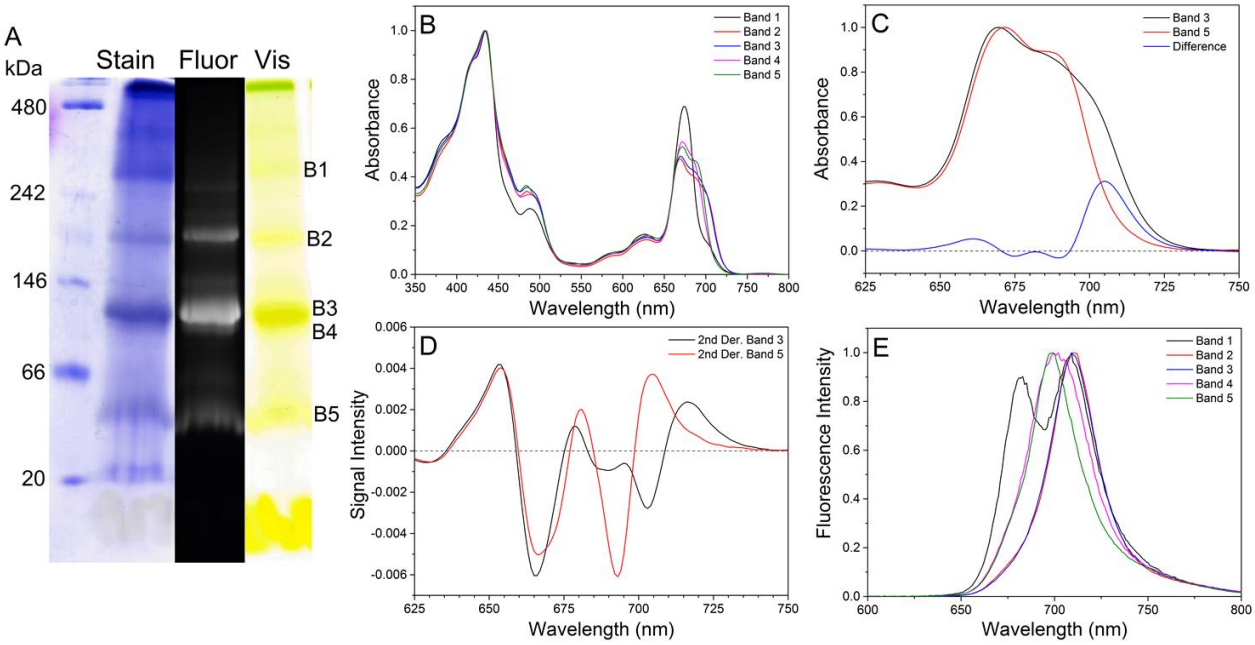

Figure 3.6: Composition of the FR-LHC using clear native PAGE and spectroscopy of gel slices. (A) Clear native PAGE gel of gel filtration purified FR-LHC. A visible scan, a 705 nm fluorescence image when the gel was illuminated with blue LED light, and a Coomassie stained gel with a native protein standard are shown. (B) Absorption spectrum of excised gel bands, normalized to unity at their maxima. (C) Close-up view of the Q_y region of B3 and B5 and the difference spectrum, calculated by subtracting B5 from B3. Spectra were normalized to unity within the Q_y absorption range. (D) Second derivative of absorption spectra of B3 and B5. (E)

Fluorescence emission spectra of whole excised gel bands at room temperature, 435 nm excitation, normalized to unity.

3.2.5 2D Polyacrylamide Gel Electrophoresis

A second, denaturing dimension was run from a vertical slice of a native gel. The first dimension was the non-denaturing CN-PAGE, which maintained the pigment-protein complexes in their native state. A vertical slice of the gel was excised, chemically denatured with SDS and reduced using βME, and run in the second, denaturing dimension along with a molecular mass ladder.

Regardless of the spectroscopic properties of the four native gel bands, all appeared to have similar polypeptide compositions: two major bands migrating as 18 and 21 kDa species, with the addition of two weaker, lower molecular weight bands (Fig 3.7). These same two major bands also appear to be the primary constituents of whole solubilized membrane material as well as the various gel filtration fractions (Fig 3.5). The 18 kDa polypeptide appeared to be more abundant than the 21 kDa polypeptide in the native complexes. A faint, high molecular weight bands (B1 and B2) on the native gel additionally contained 30 kDa and 40 kDa polypeptides, which likely correspond to components of photosystem II, which we would expect to see complexed in higher oligomers with our purification protocol.

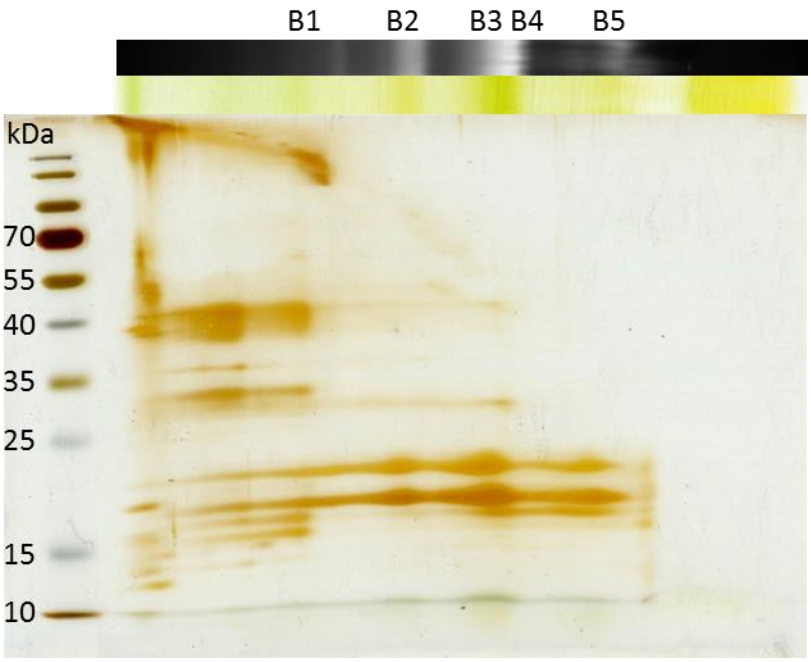

Figure 3.7: 2D PAGE of the FP5 FR-LHC. The first dimension was a non-denaturing clear native PAGE gel, and using identical adjacent wells, slices were analyzed spectroscopically. The visible and FR fluorescence when excited with a blue LED are shown along the top of the gel, and the assigned bands on the native PAGE are indicated. The second dimension was a 12% SDS-PAGE gel.

3.3.6 Purification of Protein Complexes using Preparative CN-PAGE

Protein-pigment complexes were eluted from each slice of the CN-PAGE gel, yielding several protein complexes, including forms of the FR-LHC (B2 and B3), as measured by absorption and fluorescence emission spectroscopy (Fig 3.8). The 77 K absorption spectrum of the eluted proteins showed several features in the Q_y region (Fig 3.8A). Comparing B3 and B5 by their difference spectrum, we find that the far-red and red antenna components are enriched in B3 (Fig 3.8B). Comparing the second derivative spectra of these two bands, five negative peaks are present in B3 at 660, 668, 682, 693, and 709 nm, while negative peaks in B5 are observed at 671 and 697 nm (Fig 3.8C). These peaks indicate that the FR-LHC complex in B3 includes pigments absorbing light at far-red wavelengths, while other, lower molecular weight antennas also present in the FP5

light-harvesting system notably lack pigments absorbing in the far-red. The farthest red-shifted negative peak in B3 is located at 709 nm, which likely corresponds to the most red-shifted form of Chl *a* in the FR-LHC.

The room temperature fluorescence maximum of B3 after elution was at 707 nm (Fig 3.8), but when the sample was cooled to 77 K, this maximum shifted to 716 nm (Fig 3.9D), consistent with measurements taken *in vivo*, which also show a 718 nm fluorescence peak at 77 K (Fig 3.1B). However, other bands lacking far-red fluorescence at room temperature in the eluted material (Fig 3.8) or in-gel form (Fig 5E) still maintained this far-red fluorescence at 77 K. Although B2 and B3 were made up of almost entirely a single component at 716 nm, B1, B4, and B5 contained notable features in the red region in addition to this far-red component (Fig 3.9D).

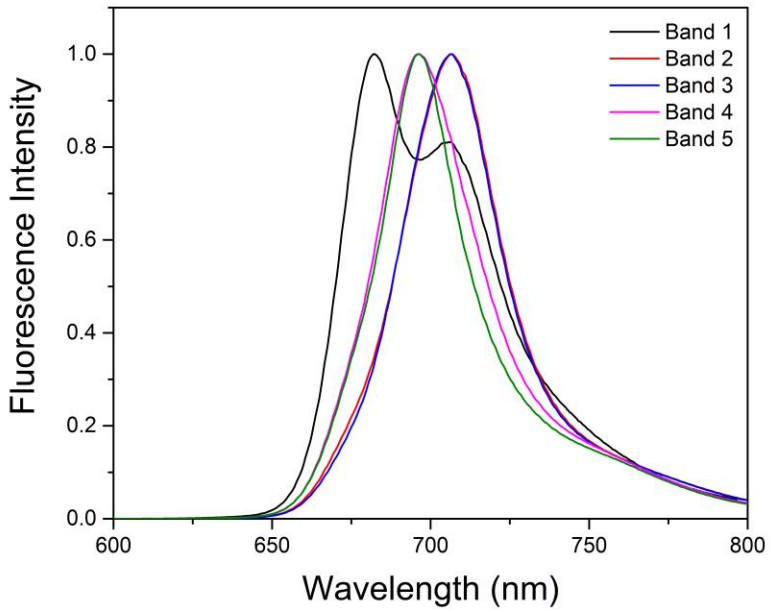

Figure 3.8: Room temperature fluorescence emission of eluted gel bands. Spectra were normalized to unity at their maxima.

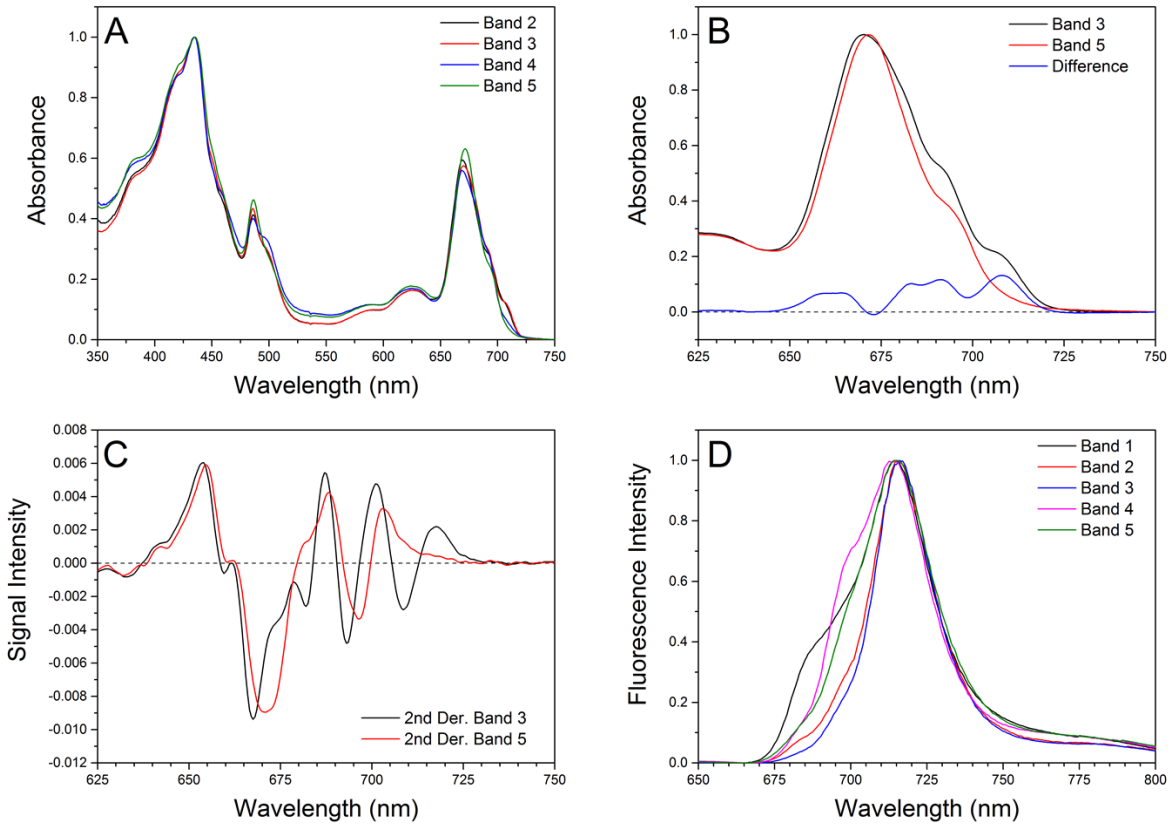

Figure 3.9: 77 K spectroscopic analysis of native pigment-protein complexes eluted from clear native PAGE gel slices. (A) 77 K absorption spectrum of eluted proteins, showing several components of the Q_y region, normalized. (B) Close-up of the Q_y region from of B3 and B5, difference spectrum. Spectra were normalized within the range of absorption of the Q_y region. (C) Second derivative of the absorption spectrum of B3 and B5. See text for peak assignments. (D) Fluorescence of eluted bands at 77 K with 435 nm excitation, normalized.

3.3 Discussion

Eustigmatophyceae sp. FP5 is able to utilize the normally unavailable wavelengths of light in the far-red region by using only Chl *a* and integral membrane proteins. The red-shift of Chl *a* observed in FP5 appears to be due to the protein environment surrounding the pigments. Such a protein-induced red-shift of Chl *a* has also been seen in several different Stramenopiles and other algal

clades (Wilhelm and Jakob 2006b; Tichy et al. 2013; Bína et al. 2014; Kotabová et al. 2014), and protein-environment-induced red-shifts that lead to the existence of a small amount of far-red absorbing chlorophyll were reported in the antennas of plant PSI (Wientjes and Croce 2011).

In plants, LHCII, associated with PSII, is found as a trimer in which each monomer contains eight Chl *a*, six Chl *b*, and various carotenoids (Liu et al. 2004). LHCI, associated with PSI, which also binds Chls *a* and *b* as well as carotenoids, forms dimers rather than trimers (Wientjes and Croce 2011). FP5 does not contain any Chl *b*, and it is likely that that the 18 kDa and 21 kDa antenna polypeptides making up its FR-LHC are similar to the light-harvesting proteins found in the vaucherioxanthin-chlorophyll proteins, (VCP) of the related genus *Nannochloropsis*, which are themselves similar to the FCP proteins in most diatoms (Litvín et al. 2016). Although structural modeling, sequence alignment, and pigment analysis were done on FCP, no crystal structure is available (Durnford et al. 1996; Gundermann and Büchel 2014; Llansola-Portoles et al. 2016). Phylogenetic analysis of the 18S rDNA sequence, pigment composition, and polypeptide sizes suggest that the FP5 antenna may be similar to the VCPs found in *Nannochloropsis*, which have not been reported to utilize FRL to support growth of the organism (Litvín et al. 2016).

The far-red absorption phenotype of another protein-pigment complex, the red form of the LHC in the Alveolate *Chromera velia*, was shown to require multimerization to exhibit a red-shift (Bína et al. 2014). This was observed in FP5 as well. FP5 contains several low molecular weight monomers, 18 and 21 kDa, which are similar to the FCP-like proteins found in *C. velia* (Tichy et al. 2013). Trimers of some forms of FCP were shown to form higher order oligomers as well. In the diatom *Cyclotella meneghiniana*, FCPs were shown to form both trimers made up of 18 and 19 kDa subunits and oligomers that are made up of trimers of 19 kDa subunit only (Büchel 2003). While *C. meneghiniana* FCPs were not shown to exhibit far-red absorption characteristics,

multimerization has also been shown to be important to the red-shifting of Chl *a* absorption in other species (Bína et al. 2014; Kotabová et al. 2014), indicating that it may also be at play in the FP5 system.

FP5 is capable of growing under pure far-red light (LED spectrum shown in Fig 2.1), indicating that it is able to utilize long wavelength light to drive charge separation at both PSI and PSII. Typically, LHCs absorb light at a shorter wavelength than the absorption of the special pair of chlorophylls that drives photochemistry, allowing downhill energy transfer from LHC pigments to the RC pigments. However, exceptions to this rule were reported in some of the LHCs associated with PSI (Wientjes and Croce 2011): red-shifted chlorophylls in the LHCs associated with PSI, called Lhcas, were found to absorb wavelengths beyond 700 nm, which is the absorption of the special-pair chlorophylls of PSI (P700) (Wientjes and Croce 2011). Several functions were proposed, the most interesting being the possibility that these far-red forms allow leaves to absorb far-red light in shaded environments, where FRL is enriched, and transfer it to the RC using thermally activated energy transfer (Trissl 1993; Rivadossi et al. 1999; Wientjes and Croce 2011). The far-red forms were shown to account for up to 40% of the total photons absorbed under shade conditions (Rivadossi et al. 1999). This process of increasing the absorption cross-section of a leaf allows for increased utilization of this low-energy light (Trissl 1993; Rivadossi et al. 1999). However, these chlorophylls only form only a small portion of the overall antenna pigments (Rivadossi et al. 1999).

Thermally activated energy transfer in the isolated FP5 FR-LHC was demonstrated by measuring fluorescence emission upon long-wavelength excitation that was significantly red-shifted compared to the emission band (Fig 3.10). Thermal activation was also observed in *Ostreobium*

and *C. velia*, although these measurements were taken by using whole cells and not purified complexes (Wilhelm and Jakob 2006b; Kotabová et al. 2014).

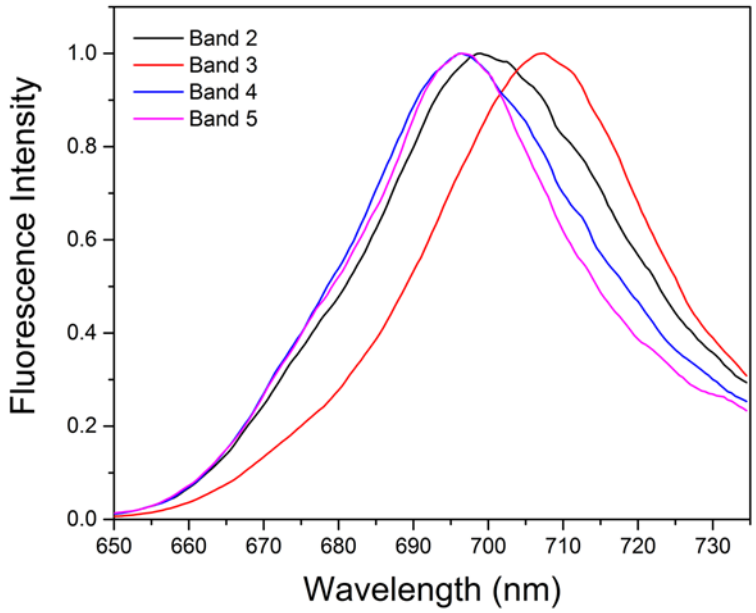

Figure 3.10: Thermally activated up-hill energy transfer in chlorophyll proteins eluted in various gel bands. Fluorescence emission spectra obtained upon 750 nm excitation at room temperature. In order to correct potential effect of light scattering the emission spectrum of pure buffer was subtracted from each of them. The spectra are normalized to unity at their maxima.

Because leaves also transmit FRL, it is likely that if such an adaptation were to be engineered into crop plants, this wasted energy could be utilized in leaves below the canopy layer (Ort et al. 2015). It is theoretically possible to absorb 19% more photons in this range that contains enough energy to drive oxygenic photosynthesis (Chen and Blankenship 2011; Blankenship and Chen 2013). It may be possible to modify the response of plants to far-red light hitting the lower leaves to optimize their efficiency (Ort et al. 2015). Although plants already do this to some extent (Pettai et al. 2005b, a), the far-red absorption cross-section is severely limited compared to FP5. By understanding how these far-red antenna systems work, we hope to provide a basis for the future transformation of these systems into crop plants to improve the efficiency of photosynthesis.

3.5 Conclusions

The newly isolated Eustigmatophyte alga *Eustigmatophyceae* sp. FP5 contains a specialized photosynthetic antenna system that extends the range of light absorption into the far-red region. This adaptation allows FP5 to grow under a solely far-red light source. We showed that this antenna system is made up of a complex of several antenna monomers, which must interact to facilitate this far-red light absorption phenotype. The antenna contains only Chl *a* and several carotenoids, and therefore we conclude that the FP5 antenna system uses the protein environment to shift the absorption of Chl *a* to the far-red.

The ability of some specialized organisms to absorb far-red light to drive oxygenic photosynthesis is challenging the notion that energies lower than that absorbed by plants are not capable of sustaining oxygenic photosynthesis. Indeed, these longer wavelengths, typically wasted in many ecosystems, are a potentially ignored source of photosynthetic energy. The antenna system of the newly isolated Eustigmatophyte *Eustigmatophyceae* sp. FP5 demonstrates the ability of Chl *a* antennas to absorb these useful wavelengths. Understanding the function of these antennas may pave the way for modifications in plants that allow these useful, but typically wasted, wavelengths to be used in driving photosynthesis.

Chapter 4: Photoacclimation in the Eustigmatophyte FP5[3]

The Eustigmatophyte alga FP5, isolated from a water system in Forest Park, St. Louis, MO, USA, has the unusual ability to subsist off of entirely far-red illumination. This environment, a partially shaded, eutrophic water system with a low rate of flow, provides the organism with a varied environment that ranges from strong daylight to far-red enriched shade light. Although the latter requires adaptations allowing it to extend its photosynthetic spectrum into the far-red, the former requires a resilient and adaptable antenna system that can withstand the strong light. To understand how this organism responds to changing light conditions from a whole-cell physiological perspective, we observed cells grown under either blue or far-red illumination using hyperspectral confocal fluorescence microscopy and analyzed protein-pigment complexes from cells under each condition using clear-native gel electrophoresis and in-gel spectroscopy. We show a significant chromatic acclimation in far-red antenna composition under varied light conditions in addition to a fluorescent punctate structure of unknown function, which we think corresponds to a characteristic red spot in Eustigmatophytes, and carotenoid-containing bodies outside of the plastid that do not appear to respond as strongly to light condition. Through this view of chromatic adaptation in FP5, we have shown the ability of this organism to adapt to laboratory conditions mimicking its natural environment and have provided a platform on which to base further studies describing the architecture of the far-red light harvesting system in specialized Eustigmatophytes.

[3] Much of this text has been submitted as a manuscript under the title "Photoacclimation in a Newly Isolated Eustigmatophyte Alga Capable of Growth Using Far-Red Light" with the authors Benjamin M. Wolf, Meghan C. Barnhart-Dailey, Jerilyn A. Timlin, and Robert E. Blankenship.

4.1 Introduction

During photosynthesis, plants, algae, and cyanobacteria capture light to generate cellular energy and produce biomass for growth. In most cases, the photosynthetic spectral range is limited to the traditionally-defined photosynthetically active radiation (PAR), 400-700 nm (Chen and Blankenship 2011). However, some specialized oxygenic phototrophs are capable of harvesting photons with wavelengths longer than 700 nm, called far-red light (FRL), to drive photosynthesis (Miyashita et al. 1997; Chen et al. 2012; Kotabová et al. 2014; Wolf et al. 2018). FRL is transmitted by phototrophs such as species in algal mats and is therefore enriched in shaded environments (Kühl et al. 2005).

To better understand how FRL is harvested and utilized, we sampled the environment and used selective FRL growth chambers to isolate species that could survive on FRL as their sole energy source. One such organism is the Eustigmatophyte alga Forest Park Isolate #5, or FP5. Although we have extensively characterized the antenna system of FP5 biochemically and spectroscopically when grown under FRL (Wolf et al. 2018), we have just begun to explore the chromatic acclimation of this organism. In its natural environment, FP5 and indeed any other alga that is capable of drifting through the water column must be capable of surviving widely varied light conditions. As it contains an antenna complex capable of shifting the absorption of Chlorophyll *a* (Chl *a*) into the far-red region, FP5 is clearly well-adapted to far-red light growth conditions (Wolf et al. 2018). However, it was unclear how FP5 would respond to illumination from strong, visible light.

In order to survive under strong visible light, cells that have adapted to dim, far-red illumination must respond by reorganizing their light harvesting systems. This has been observed in several

cyanobacteria recently. *Leptolyngbya* JSC-1 was recently found to undergo an extreme response when changed between white light and far-red light illumination, with significant changes in differential expression observed in nearly 3000 genes (Gan et al. 2014b). Another species, *Synechococcus* sp. PCC 7335, has been shown to reorganize its phycobilisomes as well as its transcriptome, while producing the far-red absorbing Chl *f* (Ho et al. 2016b, c).

Some algae, including diatoms, do appear to respond quite strongly to alterations in light conditions. Diatoms are stramenopiles, as are Eustigmatophytes, but are different in a variety of ways, including the existence of Chl *c* in diatoms and its absence in Eustigmatophytes. The pennate diatom *Phaeodactylum tricornutum* has been shown to have a strong response to *red* light when compared to daylight (Herbstová et al. 2015). In this species, a significant shift was observed in the fluorescence spectrum of whole cells and in their antenna makeup under red light conditions (Herbstová et al. 2015). Such responses have also been observed in the alga *Chromera velia*, in this case using red or blue light (Bína et al. 2014; Kotabová et al. 2014). To our knowledge, there has been no work describing how Eustigmatophytes capable of utilizing far-red light respond under far-red illuminated conditions as compared to intense visible light.

Under varying light conditions in some species, localization of pigments and proteins within the cells form an important aspect of chromatic adaptation. In the cyanobacteria *Halomicronema hongdechloris* and *Synechococcus* sp. 7335, changes in the location of various light harvesting complexes, primarily phycobilisomes, were observed under far-red vs. white light conditions (Majumder et al. 2017). Hyperspectral confocal fluorescence microscopy (HCFM) and multivariate curve resolution (MCR) analysis were used to view the spatial reorganization of highly spectrally overlapped photosynthetic pigments and proteins. HCFM in combination with MCR has proven utility in identifying photosynthetic pigments with strong degrees of spectral

overlap in living photosynthetic organisms (Vermaas et al. 2008; Collins et al. 2012; Majumder et al. 2017).

Understanding how FP5 responds to different light conditions is crucial for identifying the specific antenna proteins involved in FRL harvesting, which has broad implications for the improvement of agriculturally-important plant species (see Discussion). In *P. tricornatum,* comparison of daylight and red light grown cultures was sufficient to implicate at least one specific LHCF protein in light harvesting, LHCF15 (Herbstová et al. 2015). In FP5, comparing cells grown under FRL that are expressing far-red absorbing light harvesting complexes (FR-LHC) to cells grown under blue light has enabled us to improve our understanding of the properties of the FRL harvesting system, as well as how the organism as a whole reacts to changing light conditions.

4.2 Results

FP5 responds strongly to the chromatic quality of the light environment. Under blue light (BL), white light (WL), and far-red light (FRL) of equivalent intensities (Figure 4.1A), FP5 responds very strongly only to blue light. Room temperature fluorescence emission of whole cells when excited in the Soret region of Chl *a* (435 nm) was used to indicate the presence or absence of low energy pigments. Under white and far-red light, a far-red antenna was apparent (indicated by an arrow in Figure 4.1B), but was reduced to a minor shoulder under blue light, while another peak likely corresponding to reaction centers (Chl *a*) was visible in the red emission range (Figure 4.1B). Although the white light contains some blue and far-red light, it does not constitute the majority of the available photons due to the white LED phosphor emission in yellow and green wavelengths. Absorption spectroscopy allowed us to measure the extent of far-red absorbing pigments in FP5, and analysis via the 2nd derivative of absorption highlighted those differences. Although cells

grown under FRL contain a significant absorption feature at 705 nm (indicated with an arrow in Figure 4.1C), cells grown under blue light entirely lack this feature (Figure 4.1C). This observation is confirmed using the 2nd derivative of absorption, which shows a lack of a characteristic negative peak at approximately 710 nm only under blue light. Under white and far-red conditions, this negative peak is present, indicating an inflection point on the spectrum and an underlying far-red absorption band (Figure 4.1D).

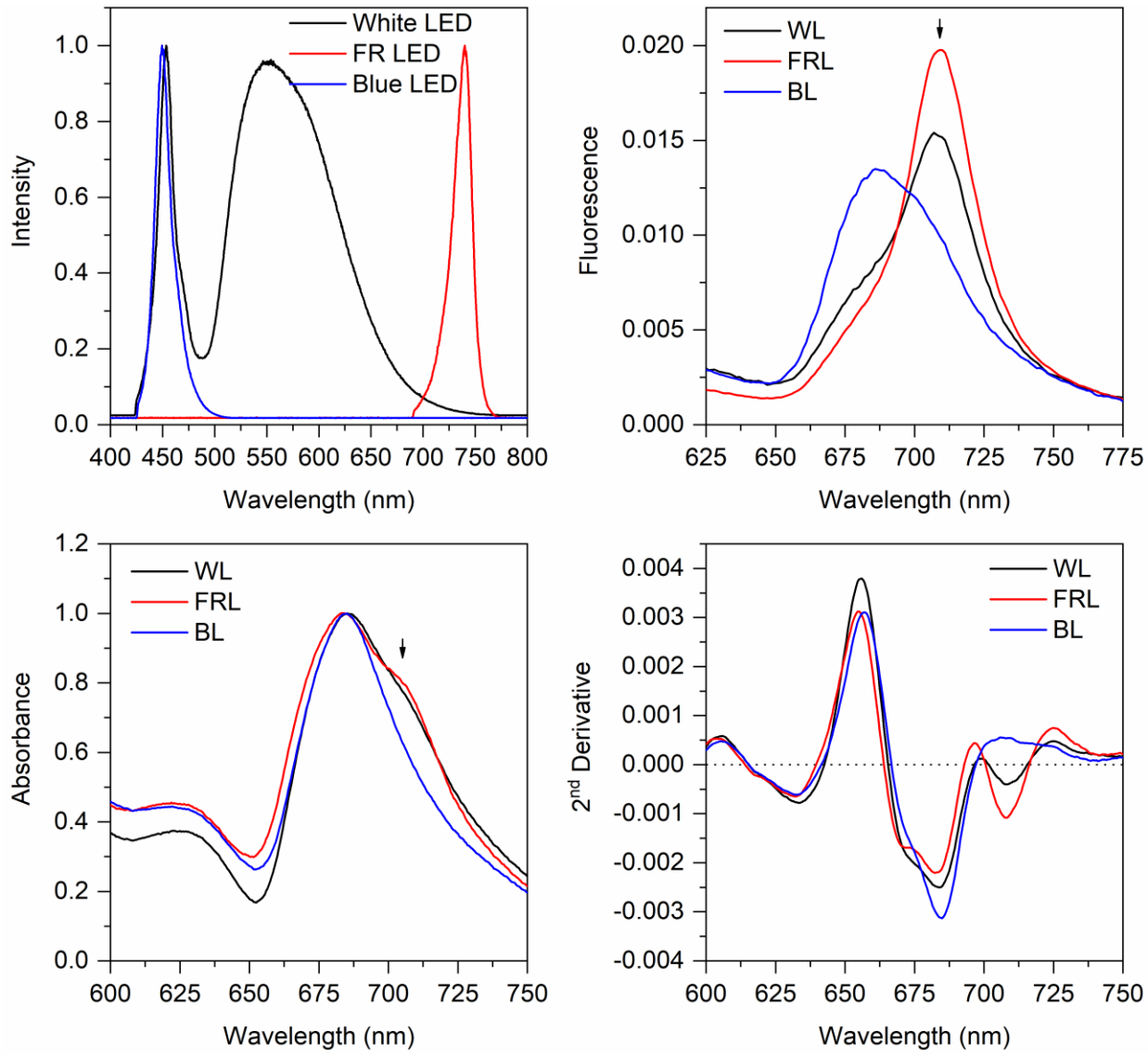

Figure 4.1: FP5 grown under various light conditions for 13 days in 200 mL culture volumes. Spectra are representatives taken from a pool of 3 replicates, with an average OD750 for all 9 cultures of 0.065. A) Spectra of the growth LEDs, normalized to unity. B) Fluorescence emission spectra of FP5 grown under each condition normalized to peak area. An excitation wavelength of 435 nm was used. Arrow indicates FR-LHC emission peak. C) Q_y region of absorption spectra of whole cells following sonication and resuspension in 50% sucrose highlighting changes in photosynthetic antennas. Normalized to unity. Arrow indicates the FRL absorption feature of FR-LHC. D) 2nd derivative spectra of absorption spectra highlighting negative peaks in WL and FRL cultures, but not BL. Derivative spectra are not normalized, but input spectra were normalized to unity and smoothed using a Savitzky-Golay algorithm.

Although blue light of equivalent intensity causes significant changes in low-density cultures, this change does not appear to be the result of chromaticity alone. Even under pure blue light, in more mature and denser cultures, self-shading can reverse this FR antenna reduction response if the light intensity is not adjusted to account for this densification of the culture. For instance, the same blue-light cultures shown in Figure 1, which were taken after 11 days, had a far-red fluorescence peak after a month, though their absorption properties were relatively unchanged. Considering the increase in optical density during this time, from an average OD_{750} of 0.085 at 11 days to an average of 0.499 at day 29, this indicates a change due to self-shading. Interestingly, there is not a strong difference in growth rate between white and blue light despite the significant spectral differences (Figure 4.2). Furthermore, when cells are subject to far-red conditions after being grown under and acclimated to blue light, they will revert within 4 days to their far-red acclimated state.

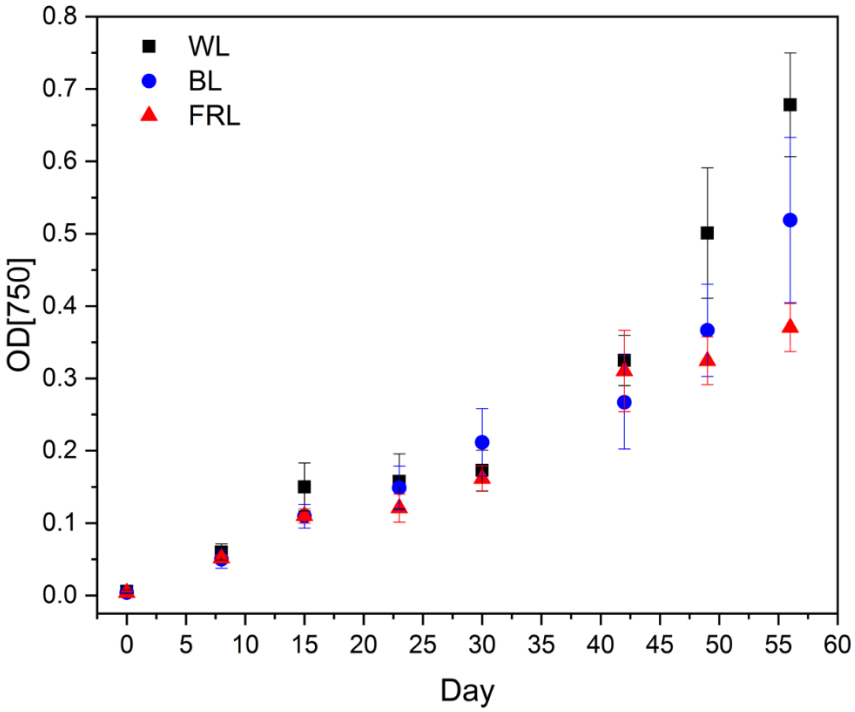

Figure 4.2: Growth curve of FP5 cells grown under white, blue, and far-red light. Three replicates from each condition were sampled. Error bars are 1 standard deviation. Optical density was measured at 750 nm to avoid absorption from the far-red antenna system.

Although spectroscopy of whole cultures can provide information on the global responses of FP5 to blue light, this gives little information about the cell-to-cell variation and any photosynthetic pigment- protein rearrangement at the subcellular scale. To characterize the spectral changes occurring within the chloroplasts, as well as the other fluorescent cellular features, we utilized hyperspectral confocal fluorescence microscopy (HCFM). A significant advantage of HCFM over conventional confocal fluorescence microscopy techniques is that HCFM collects the entire emission spectrum for each image pixel, which when coupled with spectral analysis methods allows identification of the independently-varying component spectra. Data sets consisting of HCFM images encompassing varying conditions to be compared are processed using multivariate curve resolution (MCR), a self-modeling curve resolution method. A spectral model is identified consisting of a reduced set of independently varying, underlying spectral components that describe

the data within and across conditions. Images that correspond to the location and relative abundance of each spectral component within every image pixel are also calculated.

4.2.1 Cellular Structure Analysis through HCFM

Two instrument configurations were used for imaging, one with a cyan emission filter placed to reduce the intensity of the chlorophyll bands in the 640 – 800 nm region of the spectrum, allowing visualization of the lower intensity fluorescent components in the 500 - 625 nm region of the spectrum, and one configuration without this filter. For hyperspectral image data collected with the cyan filter in place, a 6-component spectral model was built (5 pigment components and 1 linear offset from the detector) (Figure 4.3). These components included three spectral signatures with Chl *a* spectral characteristics and two additional, likely non-photosynthetic, components outside of the chloroplast, with wide emission bands at 500-650 nm and 525-700 nm.

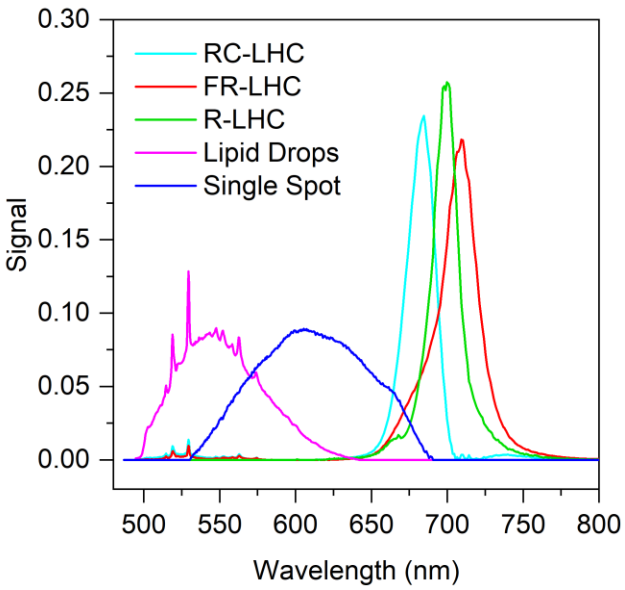

Figure 4.3: MCR output spectra from blue light and far-red light grown FP5 cellular imaging. A cyan filter was used to attenuate the signal from chlorophyll (LHC channels) and effectively enhance sensitivity to the 500 – 625 nm region of the spectrum. Line colors correspond to channel colors in Figure 3.

The three photosynthetic components were assigned as light-harvesting complex (LHC) pigment proteins and reaction centers. Due to distortions caused by the filter, all photosynthetic components are blue-shifted by several nanometers compared to the images without the filter, which will be described later. With the filter in place, the most blue-shifted peak is at 685 nm and is described as reaction centers (RC), possibly complexed with a non-far-red LHC protein (RC-LHC). The other two represent two red-shifted LHC proteins, the Red-LHC (R-LHC) and the Far-Red LHC (FR-LHC) with emission maxima at 700 nm and 709 nm, respectively (Figure 4.3). All of the photosynthetic components exhibit a strong fluorescence emission in the red to far-red regions, as is expected given their Chl *a* pigmentation. However, also co-varying with these strong Chl *a* spectra are Raman scattering peaks from carotenoids, which can be observed in the shorter wavelength ranges of the red and teal traces in Figure 4.3. These represent carotenoids associated with chlorophyll-binding proteins and co-vary along with the Chl *a* signal. This indicates that these components interact within the protein.

The photosynthetic components are strongly influenced by the light condition, as can be seen in Figure 4.4. In Figure 4.4, for each spectral component displayed, the maximum pixel intensities for blue light and far-red light images were set equally, thus allowing the visual intensities to be compared between light treatments. Under far-red light, a clear shift is apparent to the far-red emitting components dominating compared to the blue-light condition, where the RC-LHC dominates. The localization of the various spectral components of the chloroplast is also notable. There appears to be no large-scale rearrangement of the chloroplast pigment-proteins, but rather the relative abundance of the three chloroplast pigment-proteins changes depending of the light condition. Some heterogeneity is observed amongst the cells regarding the relative intensities of each far-red component (see overlays, Figure 4.4). The ratios of the three photosynthetic

components, easily visible in the overlay in Figure 4.4, is somewhat variable between cells. However, under both conditions, there is very little difference in intensity within each cell, and all photosynthetic components seem co-localized in the cells imaged. Single-cell analysis (Figure 4.5) of cells imaged using the cyan filter indicates large changes in the 709 nm FR-LHC component intensity, with a mean intensity of 1640 under far-red light versus 277 under blue light. The range of intensity values for the 709 nm component in far-red grown cells was also greatly increased compared to blue light grown. Other components were found to change less between the two growth conditions (Figure 4.5). Using a Mann-Whitney non-parametric statistical comparison, between the light treatments, all components are significantly different.

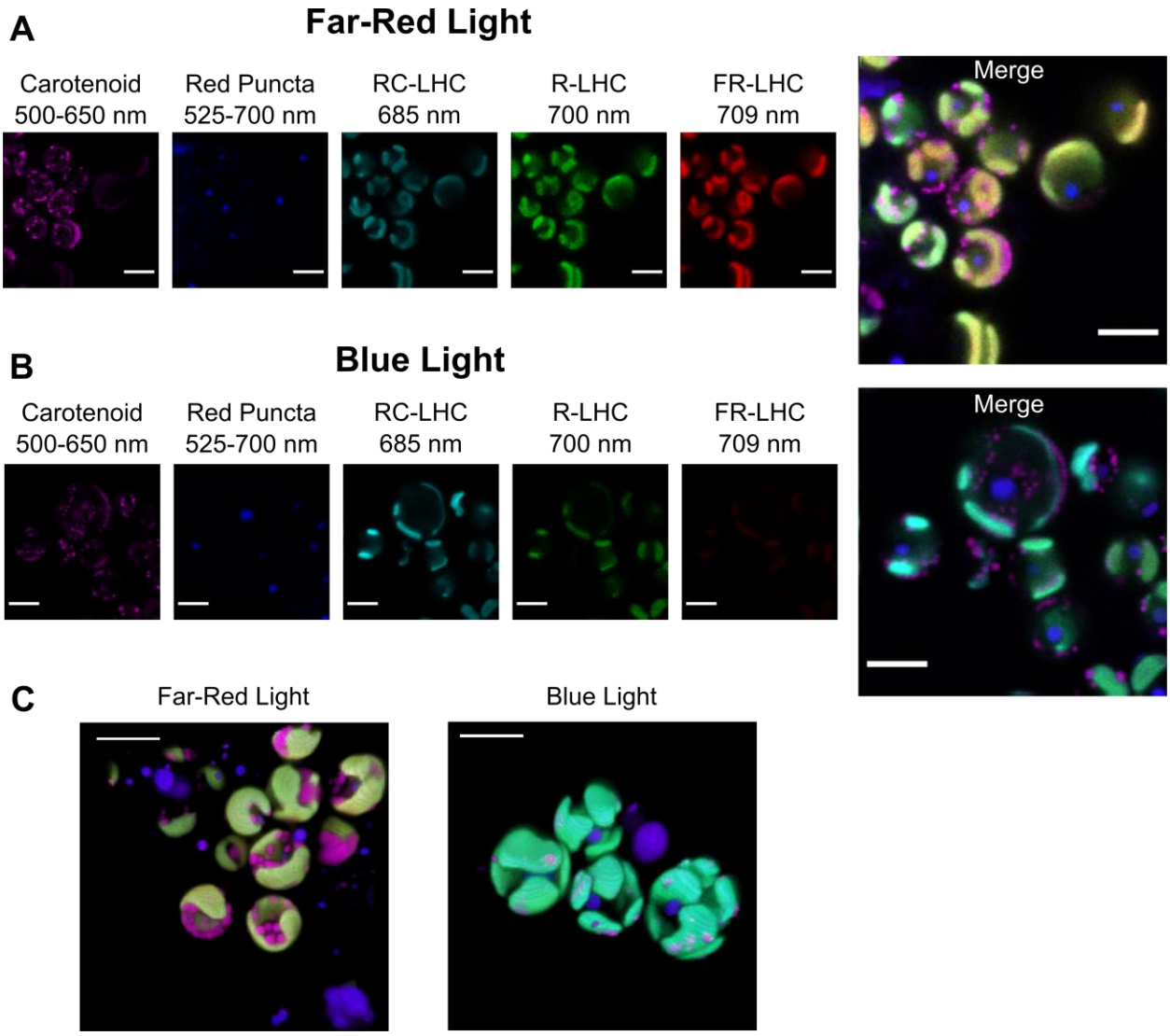

Figure 4.4: Images created using MCR output channels with cyan filter in place. In A and B, small images on the left are individual spectral components false-colored to correspond to the spectral signature from in Figure 2 they represent, which are merged in the images on the right. For each spectral component shown, the maximum intensity of both images (one from each condition) was set as the maximum pixel intensity, allowing the intensities to be compared between treatments. The blue channel labeled "red puncta" refers to the orange-red autofluorescence described in the text, and the magenta component labeled "Carotenoid" is carotenoid resonance Raman. In all images, scale bar is 5 µm. A) Cells grown under FRL. B) Cells grown under BL. C) 3D projections using the same component intensities under blue and far-red light.

The two non-photosynthetic components have been assigned based on their localization as well as spectral properties. The 525-700 nm band has properties of non-photosynthetic carotenoid-

containing lipid globules located outside the plastid. Spectrally, these carotenoids exhibit an extremely broad emission spectrum and easily discernible resonance-enhanced Raman scattering peaks (Figure 4.2) (Vermaas et al. 2008). These lipids do not strongly co-vary with the chloroplast-contained antenna complexes under differing light conditions, and little change is observed between blue and far-red light in these carotenoids (Figure 4.4, 4.5). The 500-650 nm band exhibits the properties of J-aggregates of carotenoids, which will be discussed in more detail in the Discussion. For the purposes of component description, these will be referred to as red-orange autofluorescent puncta (though these are false-colored blue in the images). Large changes in either the carotenoid containing lipid globules or the red-orange autofluorescent puncta were not observed in response to light condition (Figure 4.4, magenta and blue panels, and Figure 4.5).

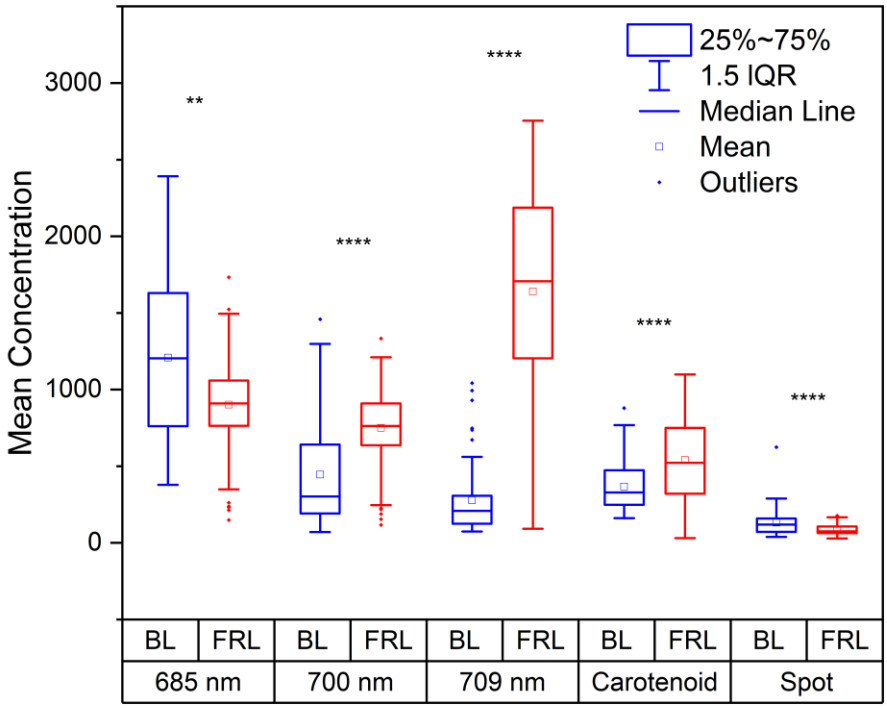

Figure 4.5: Box and whisker plot showing single cell analysis of FP5 cells when grown under blue of far-red light and imaged with a cyan filter in place. Significance computed using Mann-Whitney test, ** is $P \leq 0.05$ and **** is $P \leq 0.0001$.

3D volume renderings of Z-stacks provide further evidence to suggest that the carotenoid-containing lipid droplets are surrounding but not within the chloroplast (Figure 4.4C). Chloroplasts appear to surround the central regions of the cell, as has been previously reported in FP5 using standard confocal microscopy (Wolf et al. 2018). It is likely, from these projections, that many FP5 cells contain only a single chloroplast. In general, a single orange-red autofluorescent punctum was found per cell and these puncta appear to be localized near the center of the cells, though in some cases signal can be seen outside of living cells. This could indicate that these puncta are forming outside of cells, or that they were released from dead cells.

4.2.2 Analysis of Light Harvesting System through HCFM

We next imaged the FP5 cells in blue versus far-red light without the cyan bandpass emission filter in place. Due to the carotenoids and orange-red autofluorescence intensities being much lower, without the cyan filter in to dim the chlorophyll signal we detected only the photosynthetic apparatus. A spectral model was developed using images from 3 replicate flasks grown under blue light versus far-red light (Figure 4.6). This spectral model identified 4 spectral components (3 independently varying and 1 from detector offset): a component at 688 nm likely corresponding to a red-fluorescing LHC and photosystem II (RC-LHC), another at 705 representing an antenna protein that we call the red light-harvesting complex (R-LHC), and finally the far-red LHC (FR-LHC) at 713 nm (Figure 4.6). The far-red antenna wavelength corresponds well to the primary fluorescence emission peak of far-red grown FP5 (Figure 4.1B), and the red-LHC band appears somewhat red-shifted compared to a fully disassembled Chl-*a*-binding FR-LHC (Bína et al. 2014; Wolf et al. 2018). The RC-LHC band corresponds well to the fluorescence maximum of blue light grown cells and is interpreted as reaction centers (Figure 4.1B).

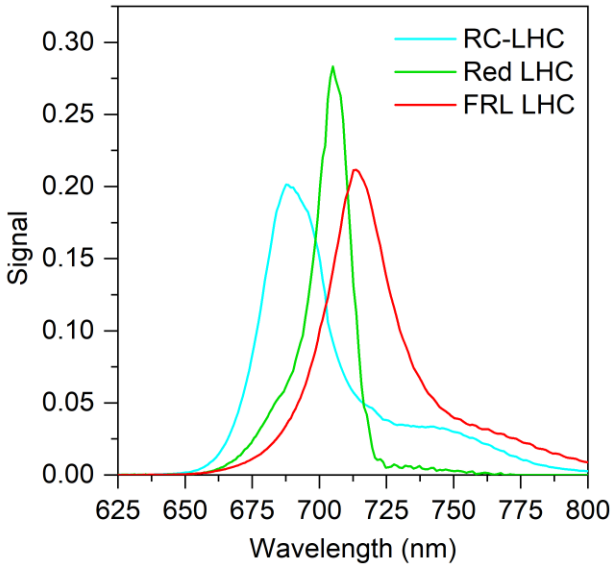

Figure 4.6: MCR output spectra from blue light and far-red light grown FP5 cellular imaging without the cyan filter to attenuate the chlorophyll bands. Only three components are visible without the filter as a result of the detector's dynamic range coupled with the strong photosynthetic pigment signal. Colors correspond to channels in Figure 4.7 From left to right, peak maxima are 688, 705, and 713 nm.

Representative image panels using the spectral model in Figure 4.6 to display the relative abundances and localization patterns of the 3 spectral components are shown in Figure 4.7. The images highlight the relative changes in antenna protein intensities between light growth conditions (Figure 4.7). Using the Figure 4.6 spectral model that has not been subjected to red-range spectral distortion by the cyan filter, three replicates from the blue light and far-red light conditions are shown. As in Figure 4.4, some level of heterogeneity in the overlays is observed, but all three photosynthetic components are co-localized within the chloroplast. Again, to allow for accurate comparison of images between treatments, for each spectral component shown, the maximum intensity of all six images (three of each condition) was set as the maximum pixel intensity.

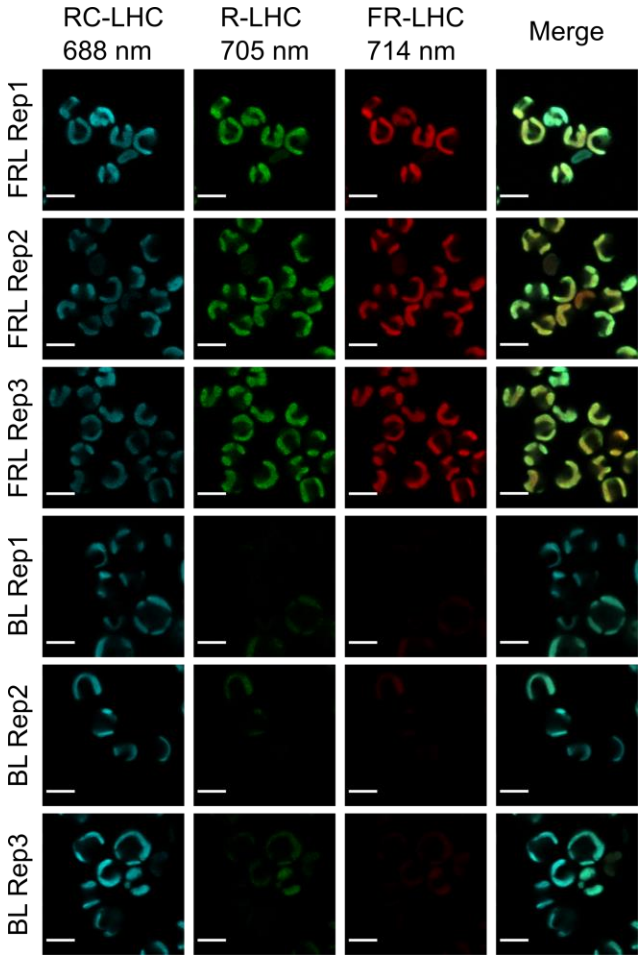

Figure 4.7: Images created using MCR channels without the cyan filter in place. For each virtual channel shown, the maximum intensity of all six images (three of each condition) was set as the maximum pixel intensity, allowing the pixels to be compared between all images from each channel. Overlays are shown to the right of all images for each replicate. Scale bars are 5 µm.

Single cell analysis of images taken of cells grown under blue or far-red light without any filter indicated large changes in the mean concentrations of fluorescence intensities in the far-red LHC component at 714 nm (Figure 4.8). For this 714 nm component, the mean intensity was 2365 when grown under far red light and 111 when grown under blue light (a 21 times decrease). Differences were also observed in the 705 nm component, with a mean of 695 versus 62 in far-red and blue light cells, respectively. However, the 688 nm channel did not show nearly as strong a change. As was the case in Figure 4.6, the far-red light grown cells show a large range of variation in the

fluorescence intensities of the far-red LHC component. Using a Mann-Whitney non-parametric statistical comparison, between the light treatments, all components are significantly different.

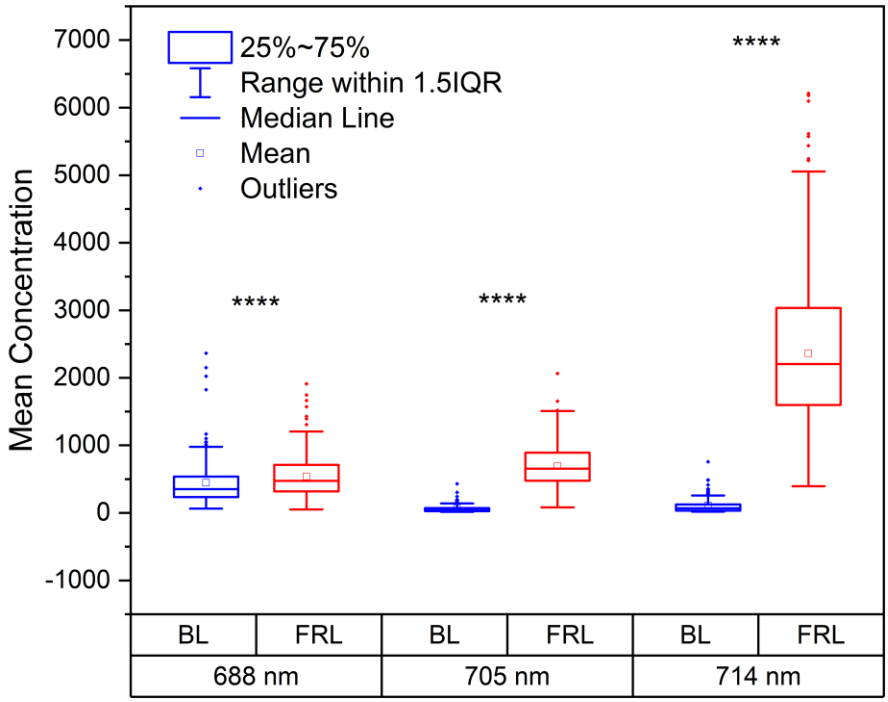

Figure 4.8: Box and whisker plot showing single cell analysis of FP5 cells when grown under blue of far-red light and imaged with no filter. Significance computed using Mann-Whitney test, **** is $P \leq 0.0001$.

4.2.3 Clear Native PAGE

Multivariate Curve Resolution analysis shows several antenna components present, and they generally seem to co-localize within the thylakoids. To understand what is happening at the protein level, we separated solubilized membranes using clear-native polyacrylamide gel electrophoresis (CN-PAGE) and analyzed the resulting bands spectroscopically. Several distinct bands are noted with differing fluorescence emission spectra were observed in both the far-red and blue light grown conditions (Figure 4.9). When cells were grown under far-red light, these peaks were at 682, 695, and 708 nm (Figure 4.9C, solid lines), as anticipated based on previous results (Wolf et al. 2018). This division of red, intermediate, and far-red fluorescence emission roughly corresponds to the

three components identified by MCR. Although these are each somewhat blue-shifted compared to the three peaks from the MCR output, this may be due to differences between the *in vivo* and *in vitro* assays. These far-red emission patterns correlate with the observed absorption spectra of each band as well, where strong far-red absorption shoulders are apparent in bands with strong far-red fluorescence, including bands 1, 2, and 3 (Figure 4.9B, solid lines). Analysis of the second derivative spectrum of Band 3, a strong far-red absorbing band that has been analyzed spectroscopically in more detail in previous works under the far-red state (Wolf et al. 2018; Niedzwiedzki et al. 2019), indicates the presence of a far-red absorbing Chl *a* pigment beyond 700 nm (Figure 4.9B, lower panel, solid line).

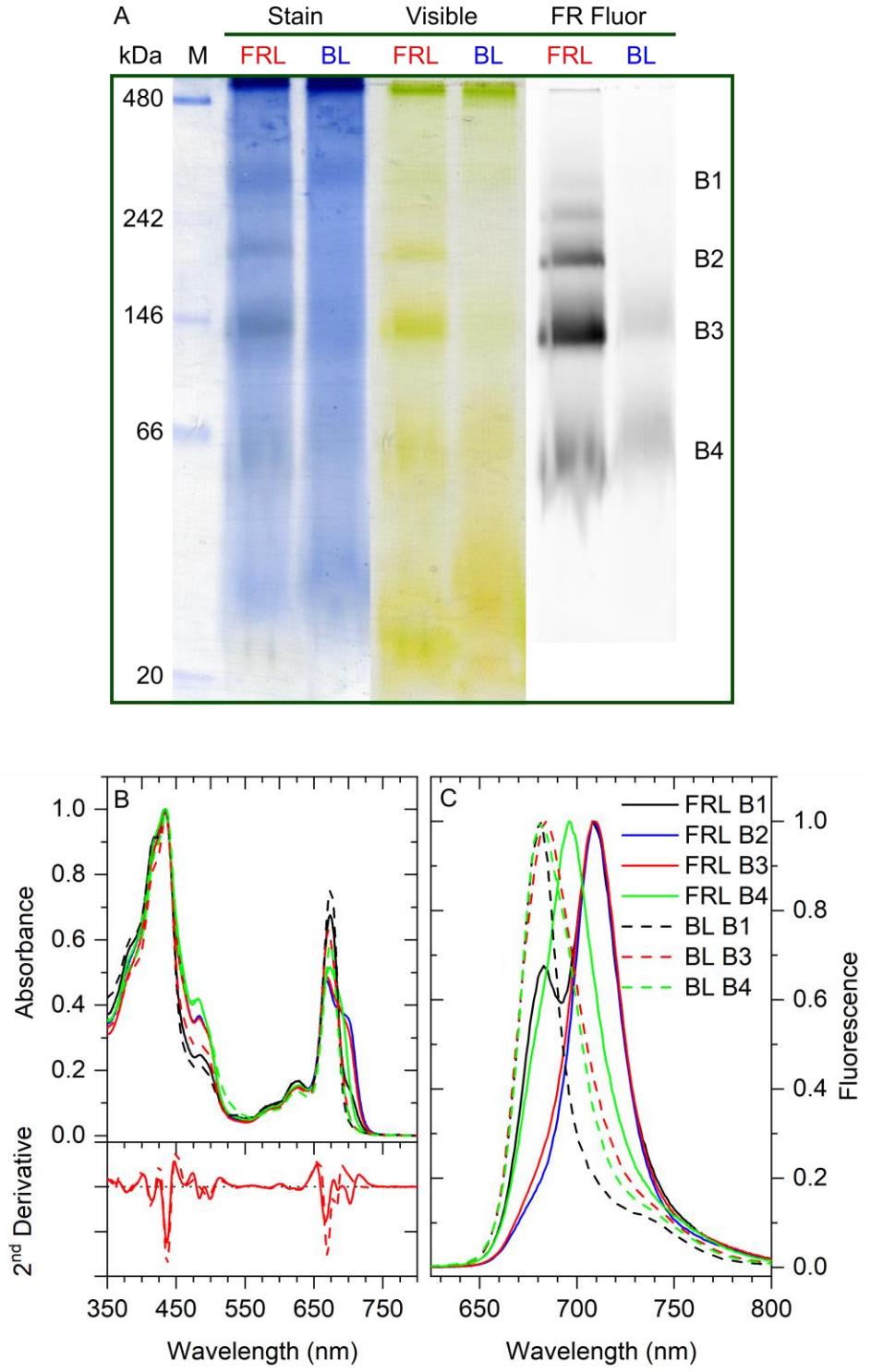

Figure 4.9: Clear native gel separating solubilized membrane proteins from FRL and BL grown FP5 cells and absorption and fluorescence spectra of excised bands. A) 9-16% native gradient gel bands viewed by Coomassie stain, visible light, and far-red fluorescence with blue light excitation. A 705LP filter was used in the fluorescence scan. Bands are indicated by numbers to the right, and

a native marker with molecular weight assignments is shown on the left. Contrast has been adjusted for clarity. Bands at the top are too large to enter the 9% gel; a 6-16% gel is shown in the supplemental material. B) Absorption spectra of excised bands with 2nd derivative spectra shown.

Under blue light, the banding pattern and the spectral signatures of the resulting bands bear marked differences. Blue light samples were observed to contain a lower chlorophyll to protein ratio than far-red samples, so pre solubilization, the concentration was adjusted to match the UV protein absorption of the far-red samples. Under blue light growth, Band 1 seems relatively unchanged compared to far-red light (Figure 4.9A), though it lacks the prominent far-red band of the far-red-light grown sample (Figure 4.9B-C, dashed lines). Band 4, a blue-shifted band under the far-red growth condition, is also relatively similar in size (Figure 4.9A), though its fluorescence emission is further blue-shifted in blue light samples (Figure 4.9C, dashed lines). The true differences can be observed in Bands 2 and 3, the "Far-Red LHC" bands. Although these bands are not absent, they are far more diffusive under blue light conditions when coomassie stained or viewed with visible light in native form, and emit nearly no far-red fluorescence. Further, their absorption and emission spectra bear no indication of a far-red antenna, and no far-red forms of Chl *a* are present in the 2nd derivative of absorption (Figure 6B-C, dashed lines).

4.3 Discussion

The eustigmatophyte alga FP5 was isolated in a pond system with a highly dynamic light regime. This study has shown how, at a cellular level, the organism responds to the stress of chromatic and perceived intensity shifts. The most striking differences were seen between the two most radically different light conditions: far-red and blue light. In nature, such wavelengths of light are highly relevant. Clear water tends to attenuate longer wavelength light, leading to a steady enrichment of blue wavelengths, while turbid water containing many phototrophic organisms tends to be enriched

in reds and far-red wavelengths (Stomp et al. 2007). In a dynamic aquatic environment, a free-living cell of FP5 might be exposed to both of these extremes on a short timescale, making acclimation a key aspect of its fitness.

When grown under either light extreme, FP5 primarily responds by altering the levels of three independently varying chloroplast-localized Chl *a* spectral forms. When imaged, these spectral forms appear to be highly co-localized, indicating that there is no spatial redistribution at the resolution of the light microscope that occurs within the chloroplast of these spectral forms. This is in stark contrast to the system that has been observed previously in some cyanobacteria when undergoing chromatic acclimation (Majumder et al. 2017). Primarily, variation is observed in the amount of far-red components present (700-714 nm), while changes in the putative reaction center (680-690 nm) remain relatively unchanged, which can be observed in Figures 4.4 and 4.7, as well as the single-cell analysis of mean intensities for each component in Figures S7 and S8. This indicated dynamic regulation of the far-red antenna system in particular, which has previously been shown to be highly labile to blue-shifting during biochemical preparation in FP5 (Wolf et al. 2018) and in another far-red absorbing eukaryote, *Chromera velia* (Bína et al. 2014). This lability might indicate changes directly to the antenna system during acclimation, which would be supported by the rapid reversion to a far-red absorbing condition.

Likely important to the observed response is non-photochemical quenching (NPQ), a process that has been shown to involve a fast and slow component and changes in zeaxanthin/violaxanthin ratios when examined in eustigmatophytes (Carbonera et al. 2014; Bína et al. 2017). FP5 does contain significant levels of violaxanthin in its antenna system (Niedzwiedzki et al. 2019) when grown under far-red light. Although NPQ is certainly an important aspect of the chromatic acclimation of FP5, biochemical evidence also indicates that a significant change is occurring at

the protein level in FP5 under varied light conditions. When FP5 light harvesting proteins are carefully solubilized (at a concentration normalized based on protein UV absorption) in low salt to avoid far-red LHC breakdown and subsequently separated using CN-PAGE, a native protein complex separation technique, a stark difference is observed between the far-red and blue adapted conditions (Figure 4.9). The intensity of the far-red LHC band at approximately 140 kDa is significantly higher in the far-red lane. Although a band in this position is present in both samples, spectrally, it behaves quite differently, with the blue light sample showing essentially no far-red absorption or fluorescence (Figure 4.9B-C). In the same gel, the upper resolved band, which has the spectral properties of an RC, is present in both treatments but with an additional far-red band when grown under far-red light. This indicates the presence of an RC-LHC complex migrating on the gel.

CN-PAGE results indicate that these forms of the photosynthetic antenna exist *in vivo*, in addition to within the context of an electrophoretic polyacrylamide gel. Given previous evidence suggesting that aggregation is important to the red-shifting of chlorophyll *a* in FR-LHC type antennas (Bína et al. 2014; Wolf et al. 2018), it is likely that the FR-LHC and R-LHC may represent aggregated and disaggregated forms, respectively, of the FP5 LHC protein. The fact that both forms are observed *in vivo* suggests that aggregation may be used to control far-red absorption in FP5, possibly to allow adaptation to highly filtered light conditions by scavenging available far-red wavelengths.

The orange-red autofluorescent puncta are observed in each cell, as has been previously reported in FP5 (Wolf et al. 2018) and other Eustigmatophytes (Eliáš et al. 2017). To our knowledge, the fluorescence emission spectrum of these puncta in Eustigmatophytes has not previously been described. The composition and function of this body remains unknown, though similarities may

be drawn to previous reports of carotenoid J-aggregates composed of violaxanthin and zeaxanthin (Gruszecki et al. 1990; Wang et al. 2012). Such aggregates have a similar broad fluorescence emission spectrum to that of the reddish autofluorescent puncta in FP5 cells. What function these aggregates could be performing in the cells is not readily apparent; indeed, they are not located within the chloroplast (Figure 4.4) and are thus not likely to be photosynthetically active. FP5 cells bear no indication of motility (indeed, a culture left standing with no disruption will quickly settle, white light microscopy has not revealed any form of motility (Wolf et al. 2018), and no taxis appears on plates), so the hypothesis that these puncta constitute an eyespot seems unsupported. However, Eustigmatophytes do typically have the ability to enter a zoospore stage (Hibberd and Leedale 1971; Eliáš et al. 2017).

FP5 seems to express its far-red antenna under normal conditions. Even when grown under white LED or fluorescent light containing some blue and far-red wavelengths and a majority of green and yellow, this antenna is present. Under this condition, cells are healthy and growing, and when allowed fresh medium, this is even more apparent. This, however, does not appear to be due to a blue light sensor, as extremely high white lights can lead to a reduction in far-red antenna, and very dim blue light will not lead to the response In these experiments, blue light was used as a stress condition, and further investigation is required to determine the method of sensing and acclimation in FP5.

The non-photosynthetic carotenoid band appears to strongly localize to lipid droplets present outside the plastid. Carotenoids were shown to localize to triacylglyceride droplets in microalgae (Davis et al. 2013) and land plants (Kilcrease et al. 2013), and these lipid droplets were observed using HCFM. When cells are grown under relatively dense conditions (Figure 3, S5 blue and far-red light), these carotenoids are readily apparent. Under rapidly dividing, diluted, and white light

conditions, they are much less apparent, though still present. This may prove important for bio-energy production applications of the strain in the form of stored lipids.

The Eustigmatophyte alga FP5 has the remarkable ability to utilize the normally wasted far-red portion of the solar spectrum, effectively expanding the solar spectrum available for photosynthesis. Investigating how the organism responds on a cellular and subcellular level will allow us to further investigate the changes in the photosynthetic machinery caused during far-red acclimation. Specifically, we found that there are three forms of antenna present, one that appears to contain reaction centers and remains relatively stable between light conditions, and two others that appear red-shifted in nature and are largely depleted under blue light illumination but make up much of the photosynthetic apparatus under far-red light. This indicates that these two antenna forms increase in abundance in response to far-red light.

Understanding how FP5 utilizes far-red light may have important implications for agriculture. In a crop field canopy, self-shading and the transmission of unused far-red light by upper canopy leaves creates a far-red-enriched environment for light-starved lower leaves. If these plants could be engineered to express a far-red utilizing antenna in their lower leaves, these leaves could contribute more photosynthetic activity to the plant as a whole, improving yield. In fact, if the spectral range of PAR could be expanded by just another 50 nm into the far-red (400-750 instead of 400-700 nm), a 19% increase in total photons absorbed could be realized (Chen and Blankenship 2011).

The idea of expanding the usable solar spectrum of photosynthesis has existed for some time (Chen and Blankenship 2011; Blankenship and Chen 2013). Much interest focuses on the utilization of red-shifted chlorophylls *d* and *f.* Although these far-red chlorophylls, when bound to their native

proteins, are capable of absorbing deep into the far-red range, their synthesis and the observed antenna system rearrangements that typically accompany their presence in cyanobacteria are complex. It is likely that one would encounter significant hurdles in trying to integrate such cyanobacterial far-red pigments into the antennas of crop plants. However, FP5 is a photosynthetic eukaryote using an ordinary pigment, Chl *a*, to absorb and utilize far-red light. Eustigmatophytes and plants alike use LHC-type proteins for light harvesting, but unlike plants, FP5 can use these proteins differently to absorb significant amounts of far-red light.

In plants, some LHCa proteins, which primarily interact with and supply excitonic energy to Photosystem I (PSI), are capable of absorbing far-red wavelengths, with fluorescence at room temperature observed out to 720 nm (Croce et al. 1996; Wientjes and Croce 2011; Wientjes et al. 2012). However, because these proteins do not interact significantly with PSII, it can be expected that PSI will preferentially absorb excitons from far-red illumination. In fact, far-red illumination can be used to preferentially excite PSI and oxidize the pool of plastiquinone (PQ) (Strand et al. 2017). PQ oxidation indicates an asymmetric excitation of reaction centers in the thylakoid, such that PQ will not be reduced by PSII activity and will only be oxidized due to the activity of PSI. Under such conditions, cyclic electron flow around PSI and concomitant ATP production are possible, but linear electron flow (LEF) supporting water oxidation and $NADP^+$ reduction is not. Without LEF, it is impossible for a far-red exposed plant tissue to contribute to the carbon pool of the plant.

The addition of the far-red light-harvesting protein complex from FP5 into the shaded, far-red exposed leaves of a crop plant would allow the cycle of LEF to be completed. The far-red light harvesting proteins of the diatom *Phaeodactylum tricornatum,* a Stramenopile (Stramenopiles also include Eustigmatophytes like FP5), have been shown to interact with PSII preferentially

(Herbstová et al. 2015). If these proteins are shown to be delivering energy directly to Photosystem II, these proteins may hold the key to unlocking far-red utilization in higher plants.

Additionally, FP5 clearly has a regulatory architecture for this antenna system that we have only partially characterized in these photo-acclimation experiments. Taken together, it seems likely that understanding the FP5 antenna system could allow for the alteration of existing LHC proteins in crop plants without the introduction of any new pigments or proteins.

Chapter 5: Photosynthetic Photoacclimation Response of FP5[4]

The antenna system of the Eustigmatophyte alga FP5 responds to its light environment in a manner that allows survival under various conditions in nature. This responsiveness allows the organism to survive under constantly varying conditions due to movement of this planktonic alga in the water column. This chapter will expound upon its response from a biochemical and photosynthetic perspective.

Chromatic acclimation is common in species capable of utilizing far-red light. In cyanobacteria, this process is termed Far-Red Light Photoacclimation (FaRLiP), and is generally observed in species capable of producing Chl *f* when exposed to far-red radiation (see Chapter 6) (Gan et al. 2014a; Gan and Bryant 2015; Zhao et al. 2015; Ho et al. 2016b, c). However, Chl *f* is not observed in eukaryotes, so algae (including diatoms and eustigmatophytes) employ different strategies that involve the red-shifting of their existing Chl *a* using the protein and pigment environment.

To further understand how the Eustigmatophyte alga FP5 responds to changes in light conditions, and to further demonstrate its response to far-red light conditions, the light-harvesting antenna proteins were separated by density using sucrose gradients and these bands were analyzed. Furthermore, whole cells were grown under far-red, white, and blue light conditions at Centrum Algatech in the lab of Ondřej Prášil during my three week visit to the Czech Republic in December 2017. We measured oxygen evolution rates under various wavelengths of light, used PAM

[4] Much of the content of this chapter will be detailed in a manuscript in preparation with the authors Benjamin M. Wolf, Gabor Bernat, Eva Kotabová, David Bína, Jiří Šetlík, Ondřej Prášil, and Robert E. Blankenship.

fluorometry to probe the quenching response of cells when grown under these light conditions, and performed additional experiments as detailed below.

5.1 Association of Far-Red Antennas with Reaction Centers

To efficiently harvest far-red light and use it to drive oxygenic photosynthesis, it is important that the far-red absorbing component of the antenna system interact with the reaction centers. In FP5, this component is ~20 kDa (see Chapter 3) and has a pigmentation corresponding to the Violaxanthin-Chlorophyll *a* binding Protein (VCP) in Eustigmatophytes (Niedzwiedzki et al. 2019). Through native separation techniques, the antenna may be purified and identified by its far-red absorption and fluorescence techniques (Chapters 3-4) (Wolf et al. 2018). Sucrose density gradients provide a powerful method to perform a rough separation of antenna complexes within eustigmatophytes and other species (Guglielmi et al. 2005; Bína et al. 2014; Kotabová et al. 2014; Litvín et al. 2016). The method allows for a course-grained localization of the far-red system compared to other photosynthetic complexes.

To understand what changes were occurring on a broad scale biochemically under blue light, sucrose gradients were used to separate antenna pigment-proteins in FP5. Four primary bands were observed (Figure 5.1). The banding pattern bears similarity to the system in the eustigmatophyte *Nannochloropsis* (Litvín et al. 2016). Under both far-red and blue light conditions, this banding pattern was observed.

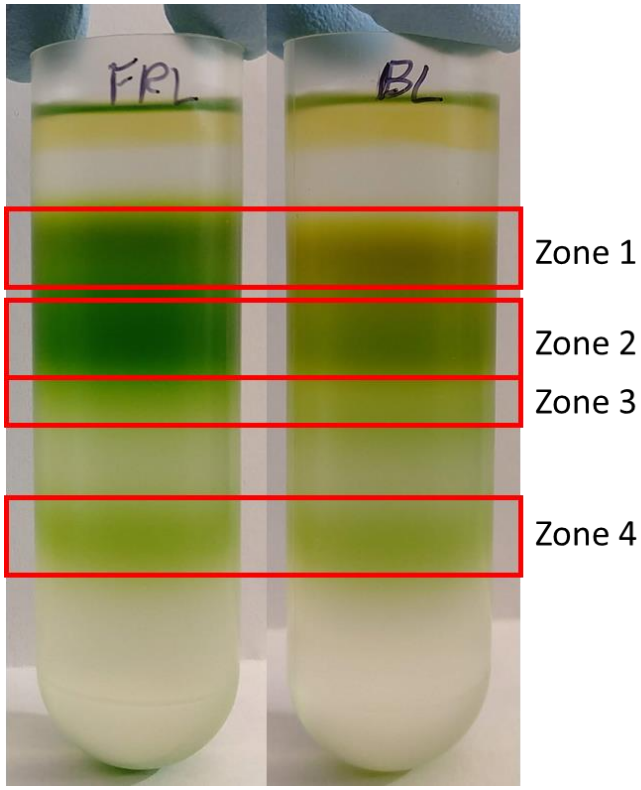

Figure 5.1: Sucrose density gradients of solubilized membranes of FP5, showing four zones that were collected for further analysis.

Each zone of the gradient was analyzed spectroscopically. Although the banding pattern did not significantly differ between the far-red light and blue light conditions, there were considerable differences in the absorption and fluorescence emission spectra (Figure 5.2). The most interesting differences were observed in zones 2 and 3. In Zone 2, the absorption spectrum of the far-red sample (Figure 5.2A-B) shows a significant far-red shoulder, but the blue light sample entirely lacks this feature. Zone 3 also has such a feature in the far-red condition only. The fluorescence emission spectrum also shows strong differences between the two conditions (Figure 5.2C). Although Zone 2 under the far-red condition (and only in this condition) is primarily composed of a far-red component with only a small red emission, Zone 3 is almost evenly split between the two. This indicates that while Zone 2 is likely a more pure form of the far-red antenna, Zone 3 likely

contains the antenna complexed with another protein or protein complex. Interestingly, despite very little red-shifting in the far-red Zone 4 compared to blue light, when grown under far-red light the fluorescence emission spectrum of Zone 4 shows a similar emission peak pattern to Zone 3.

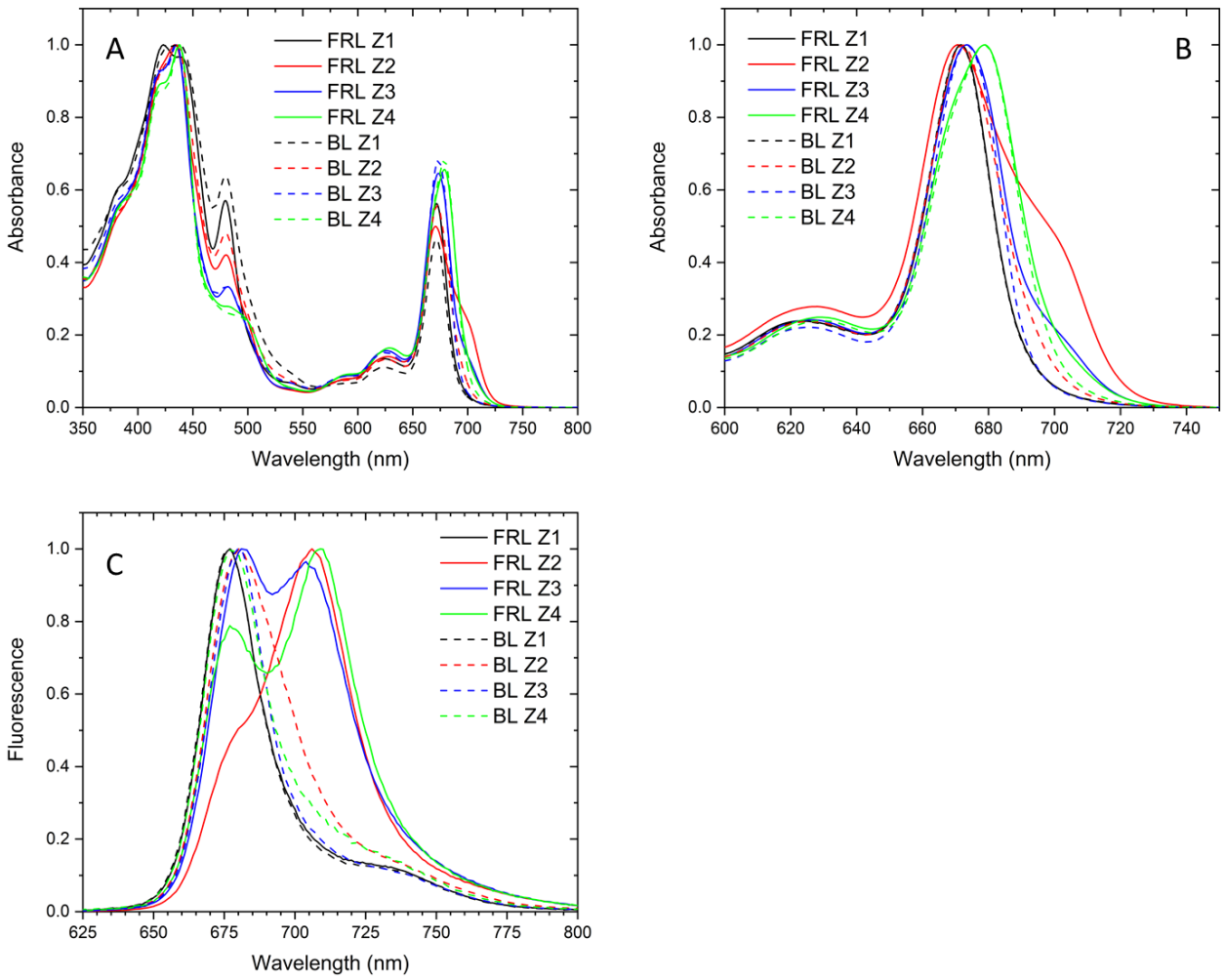

Figure 5.2: Spectroscopic analysis of individual bands of sucrose gradients for both blue light and far-red light treated FP5 cultures. In all cases, solid lines represent zones collected from the far-red culture gradient and dashed lines represent blue-light cultures. A) Absorption spectrum of sucrose gradient bands, normalized to unity. B) Absorption spectrum, showing a narrowed range to indicate changes in the Q_y region. Spectra normalized to unity within the field of view. C) Fluorescence emission spectrum when excited at 435 nm at room temperature. Spectra normalized to unity.

In similar systems, the position of Zone 3 contains PSII proteins and Zone 4 contains PSI (Guglielmi et al. 2005). To provide a second dimension of purification, material from each zone was run on a native polyacrylamide gel (Figure 5.3). Each zone, except for Zone 1, contains a prominent band or, in the case of Zone 4, two prominent bands. Unsurprisingly, under native conditions, the densest Zone contains no detectible low molecular weight components when run on the native gel. The bands here show a separation by density of components that are found on whole-membrane gels (Figure 5.4).

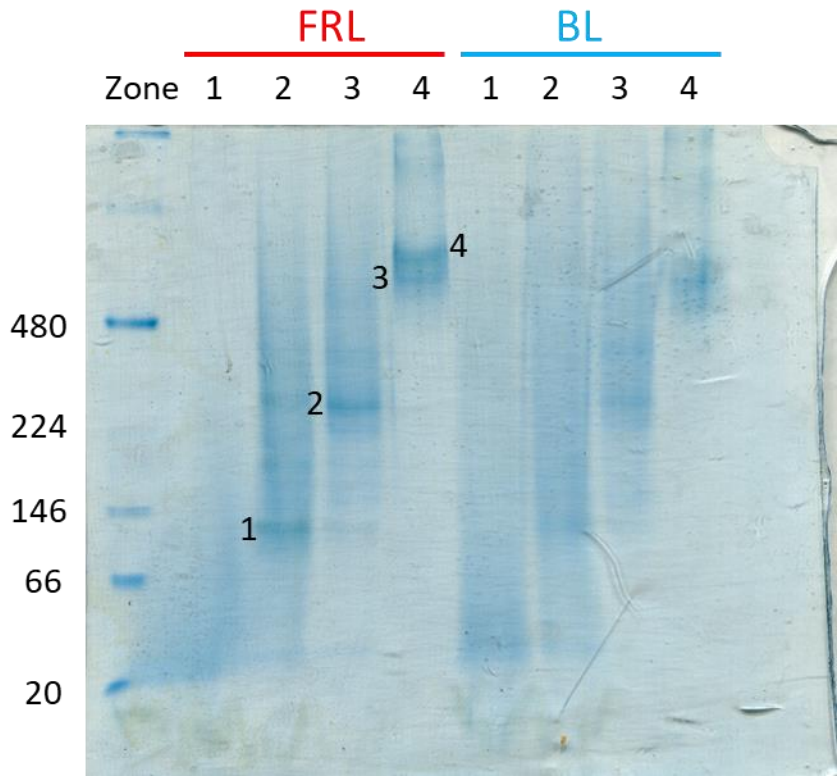

Figure 5.3: Coomassie stained native polyacrylamide gel electrophoresis of sucrose gradient zones. Ladder molecular weights are indicated to the left in kDa. Lanes are numbered based on sucrose gradient zone for both blue light and far-red light conditions. Bands on the gel are marked for LC-MS/MS analysis.

LC-MS/MS analysis indicates the presence of PSII proteins (D1, D2, CP43, CP47) heavily concentrated in the sample of Band 2. Bands 3 and 4 contain an enrichment of PSI components.

The identification of antennas in Band 1 has been particularly challenging due to a lack of sequence data for this organism (see Chapter 5.4). However, CP43 and CP47 are generally found even in these low molecular weight components, indicating that these PSII subunits may be important to the far-red absorption system of FP5.

The location of PSII was also analyzed by western blot analysis. The D1 protein of PSII was labeled in the native gel using an αD1 antibody (Figure 5.4). To align the labeling to an absorption spectra, multiple lanes were run, and one was used for in-gel fluorescence emission spectroscopy. Although PSII D1 protein forms a high molecular weight blob on the gel above Band 1, there is a concentration effect at the visible Band 1. This indicates that D1 protein is present in this higher molecular weight band, but also in higher molecular weight components. The fluorescence emission spectrum of Band 1 (Figure 5.4B, red trace) shows a small shoulder at ~680 nm, likely PSII emission.

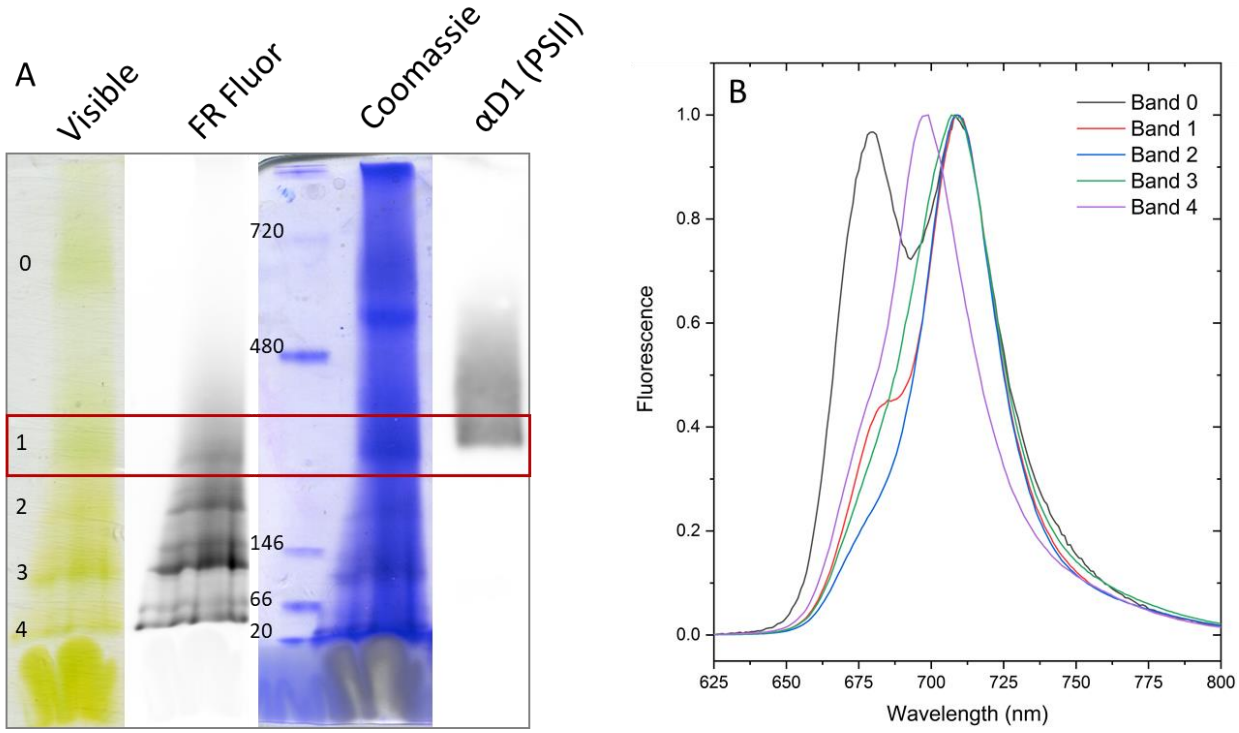

Figure 5.4: Native gel electrophoresis of whole intact membranes and αD1 Western blot. The gel is 6-16% to allow the resolution of high molecular weight species. A) Visible, far-red fluorescence (705 nm LP with blue excitation), Coomassie stain, and αD1 Western Blot of a native gel. The red box indicated the location of Band 1. B) Room temperature fluorescence emission spectra of all five bands collected. Spectra taken in-gel.

5.2 Photosynthetic Response of Whole Cells to Light Changes

Chapter 4 detailed the spectral response of FP5 cells using HCFM. Here, we have shown additional changes to the spectral properties of whole cells when responding to a wide range of light conditions. Because FP5 would likely need to be able to respond to various levels of filtering of sunlight in the water column, we grew the cells in a temperature controlled culturing device, a Multicultivator (PSI). The device allows cells to be grown in bubbled flasks at 405, 450, 540, 610, 735+blue, and 735 nm. The response of FP5 cells to each of these wavelengths followed an expected pattern, with the 405 and 450 nm wavelengths leading to a complete lack of the far-red

absorbing feature of FP5, both treatments containing far-red 735 nm light containing a strong far-red component, and 540 and 610 nm illumination leading to an intermediate state between the two extremes (Figure 5.5).

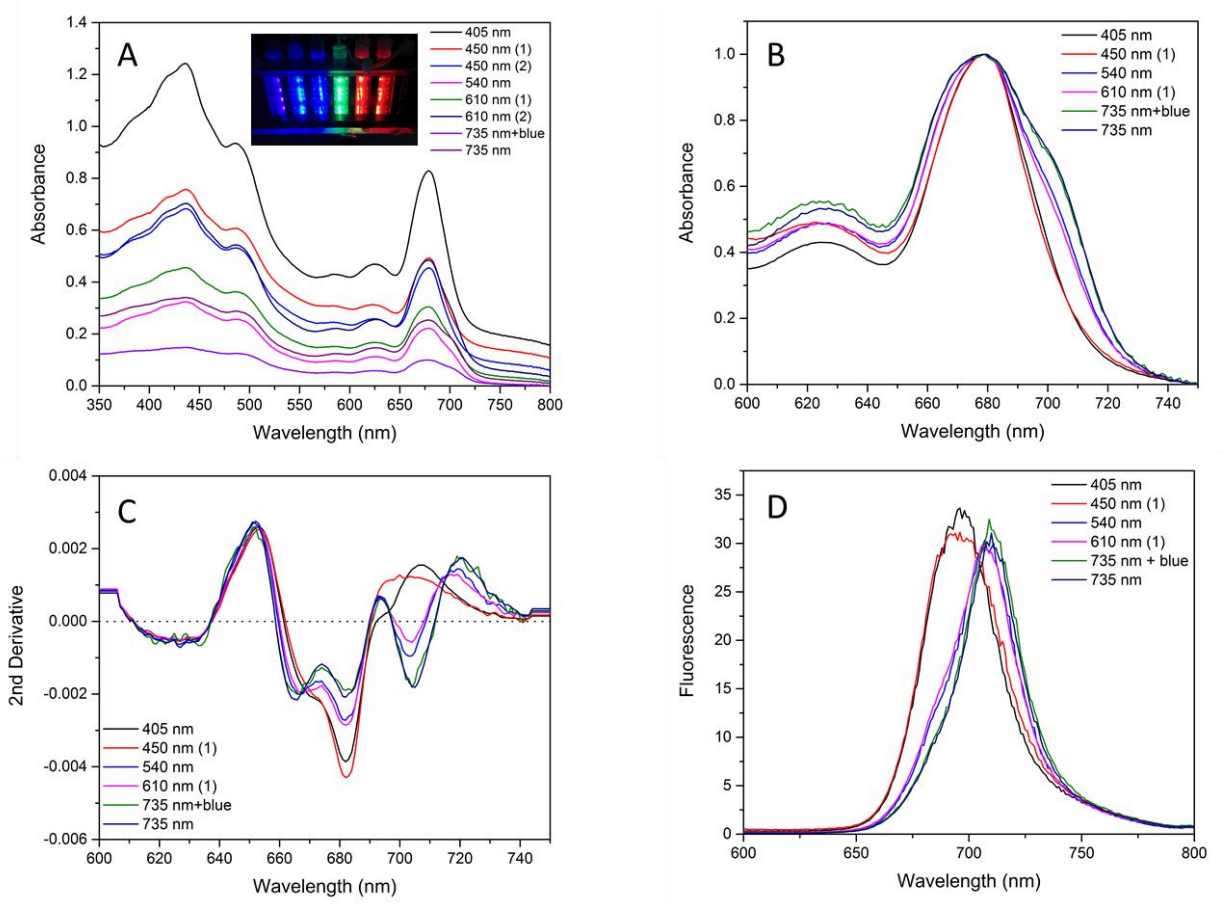

Figure 5.5: FP5 grown under varied light conditions in a PSI Multicultivator. A) Undiluted absorption spectra of cells after several days in the multicultivator at the indicated wavelengths. B) Absorption spectra normalized to the Q_y maximum. C) 2nd Derivative of absorption spectra shown in B. Dotted line indicated a derivative of 0. D) Fluorescence emission spectra of cultures with excitation at 435 nm.

Interestingly, the combination of a separate blue LED and the 735 nm illumination of the Multicultivator did not have any different effect from the 735 nm illumination (Figure 5.5). This could indicate a preferential response to far-red illumination compared to visible (this has also

been observed under white light illumination, where a small amount of far-red light is available and FP5 does not completely lose its far-red absorption feature. However, it could also be the result of self-shading. The multicultivator uses bubbling to mix the culture medium, but FP5 is very dense and tends to settle out of solution even when bubbled. Tubes were manually disturbed when this occurred, but some level of biofilm formation did occur nevertheless.

To assess the effect of self-shading on FP5, we stacked four culture flasks of FP5 on top of each other and wrapped the sides in opaque aluminum foil. The top was left open, and the whole stack was placed under a white light source to illuminate the top of the stack at 100-200 µmol $m^{-2}s^{-1}$. The FP5 predictably formed a biofilm after a week of growth, which was scraped before spectral measurements were taken. The experimental setup with the foil peeled back is shown in Figure 5.6A.

FP5 responds to self-shading in the same way as it responds to chromatic alterations in the incident light. Filtering by the culture above leads to enrichment of far-red light below. This can be roughly visualized using the absorption spectrum of the upper layer (Figure 5.6B). As each successive layer becomes more heavily shaded, it increases the strength of the far-red absorption feature, down to the fourth flask (Figure 5.6B). By subtracting each spectrum from the upper layer, it is apparent that a stepwise increase is occurring in the far-red component at 703-706 nm (Figure 5.6C).

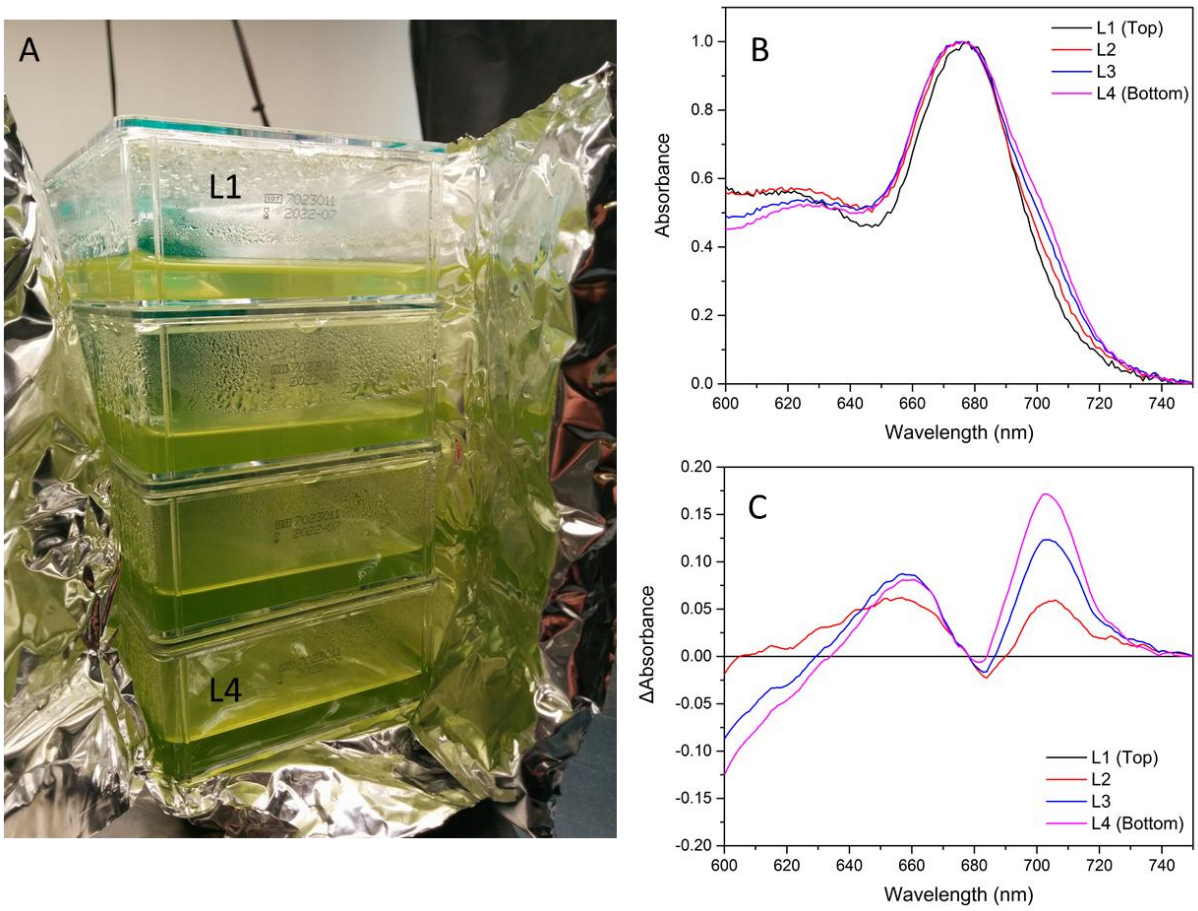

Figure 5.6: FP5 grown in a condition of controlled self-shading. A) Image of the experimental setup. During growth, the foil is wrapped around all four flasks to allow light to penetrate only from the top. B) Absorption spectra normalized to the Q_y maximum of each culture. C) Absorbance difference spectrum relative to the top layer. Input spectra are the normalized spectra in B.

Pulse Amplitude Modulation (PAM) fluorometry (Schreiber 2004) shows that cells grown under far-red light are deficient in their non-photochemical quenching (NPQ) effect, which is significantly slowed in far-red grown cells upon illumination with red light (Figure 5.7A). However, the deficiency in quenching does not necessarily correlate with an increase in the efficiency of photochemical quenching. The photochemical quenching recovery time (Figure 5.7B) is also reduced in far-red cells, as well as the quantum yield of PSII (Figure 5.7C). The

quantum yield of PSI, however, does not show the same effects (Figure 5.8D) and is quite similar in all treatments, indicating possible quinone diffusion limitations in far-red cells.

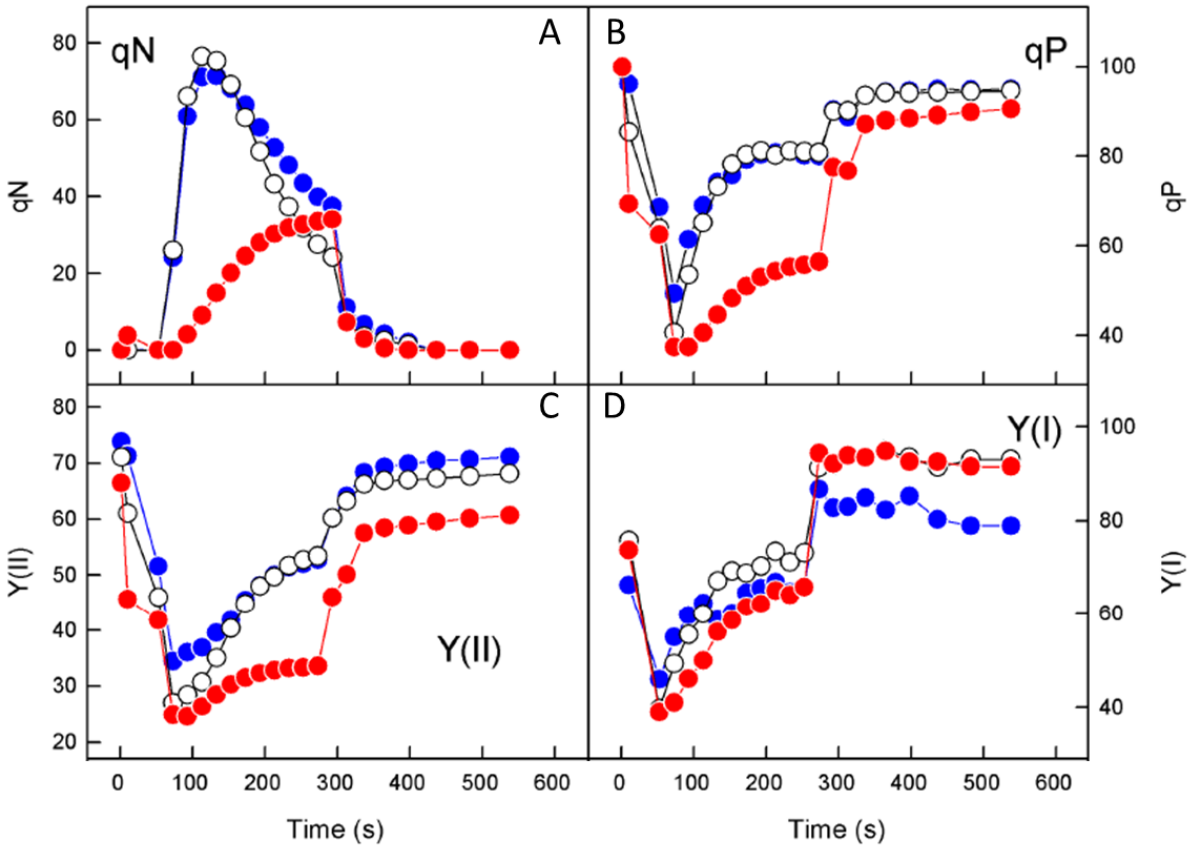

Figure 5.7: Pulse-Amplitude Modulation (PAM) chlorophyll fluorescence measurements of photosynthetic parameters in photoacclimated cells. A) Non-photochemical quenching, B) photochemical quenching recovery, C) the quantum yield of PSII, D) the quantum yield of PSI.

Despite differences in the photosynthetic properties of FP5 under varied light conditions, there is not a particularly noticeable difference in the carotenoid-to-chlorophyll ratios or the types of carotenoids present (Figure 5.8). As we have described previously (Niedzwiedzki et al. 2019), FP5 contains primarily violaxanthin, vaucheriaxanthin, and ß-ß-carotene in addition to Chl *a*. This composition is extended to varied light conditions as well (Figure 5.8).

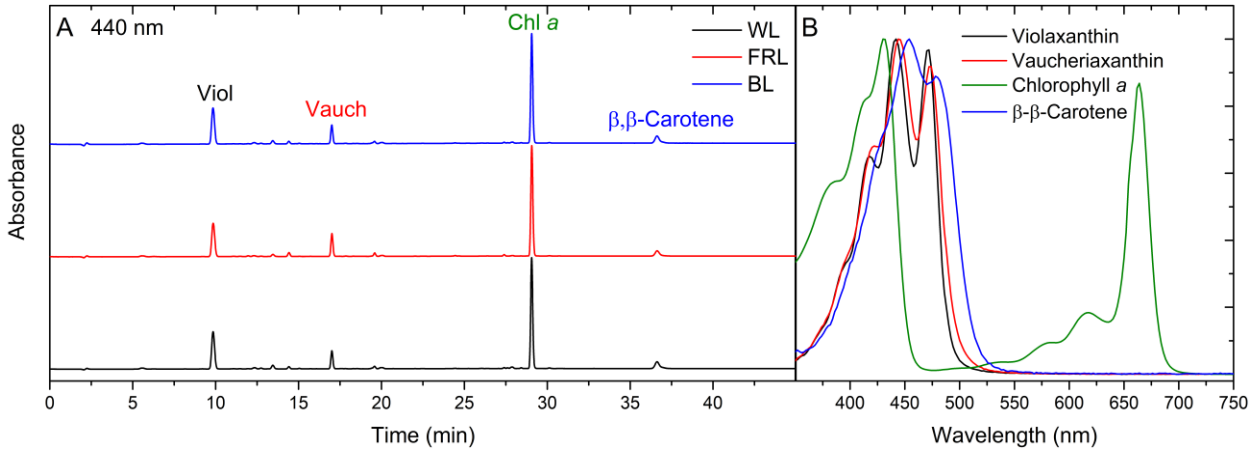

Figure 5.8: HPLC chromatograms, normalized to Chl *a* absorption, show three major carotenoids and Chl *a* (A). The spectra of these pigments are shown. Cells were grown at 28°C shaken under 100 µE m^{-2} s^{-1} light.

5.3 Oxygen Evolution

A direct indicator of photosynthetic output is oxygen evolution and has frequently been used to assess the photosynthetic activity of far-red light harvesting systems (Pettai et al. 2005b; Gloag et al. 2007; Gan et al. 2014b; Nilsson et al. 2014). To assess the rate of oxygenic photosynthesis using varied light wavelengths in FP5 cells grown under various conditions, the cells were subject to various wavelengths of dim light (<30 µmol $m^{-2}s^{-1}$) from a monochrometer. The raw traces are shown in in Figure 5.9 for each light condition. Both light on and light off slopes were calculated to provide an indication of dark respiration and light oxygen evolution.

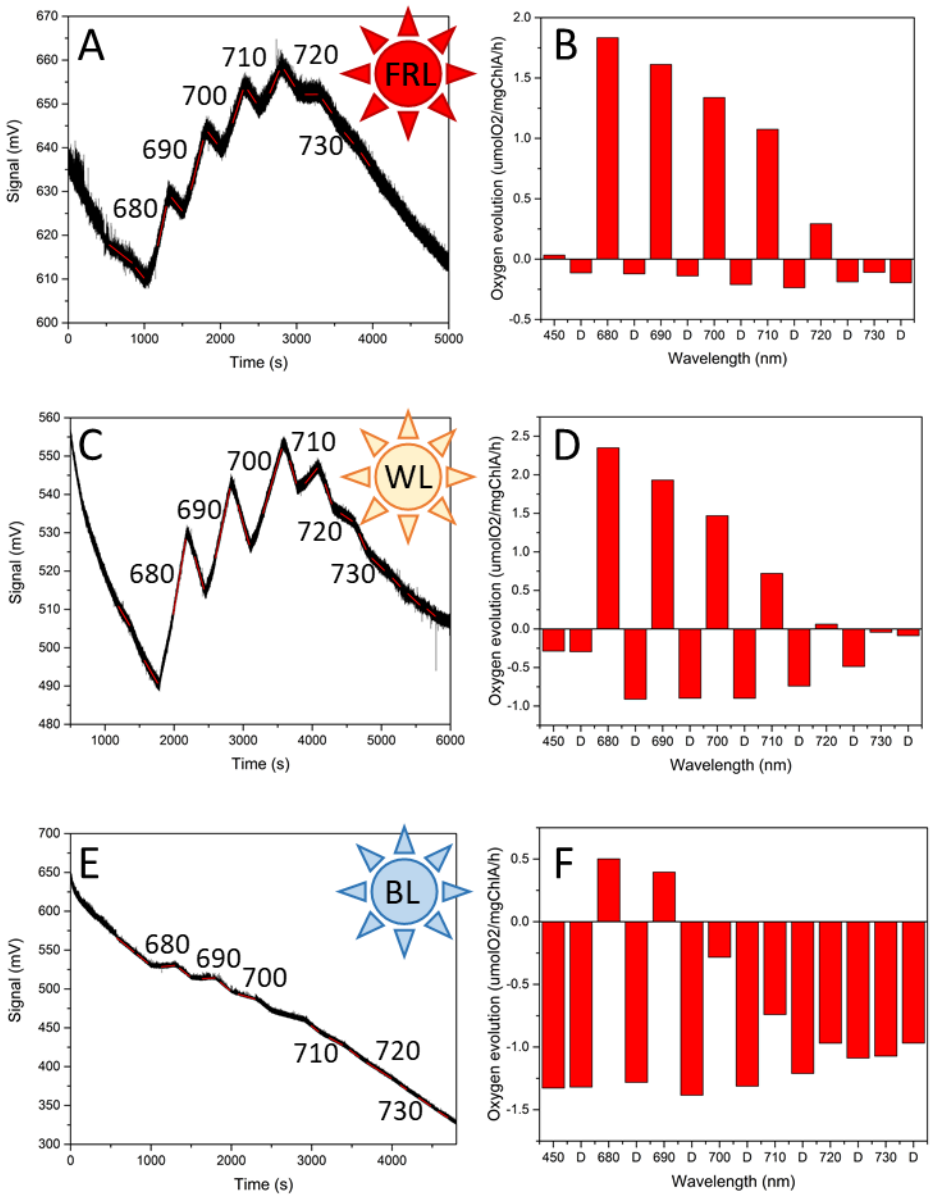

Figure 5.9: Uncorrected oxygen evolution using an oxygen electrode and measured in mV (A, C, E) and computed oxygen evolution per mg of Chl *a* based on pigment concentration and baseline and saturated solution measurements (B, D, F). Cultures were grown under different light conditions using various wavelengths of light passed through a monochromator. Culture light conditions are indicated in the sunbursts (FRL: far-red light, WL: white light, BL: blue light). On the traces, monochromator wavelengths are indicated. Red lines indicate areas of the traces used to compute slopes. Light and dark were alternated; dark regions are also calculated based on the red lines.

When cells are grown under far-red and white light, they are able to evolve oxygen at net positive rates all the way out to 720 nm (Figure 5.10A). However, blue light adapted cells are not adept at oxygen evolution under the same conditions, and cannot produce a net positive oxygen evolution rate at 700 nm (Figure 5.10A). Even at 680 nm, these cells cannot utilize the dim light as effectively as the white-light grown far-red grown cells. When the dark respiration is subtracted, blue-light adapted cells still drop off in oxygen evolution rates more quickly than far-red. Interestingly, here, the white-light cells were the most efficient (Figure 5.10B).

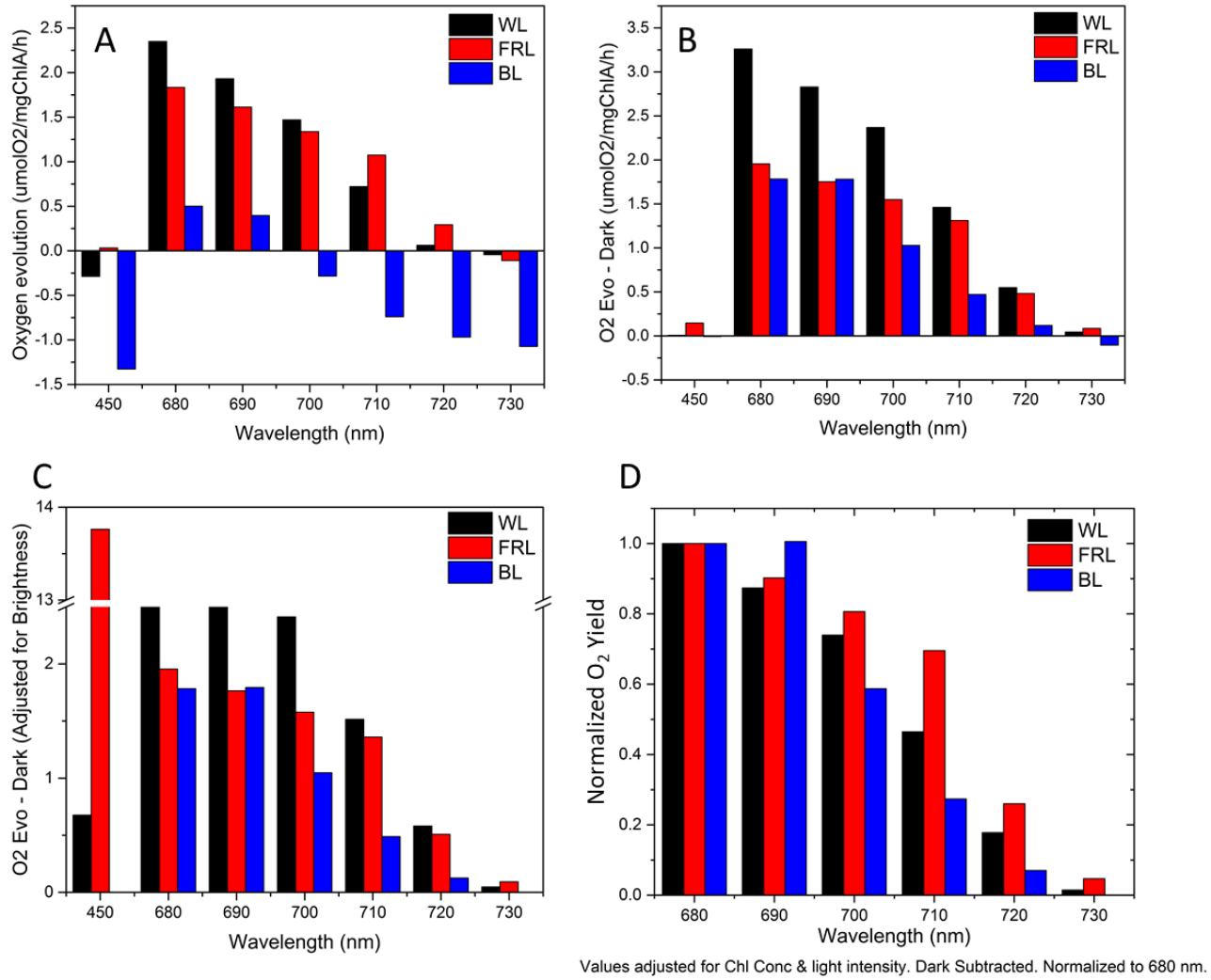

Figure 5.10: Oxygen evolution at each wavelength based on the traces in Figure 5.9. A) Raw illuminated oxygen evolution rates, not accounting for respiration, at various excitation wavelengths. B) Oxygen evolution rates with the dark respiration rates subtracted. C) Dark-subtracted oxygen evolution rates adjusted for the brightness of the light. Measurements are relative to one another. D) Oxygen evolution rates adjusted for brightness and normalized to unity at 680 nm for ease of comparison of excitation wavelength-induced changes to oxygen evolution.

Since the monochromator was using a halogen light as its white light input source, the intensity of each wavelength is not the same. For this reason, adjustments were made based on the intensity of light at each wavelength used. However, the trends remain essentially the same (Figure 5.10C). Finally, a relative comparison may be drawn regarding the strength of the far-red light utilization when all samples are normalized to 680 nm (Figure 5.10D).

Future work will focus on improving the range of conditions tested during the oxygen evolution and chromatic acclimation experiments. Due to the short duration of my visit to the Czech Republic to perform these experiments and equipment limitations, light intensity changes were not attempted on these experiments. It would be ideal to repeat the oxygen evolution experiments using a range of intensities of each wavelength, though the monochromator may not be able to be used for these experiments due to the high output intensities needed. This would allow us to separate intensity-based effects from wavelength effects more easily, especially between cultures.

5.4 Conclusions

FP5 responds strongly to its light conditions. In nature, varied spectra would be expected to occur throughout the water column. FP5 responds to these changes using its far-red antenna complexes, as can be seen by layering and chromatic acclimation experiments. However, it is interesting that

there do not appear to be significant differences between the banding patterns of the antenna system on sucrose density gradients or native gels, which may indicate that subtle changes are responsible for the red shifting of the FP5 antenna system under far-red light. In addition, cells grown under blue or white light are significantly more efficient at non-photochemical and photochemical quenching, which may indicate a disadvantage to the far-red antenna system under conditions under which it is not needed. This may explain why FP5 does in fact possess an acclimation mechanism.

Initial results shown by the low light intensity oxygen evolution experiments indicate a potential change in photosynthetic action spectrum based upon the growth condition. This hypothesis could be further tested using higher light intensities. A course-grained approach is to use extremely bright but wider bandwidth LEDs with emission peaks at different wavelengths. However, more wavelength accuracy may be attained by using a more powerful light source with a monochromator capable of handling higher photon fluxes. These results would provide a higher degree of confidence regarding the effects of photoacclimation on photosynthetic action spectra.

Chapter 6: Chlorophyll *f*-Containing Species

6.1 Introduction[5]

In coastal marine environments, corals and oxygenic phototrophs form complex interactions, resulting in incredibly diverse ecosystems. In this rich environment, phototrophic algae and cyanobacteria compete with one another for available light using various types of antennas and pigments (Fork and Larkum 1989; Miyashita et al. 1996; Kühl et al. 2005; Chen et al. 2012). These phototrophs often form layers, with the top layers composed of *Prochlorophytes*, a group of cyanobacteria containing chlorophyll (Chl) *a* and *b*, as well as other cyanobacteria and algae (Raymond and Swingley 2008). In addition to these Chls, many cyanobacteria also utilize bilin-containing phycobilisome (PBS) antennas that harvest light energy in the green wavelengths (Gantt 1981). The combination of these antennas absorbs primarily visible light, while transmitting the red and far-red wavelengths.

In the niche layers where transmitted far-red wavelengths are available in abundance, cyanobacteria containing the modified FRL absorbing pigments Chl *d* and Chl *f* are found (Miyashita et al. 1996; Kühl et al. 2005; Chen et al. 2010, 2012; Behrendt et al. 2011, 2015). Chl *f* is a red-shifted Chl with a formyl group at the C2 position, as opposed to the C2 methyl in Chl *a*, and is synthesized by a variant PsbA protein (Willows et al. 2013; Ho et al. 2016a). Chl *f* is the most red-shifted Chl and was originally discovered in stromatolites, which contain complex communities of phototrophs (Chen et al. 2010, 2012; Chen and Blankenship 2011). Chl *f* has garnered attention for the ability to expand solar spectrum coverage and for applications in

[5] The introduction to this chapter contains text originally published as Majumder, E. L. W., Wolf, B. M., Liu, H., Berg, R. H., Timlin, J. A., Chen, M., & Blankenship, R. E. (2017). Subcellular pigment distribution is altered under far-red light acclimation in cyanobacteria that contain chlorophyll f. Photosynthesis Research, 134(2), 183–192. https://doi.org/10.1007/s11120-017-0428-1

synthetic biology (Li et al. 2012, 2013; Chen 2014; Hou et al. 2014; Xu et al. 2014). One species containing this accessory pigment, which absorbs light at a maximum of 706 nm in methanol, is the filamentous marine cyanobacterium *Halomicronema hongdechloris* (Chen et al. 2010, 2012). Since the discovery of Chl *f* in *H. hongdechloris,* this pigment has been found in other cyanobacterial species as well, such as *Leptolyngbya* sp. strain JSC-1 and *Synechococcus* sp. PCC 7335 (Gan et al. 2014b; Ho et al. 2016b, c).

Chl *f* is a niche-adapted accessory pigment and its production is induced by FRL conditions in several species (Chen et al. 2012; Gan et al. 2014a). Although Chl *f*-containing organisms are capable of collecting light energy within the far-red region and driving oxygenic photosynthesis using this energy, many of them also have an additional strategy for FRL absorption: red-shifted PBS (Ho et al. 2016b, c; Li et al. 2016). The PBS is the primary pigment-protein antenna complex in most cyanobacteria, and these megadalton soluble antenna complexes absorb visible light in the range where Chl *a* absorbs poorly (Li et al. 2016).

These changes in antenna composition are manifestations of extensive transcriptional alterations that were observed when Chl *f*-containing cyanobacteria are exposed to FRL growing conditions, termed Far-Red Light Photoacclimation (FaRLiP) (Gan and Bryant 2015). In *Leptolyngbya,* substantial alterations in the gene expression profile of the organism were reported when switched between FRL and white light (WL) growing conditions (Gan et al. 2014b). In addition to spectral and proteomic changes, this suggests that a massive alteration of the cell is required for growth under FRL. Responses to far-red light include significant changes to photosynthetic antennas in *Synechococcus* sp. PCC 7335 (*Syn* 7335). The organism has been shown not only to produce Chl *f* during FaRLiP, but also to remodel PSI, PSII, and PBS (Ho et al. 2016b, c). PBS size, structure, absorption properties, and polypeptide structure are all significantly

modified under far-red light grown conditions (Ho et al. 2016b, c). *H. hongedechloris* has also been reported to contain a version of the FaRLiP gene cluster and to change the PBS structure under FRL (Li et al. 2016).

In many species of cyanobacteria, significant spectral and proteomic changes have been observed when switched between FRL and WL conditions (Gutu and Kehoe 2012). However, the subcellular pigment organizational changes that occur under these conditions have remained an open question. Here we demonstrate extensive composition and subcellular localization changes of photosynthetic antennas within *H. hongdechloris* and *Syn* 7335 when grown under FRL conditions using live cell fluorescence imaging, spectral, and electron microscopy techniques.

6.2 Isolate LSP65

The isolate LSP65 is a filamentous cyanobacterium that contains Chl *f* when grown under far-red light. It was originally isolated from a scraping on the bottom of a lily pad in Ludington State Park, Ludington, MI. The scraping was accomplished using a clean cotton swab, which was swirled in a tube of sterile BG-11 growth medium. The tube was kept in the deep shade (which is enriched in far-red radiation) for several days before being transferred to a far-red selective growth chamber for enrichment. After the tube greened up, a few microliters of culture were transferred to an agarose plate, streaked out, and placed under far-red illumination again. The colonies that formed were re-streaked until a unialgal culture was obtained.

The organism bears similarity to the genus *Phormidesmis* by 16S ribosomal RNA gene sequencing. *Phormidesmus,* also known as *Phormidium,* is a genus of filamentous cyanobacteria that live in groups of filaments or individual filaments, which are normally fairly short at about 30 cells, but can be much longer, they do not produce heterocysts, and are not motile (Anagnostidis

and Komárek 1988). In addition to the 16S sequencing, these features are also observed in the isolate LSP65. Unlike some filamentous cyanobacteria, which possess a form of gliding motility (Majumder et al. 2017), such features have not been observed in this isolate. Previous studies in *Phormidium foveolarum* indicated no atmospheric nitrogen fixation in this species (De 1938). Pilot experiments in nitrogen-free BG-11 did not yield any growth in LSP65. Heterocysts have not been observed in LSP65.

This isolate is filamentous in nature, but grows very well in suspension as long as it is properly agitated by vigorous bubbling or shaking. It is not necessary for this species to form a biofilm to survive, though it grows well as a biofilm, particularly on plates (Figure 6.1A). The cells tend to form into short filament fragments (Figure 6.1B), but large clumps can also form.

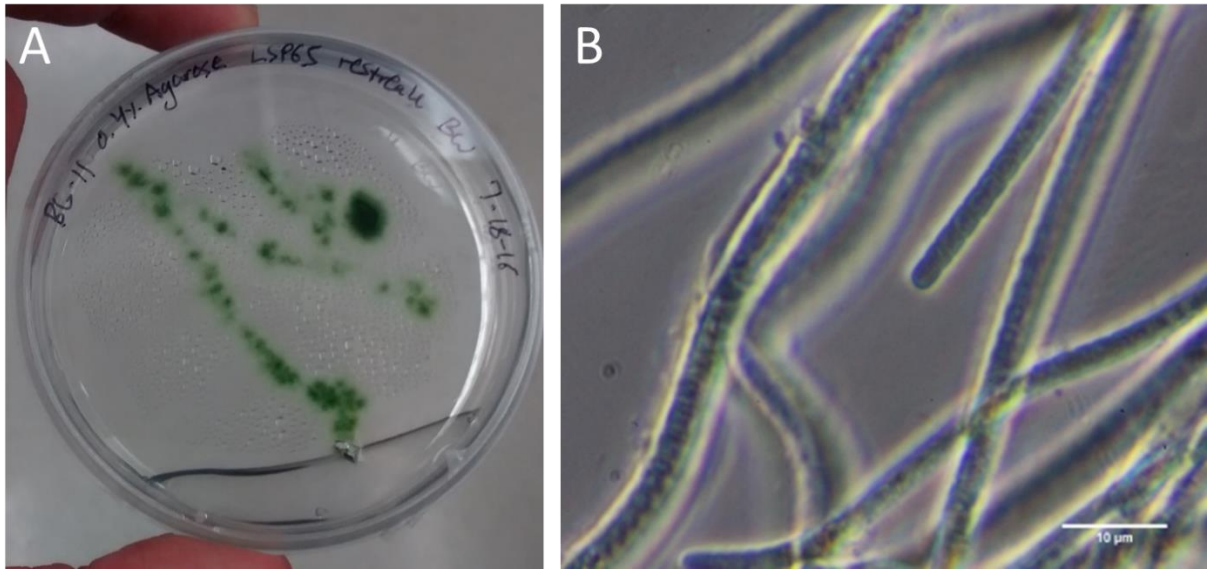

Figure 6.1: LSP65, white light images. A) LSP65 growing on a 0.4% Agarose BG-11 plate following streaking. B) LSP65 cells under a phase contrast white light microscope. Scale bar is 10 µm.

6.2.1 Biochemistry: Photoacclimation Response

LSP65 possess the ability to acclimate to changes in light quality. In particular, a significant response is observed in response to far-red or white light. Unlike FP5, which does not respond strongly to white light compared to far-red, LSP65 responds to white irradiation and far-red irradiation very differently. Under the white light condition, the organism produces Chlorophyll *a* as the only chlorophyll present. Under far-red light, the species undergoes far-red light acclimation (termed FaRLiP by some authors (Gan et al. 2014a; Gan and Bryant 2015; Ho et al. 2016b, c)) by producing Chl *f* in addition to Chl *a*. Under these conditions, approximately 5% of the total chlorophylls are Chl *f* (Figure 6.2).

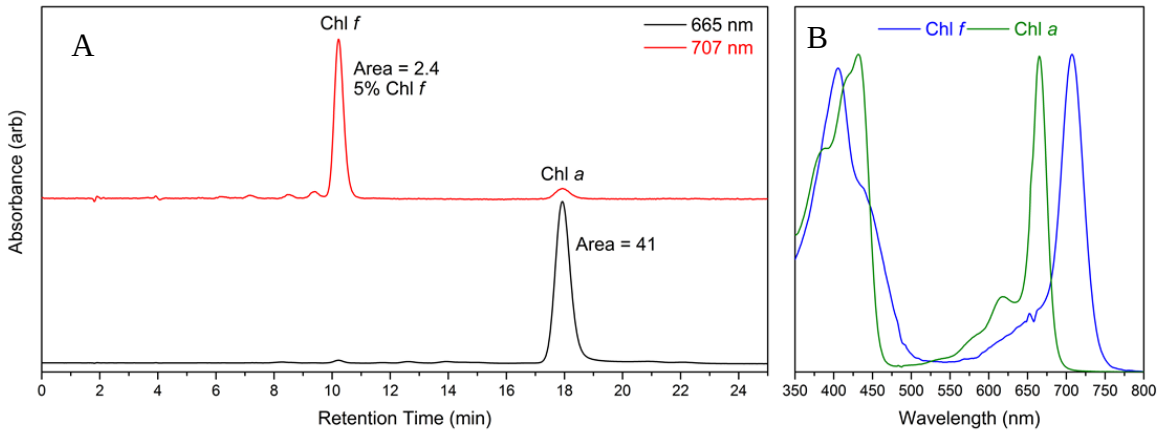

Figure 6.2: HPLC chromatogram and spectrum of pigments extracted from whole cells of LSP65. A) Chromatogram of the absorption signal at 665 nm and 707 nm. Peak areas are indicated. Percent Chl *f* was calculated using area and extinction coefficient. B) Absorption spectra at the labeled peaks.

This change in pigmentation, and perhaps other acclimation effects as well, contributes to some striking changes in response to a change from far-red to white light. When grown under far-red light, a strong far-red shoulder is observed on the absorption spectrum of whole cells, and the

difference spectrum between the two conditions shows a prominent positive peak at 716 nm, indicating a new pigment with this absorption under far-red light (Figure 6.3A). Additionally, a broad negative peak is observed at 627 nm in the difference spectrum, which can be interpreted as a decrease in green-absorbing phycobiliproteins when cells are grown under far-red conditions (Figure 6.3A). Significant differences are also discernible on the fluorescence emission spectra of whole cells. Under white light, there are three primary emission components: ~653 nm, ~678 nm, and ~712 nm. A spectral shoulder at 653 nm and a minor peak at 679 nm are still visible in the far-red cells, but a 731 nm peak dominates (Figure 6.3B). The 653 nm component in each sample can be attributed to phycobiliproteins, and is the dominant peak in white light cells, but the most minor under far-red. The 731 nm peak is only observed in far-red grown cells, indicating that it can be attributed to the far-red induced Chl *f*.

Because of its filamentous nature, spectroscopy of LSP65 is most easily performed on membranes. This tends to reduce scattering significantly compared to other techniques while not necessitating any filter paper or integrating sphere. Filter paper can be used to take an absorption spectrum, but the resulting spectrum is often noisy in the Soret region because of the strong blue and UV absorption of the filter paper itself. Fluorescence emission spectroscopy of isolated total membranes from LSP65 cells grown under white or far-red light shows a significant change in the primary fluorescence peak, particularly at 735 nm (figure 6.3D). Even in these room temperature spectra, there are two prominent peaks when cells are grown under far-red light. One at 680 nm appears to be an emission spectrum from a lower-energy pigment, assigned as Chl *a*, while the peak at 735 nm is likely Chl *f*. The interesting aspect is the fact that, as they both emit when 435 nm light is absorbed, fluorescence is successfully competing with excitation energy transfer (EET) between these components, possibly indicating a low rate of EET.

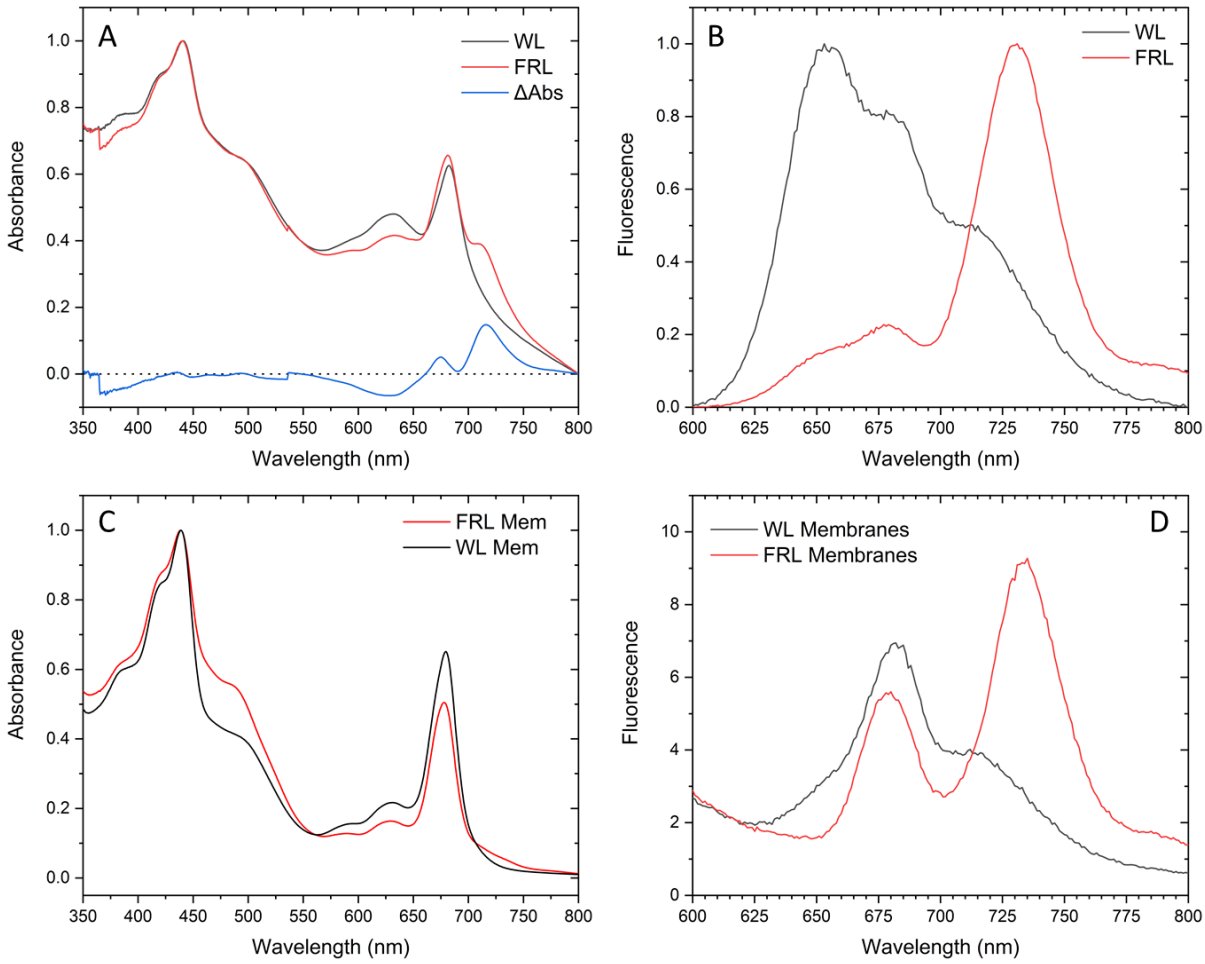

Figure 6.3: Spectroscopy of intact cells and isolated total membranes of LSP65. A) Absorbance spectrum of whole cells, including the difference spectrum of far-red minus white light absorbance. Far-red and white light cell spectra were normalized to unity. B) Fluorescence emission spectrum of whole cells with excitation at 435 nm, normalized to unity. C) Absorption spectra of membranes, normalized to unity. D) Fluorescence emission spectrum of cell membranes with excitation at 435 nm.

When the absorption spectrum of the membranes is measured, it is apparent that while the 680 nm component makes up most of the Q_y absorption under both growth conditions, the far-red cells also possess a significant shoulder in the far-red (figure 6.3C). This can be attributed to Chl *f*.

Absorption and fluorescence spectroscopy constitute an initial view of the photoacclimation response of LSP65, but to determine what changes are occurring at the biochemical level to lead

to these effects, the membranes were solubilized and the resulting native proteins separated by density on sucrose density gradient (Figure 6.4). By using isolated membranes, the phycobilisome antenna can be discarded and only the membrane-associated proteins investigated.

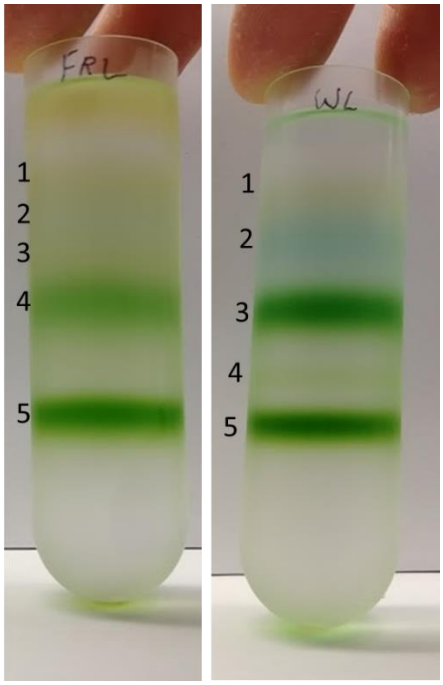

Figure 6.4: Sucrose density gradients separating solubilized membrane antenna complexes from LSP65 when grown under far-red or white light. FRL: far-red light, WL: white light.

In Figure 6.4, several differences are observed in the banding pattern of each gradient, based on the light condition of the cells. Particularly, under white light, a light green zone between the two primary green zones is apparent, which is not apparent in the far-red version. Also, the cells grown under white light have some phycobilisome contamination owing to their high levels of these soluble antennas (more below). However, the two strong dark green zones are easily visible in each condition. These will be described in detail below.

The absorption and fluorescence emission spectra for all zones under each condition are shown in Figure 6.5. Although some zones do not show significant differences in peak wavelength or peak

shape, there are a few key distinctions between the two sucrose gradients. The second band, which was a brilliant blue only in the white light gradient, has a telltale phycobilisome peak in the white light condition (Figure 6.5B). This may represent simple contamination or phycobiliproteins that remained associated with the reaction center cores during the membrane preparation. Zone 4 under FRL, which corresponds to Zone 3 in white light (see Figure 6.4), has a significant absorption shoulder in the far-red region (Figure 6.5 A-B). The same trend is reflected in the fluorescence emission spectrum (Figure 6.5 C-D). The fluorescence spectra also show some significant differences in the lowest zone, Zone 5, between the two conditions (Figure 6.5 C-D). Though it has a unique position on the gradient, the Zone 4 under white light does not appear to have an absorption or fluorescence spectrum very different from the neighboring Zone 3 (Figure 6.5 B,D). However, it does appear from the absorption spectrum that it may have a higher absorption on the blue end of the spectrum (Figure 6.5 B).

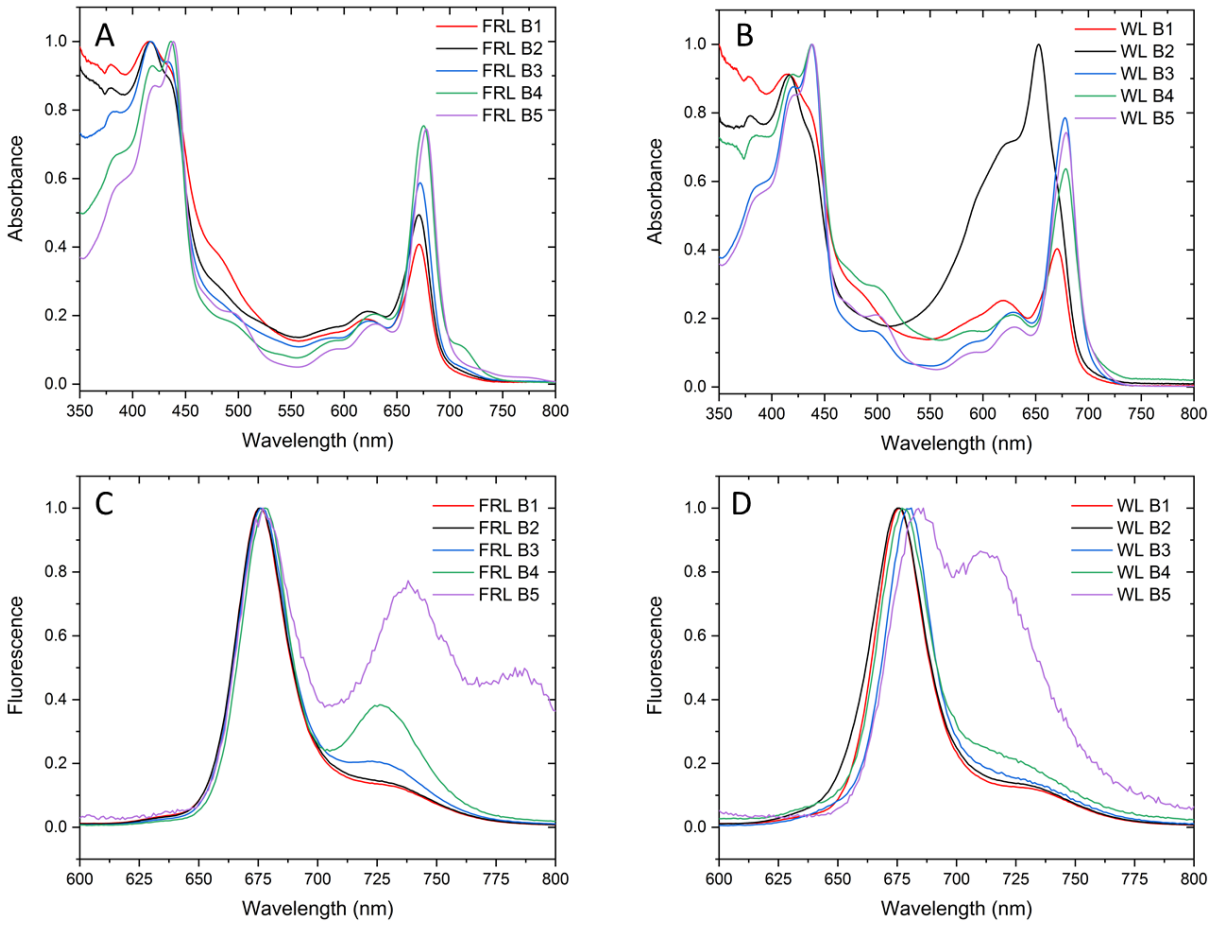

Figure 6.5: Absorption and fluorescence emission spectra of all zones (labeled B1-B5) from each of the two conditions. Absorption spectra are shown of A) far-red light (FRL) and B) white light (WL), and fluorescence emission when excited with 435 nm light are shown of C) FRL and D) WL.

Given similarity to other cyanobacterial systems described in literature (Gan et al. 2014b), it is probable that the two lowest green zones (FRL zones 4 and 5, WL zones 3 and 5) correspond to Photosystem II (PSII) and Photosystem I (PSI). As it has recently been shown that these reaction centers in Chl *f* organisms contain small amounts of this far-red chlorophyll in addition to the expected Chl *a* (Nürnberg et al. 2018), these sucrose gradient bands were investigated in greater detail.

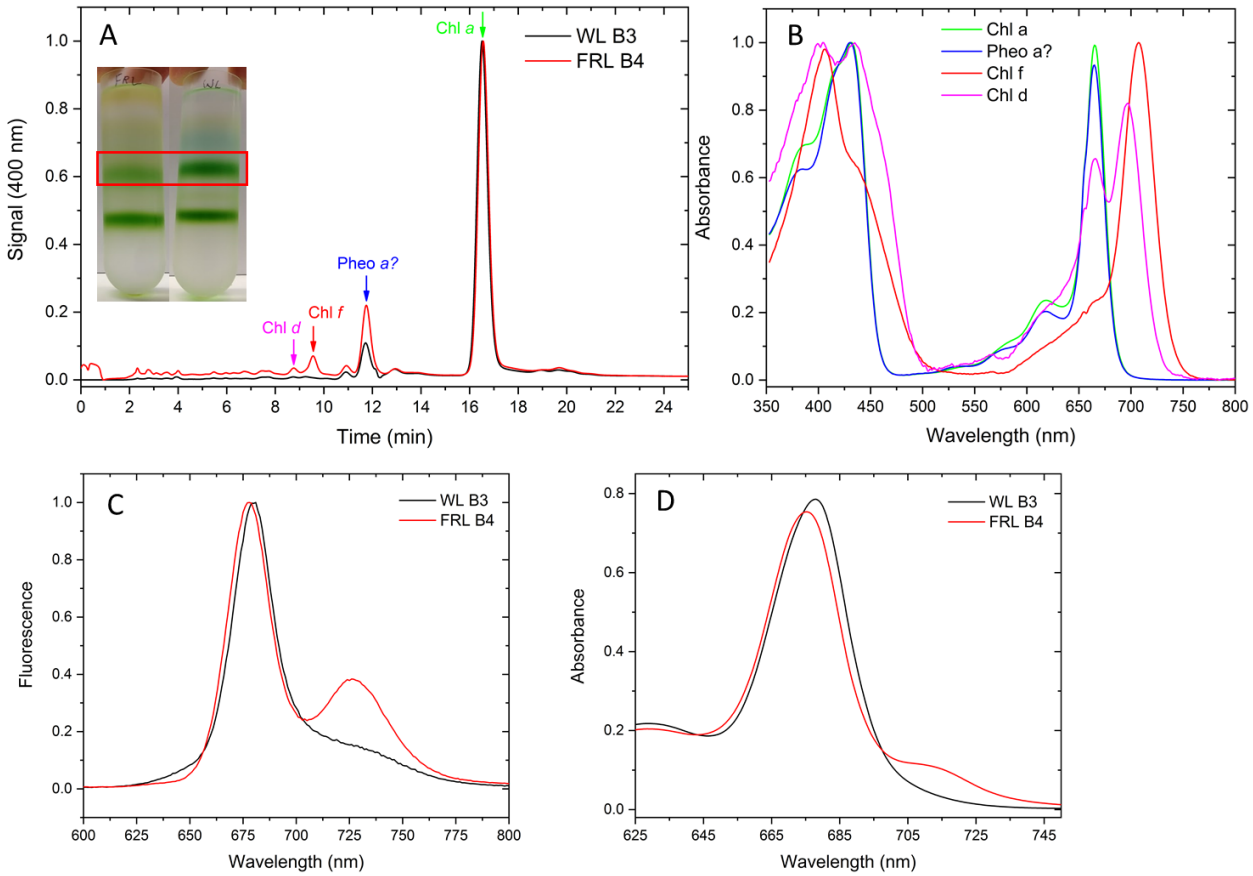

Figure 6.6: HPLC and spectroscopy of the upper green zone. A) HPLC chromatogram monitoring absorption at 400 nm with an inset indicating the zone from which pigment was extracted. Arrows indicate potential pigment assignments, and their color corresponds to the absorption spectra in B. B) Absorption spectra at each of the indicated peaks in A. C) A highlight of the fluorescence emission spectrum of the zone from each condition. D) An absorption spectrum highlight and zoom on the Q_y region to indicate subtle spectral differences.

The upper green band from far-red grown cells contains Chlorophylls *a*, *f*, and potentially *d*, as well as another pigment with an absorption spectrum similar to Chl *a* but with a much shorter retention time (Figure 6.6 A-B). The Chl *d* spectrum appears to contain some background Chl *a* as well. Chl *d*, in small quantities, has often been reported in organisms that produce Chl *f*, and its

presence has been demonstrated in PSII in a far-red adapted Chl *f* containing organism (Nürnberg et al. 2018). The unknown peak could be a molecule related to Chl *a*, such as a breakdown product of a chlorophyllide. This has not been confirmed and the exact identity of this pigment cannot be confidently assigned without additional experiments. The chromatogram of the white light pigment sample is similar in terms of Chl *a* and the unassigned pigment, but notably lacks the two far-red species. The fluorescence spectra, shown more prominently in Figure 6.6C than they were in Figure 6.5, bear a significant difference between conditions, primarily in the form of a prominent far-red emitting peak in the far-red grown condition. This can be attributed to the presence of far-red pigments not present under white light. An important difference between the conditions can also be seen in the Q_y zoom of the absorption spectra, which shows a notable absorption shoulder at 715 nm.

The lower green band also bears some differences between conditions similar to the upper band, in that far-red pigments are only found in the far-red grown cells (Figure 6.7A). However, Chl *d* is not present in this sample, which is consistent with expectations given the characterization of previous species (Nürnberg et al. 2018). The fluorescence emission spectra show a significant difference between white light and far-red light samples (Figure 6.7B). The fluorescence spectrum of the white light sample has the telltale far-red fluorescence of PSI, but the far-red sample has a far greater shift to the red (~735 nm) and also bears an additional peak even further to the red at ~780 nm. However, the Q_y zoom of the absorption spectra of the two samples is not very different between treatments.

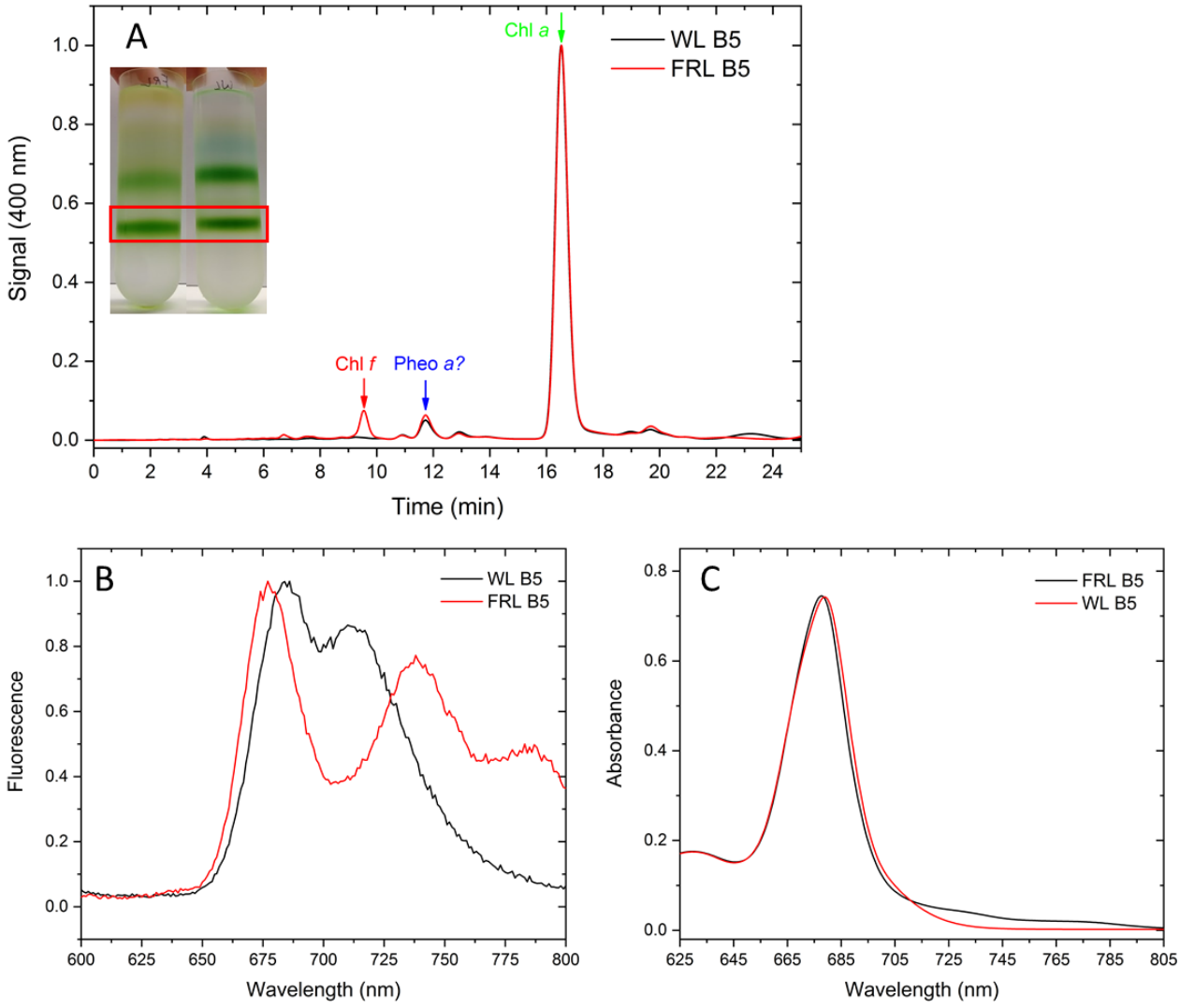

Figure 6.7: HPLC and spectroscopy of the lower green zone. A) HPLC chromatogram monitoring absorption at 400 nm with an inset indicating the zone from which pigment was extracted. Arrows indicate potential pigment assignments, and their color corresponds to the absorption spectra in Figure 6.6B. B) A highlight of the fluorescence emission spectrum of the zone from each condition. C) An absorption spectrum highlight and zoom on the Q_y region to indicate subtle spectral differences.

6.2.2 Microscopy: Photoacclimation

Far-red light grown filaments of LSP65 bear an interesting structure under a confocal fluorescence microscope, bearing strong far-red fluorescence along the margins of the cells within the filament, but strong orange-red fluorescence that is often concentrated at the poles of the cells within the

filament (Figure 6.10). Using a standard spinning-disk confocal arrangement, it is not possible to determine the precise emission peaks of each component, but it appears that the physcobilisomes are preferentially found in the septa while the far-red fluorescent components (reaction centers) are localized to the margins. This result is very similar to our findings in *H. hondechloris* cells grown under far-red light (Majumder et al. 2017). The reasons for this segregation of photosynthetic antennas under far-red light is not entirely known, but the fact that is has been observed in multiple far-red utilizing species indicates that it may serve an important function in these species.

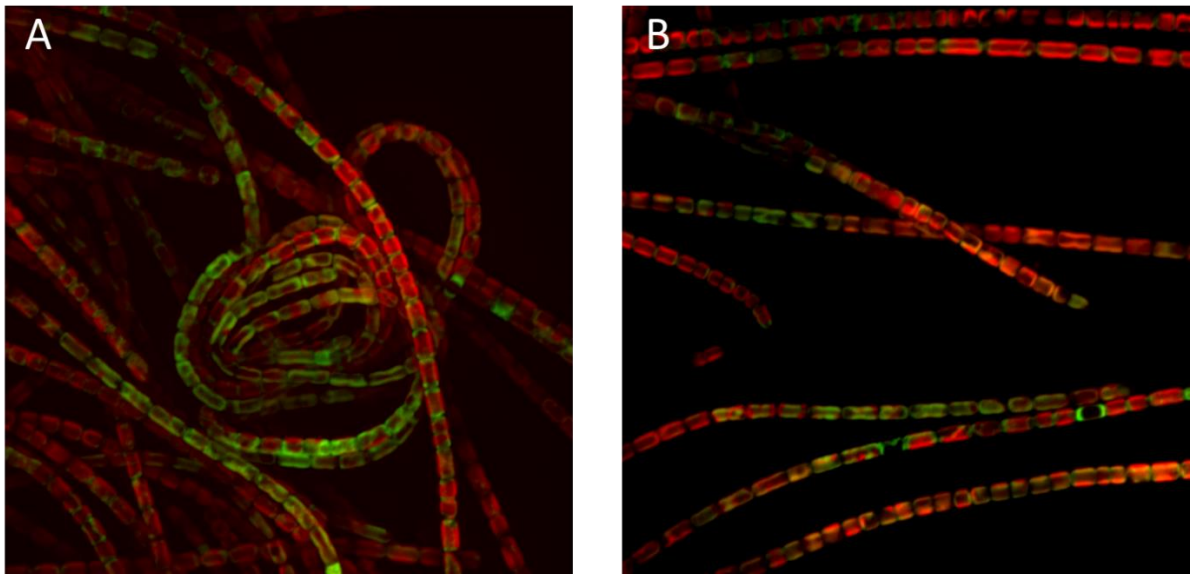

Figure 6.10: LSP65 cells grown under far-red light and viewed using a spinning disk confocal microscope. Green indicates 615 nm fluorescence emission (W70) when excited with a green 651 nm laser. Red indicates 485 nm (W60) or 705 nm (W90) emission with a 405 nm excitation. The fluorescence spectrum of whole cells does not indicate any components at 485 nm, so the signal can be interpreted as 705 nm emission. A) A knot of longer filaments. B) Straight filaments with some breaks visible.

The cells also vary in their filament structures, though they are always found in the filamentous form. They may be found in tight knots (Figure 6.10A) or in long strands (Figure 6.10B). In some

cases, cells are identified that appear to have no far-red fluorescence, but bear strong signal in the orange-red region at the septa.

Hyperspectral Confocal Fluorescence Microscopy (HCFM) was used to obtain a detailed picture of the effects of far-red and white light on the characteristics of LSP65 cells. HCFM provides advantages over standard confocal fluorescence microscopy because it can identify full spectral information for each pixel. Coupled with multivariate curve resolution (MCR), it is possible to identify the primary spectral components that make up the total signal. This can be a powerful complement to biochemical separation. It allows for a native, *in vivo* view of the actual spectra of each component. It also allows visualization of components that could be damaged during biochemical extraction, such as fragile protein complexes. The MCR analysis of LSP65 cells revealed four spectral components in the cells, at 735 nm, 726 nm, 658 nm, and 683 nm (Figure 6.11).

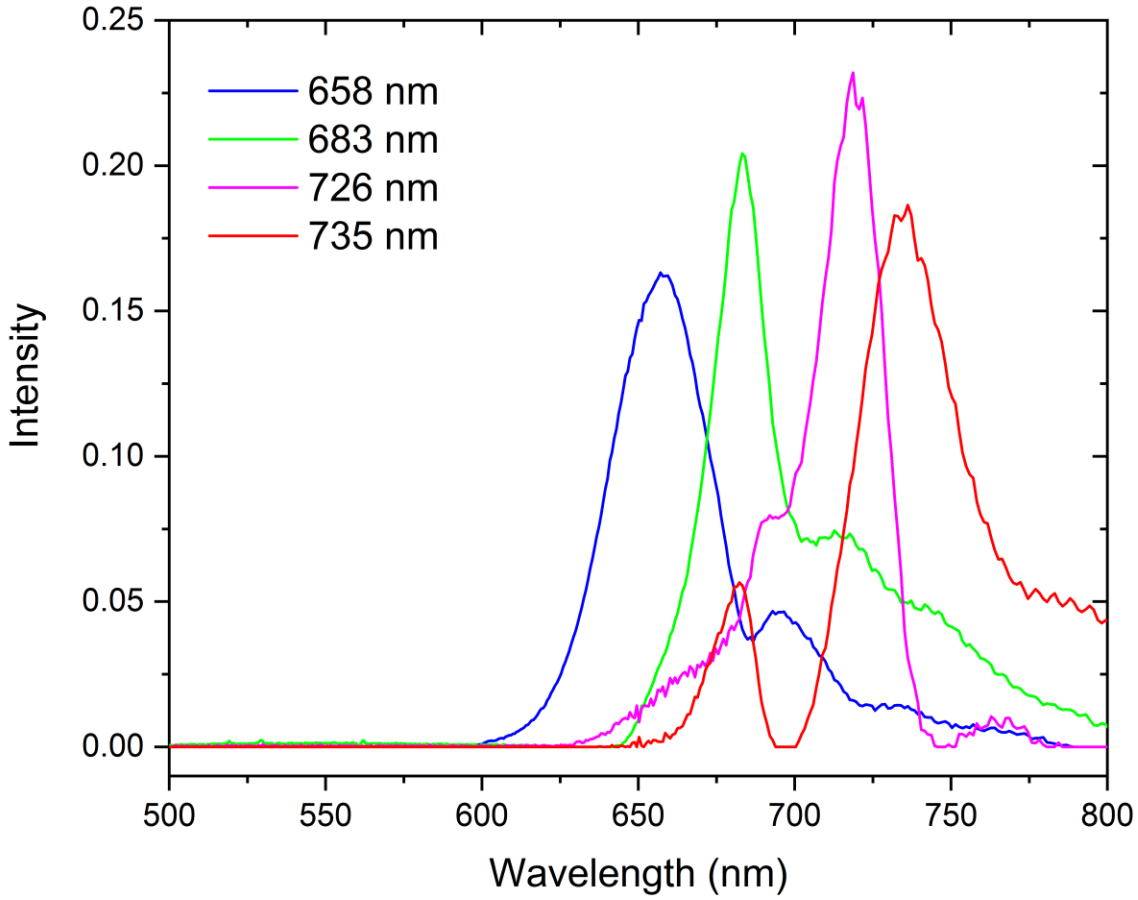

Figure 6.11: Spectral components identified by multivariate curve resolution from hyperspectral confocal fluorescence microscopy in LSP65.

The MCR spectra bear some additional complexity in the form of multiple peaks identified within each component. This can be explained by covariance. When two spectral features vary proportionally to one another, the MCR algorithm considers them a single component. This is because MCR uses variance as its criterion for identifying components. This is a useful feature of the output, as it shows when multiple pigment components are a part of the same photosynthetic pigment-protein. In this case, the 683 nm component always co-varies with two additional far-red peaks identified in far-red light cells in Zone 5 (the lowest green zone) in sucrose gradients (Figure 6.7B). A slightly blue-shifted peak in this region is also found in white light Zone 5, indicating

that the MCR may have identified these as a single component. The 735 nm component also co-varies with a ~680 nm peak, and the 658 nm peak also co-varies with signal between 690-700 nm (Figure 6.11).

The localization of these various components is rather homogenous, though it varies widely in the specific components found in cells under these conditions. Under far-red conditions, the two far-red components (735 nm and 726 nm) are strongly visible in the far-red condition, but the 658 nm component is nearly absent except at a few septa between the cells (Figure 6.12A). Under white light, the far-red components are nearly absent, but a much stronger signal is observed at 658 nm (Figure 6.12B). The 683 nm component is the only one that remains relatively constant, and is attributed to Chl *a* fluorescence. The 735 nm and 726 nm components are also visible in the membrane protein separation of the sucrose gradients (Figures 6.5C, 6.6C, 6.7B), indicating that both can be attributed to some level of Chl *f* fluorescence.

The spectral assignment of 658 nm to the autofluorescent component that moves to the cell septa provides further evidence that this is phycobilisome localization under far-red light conditions, which agrees with previous research we have published (Majumder et al. 2017). This phenomenon is only observed under far-red light, and under white light, the 658 nm signal is distributed throughout the cell. It is not surprising that the greatest signal density is observed around the margins of the cells under both conditions and for all spectral components, as all of these components would be anticipated to localize to the thylakoids.

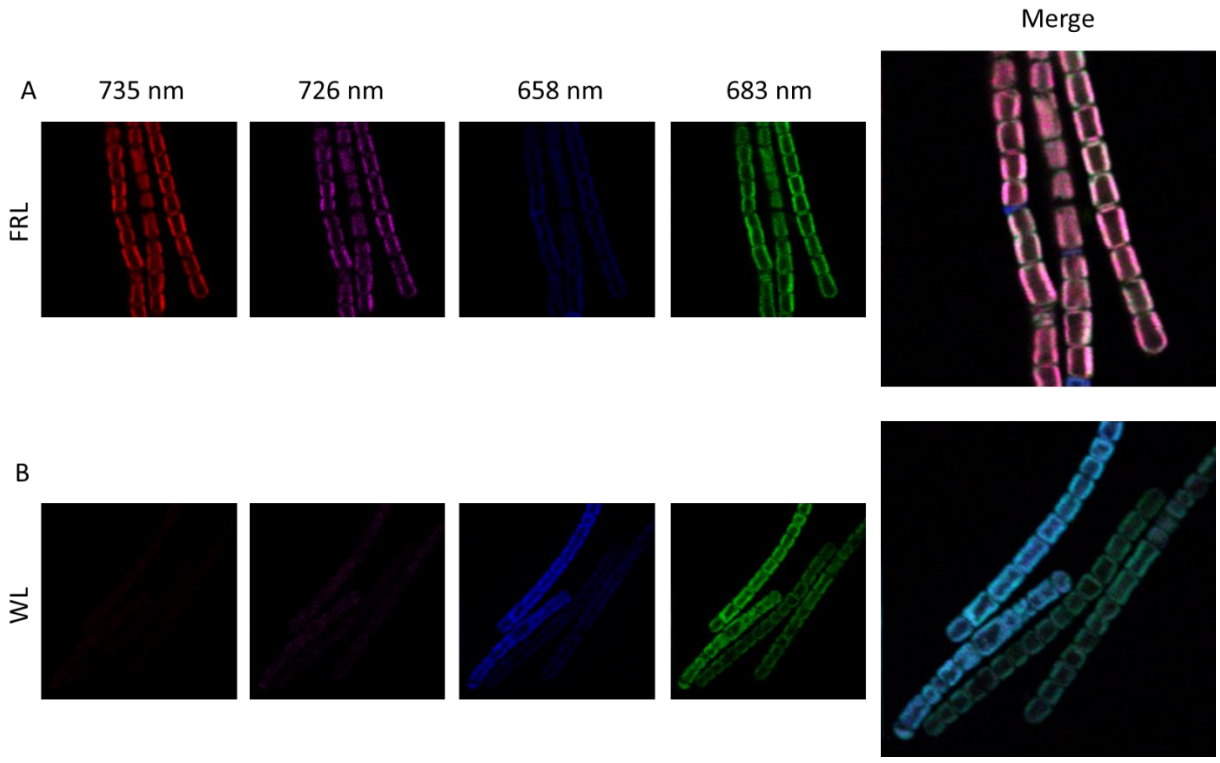

Figure 6.12: Individual component images of representative samples of LSP65 grown under white and far-red light conditions. Component images were generated using multivariate curve resolution analysis of data generated by hyperspectral confocal fluorescence microscopy. Images are labeled to indicate the spectral component they depict; the panels to the right are merged images of the 4 individual spectral components shown to the left. A) Cells grown under far-red light. B) Cells grown under white fluorescent light.

6.3 Conclusions

Chlorophyll *f* is a promising far-red pigment for expanding the usable solar spectrum of photosynthesis in crop plants. The isolate LSP65 strongly adapts to its light conditions though FaRLiP (Gan and Bryant 2015). Since many other cyanobacteria that contain Chl *f* contain red-shifted phycobiliproteins (Ho et al. 2016b, c; Li et al. 2016), a logical future direction for the LSP65 project is to investigate its phycobilisomes in greater detail. Further investigations will also be greatly benefited by the sequencing of this organism's genome, allowing for easier mass spectrometric experiments and potentially targeted mutation of putative far-red proteins, as well

as the identification of any potential nitrogen fixation genes (though the ability to grow under nitrogen depletion has not been observed).

Chapter 7: *Acaryochloris sp.*

Chlorophyll *d* is an important far-red absorbing pigment. Originally discovered in 1943 by Manning and Strain from extracts of whole red macroalgal samples collected off the cost of Northern California (Manning and Strain 1943). The pigment is not actually produced by red algae, but rather by epiphytes on their surface (Murakami et al. 2004b). These epiphytes are of the cyanobacterial genus *Acaryochloris,* which was originally discovered in 1996 and the genus described a year later (Miyashita et al. 1996, 1997). In *Acaryochloris,* Chl *d* normally makes up 95% of the pigments present, with the rest being Chl *a.*

Chl *d* is particularly interesting from a biotechnology standpoint. Its red-shifted absorption spectrum makes it a potential candidate for the expansion of the available photosynthetic spectrum in crop plants. A key aspect of this will be the identification of the Chl *d* synthase, which is not yet known (see Chapter 1 for more details). To bolster the biochemical toolkit of bio-engineers, we have set out to isolate additional organisms containing Chl *d* and to characterize a specialized *Acaryochloris* that lacks it to provide a point of comparison.

7.1 Isolation of Chl *d* Containing Species

In collaboration with Drs. Niki Parenteau (NASA Ames Research Center) and Nancy Kiang (NASA Goddard Institute for Space Studies), we sampled the same geographical region that Manning and Strain had originally sampled when they discovered Chl *d* in 1943. Our collaborators obtained a sampling permit and collected red macroalgae at low tide in the Fitzgerald Marine Reserve, Moss Beach, CA. The samples were shipped to our lab, where we scraped the tissue with a sterile pipette and removed small pieces of tissue, which were placed into a marine growth medium with low fixed carbon, MBG-11, in glass culture tubes. These tubes were subsequently

placed on a rack in the first of several far-red light growth chambers that we constructed. This chamber contained 740 nm LEDs cooled by liquid cooling rails. Although the chamber is not temperature controlled, the liquid cooling maintains the temperature near 25°C. Tubes were left in this condition for several months until visible growth appeared.

Some of the collected tissue was subject to HPLC analysis. Tissue was ground in 7:2 acetone: methanol, insoluble material was separated, and the pigment was concentrated by evaporation with dry argon or nitrogen gas. Subsequent HPLC analysis showed small amounts of Chl *d* in the total pigment extracts, demonstrating that Chl *d* containing cyanobacteria were present, but also showed that isolated samples contained a good deal of Chl *d* (Figure 7.1).

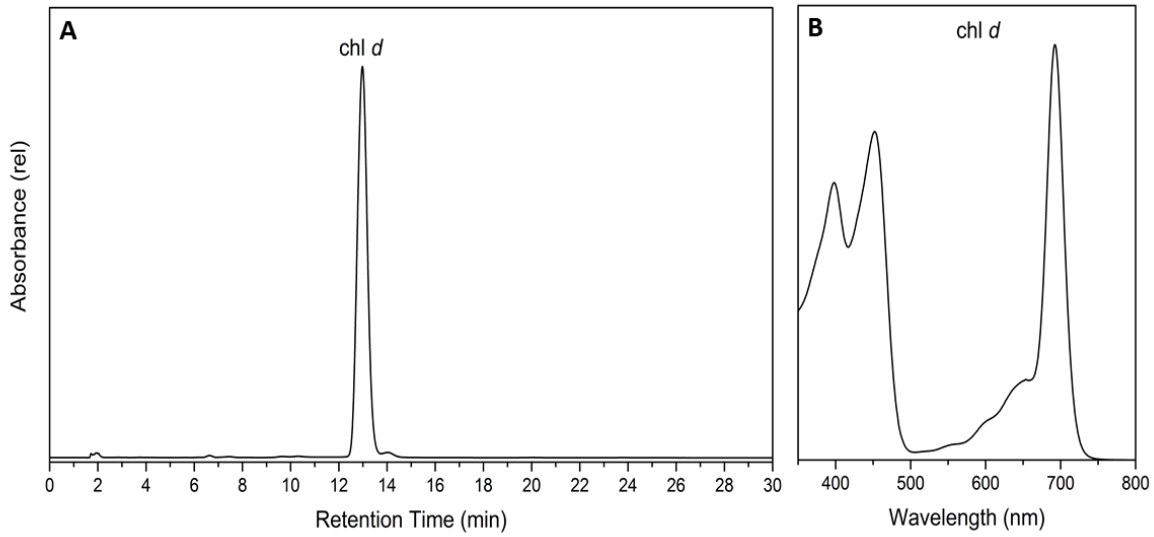

Figure 7.1: HPLC chromatogram and absorption spectrum of the primary peak of cyanobacteria isolated as epiphytes from red macroalgae. A) Chromatogram B) Absorption of Chl *d* peak.

Although initially only two tubes showed growth, then next round of sampling yielded 10 tubes with discernable cyanobacterial growth. A sample of the cell material was taken from each for PCR amplification of the 16S rDNA sequence. Universal and cyanobacterial-specific primers

were combined for a cleaner sequence, as these tubes contained many heterotrophic bacteria as well. Although not all cultures gave good sequence data, those that did appeared to be the same undescribed species of *Acaryochloris* (Figure 7.2). HPLC and absorbance analysis of pigment extracted from the cyanobacteria grown in the first round of sampling showed that they contained primarily chl *d* (Figure 7.1).

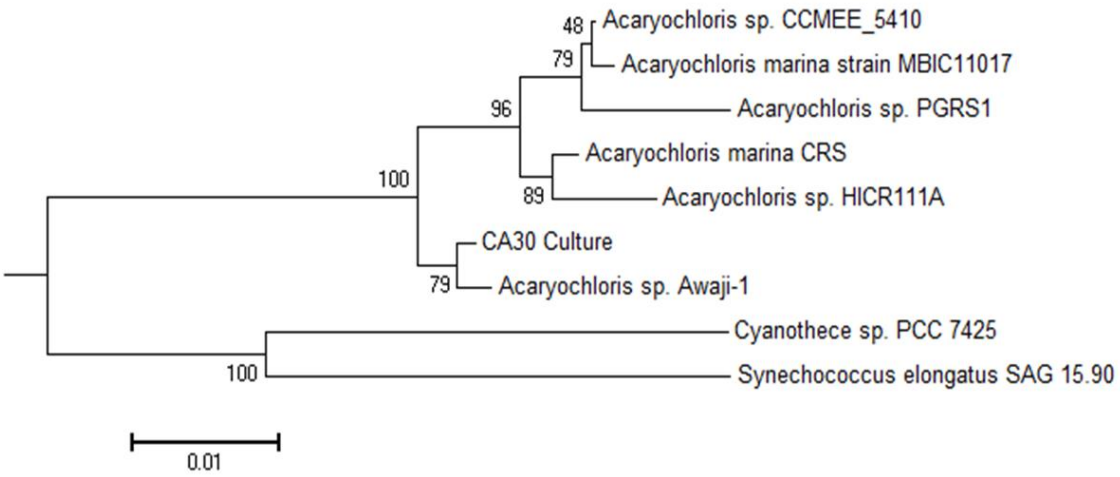

Figure 7.2: Neighbor-joining tree comparing the 16S sequence of one of the isolates, CA30, to other *Acaryochloris*.

7.2 The Enigmatic *Acaryochloris* sp. R61[6]

7.2.1 Introduction

All species of the cyanobacterial genus *Acaryochloris* discovered to date contain the far-red absorbing pigment Chl *d* except for one, *Acaryochloris* RCC1774 (abbreviated R61 in this thesis

[6] This section contains data and text derived from a manuscript in preparation with authors Benjamin M. Wolf, Jeremy D. King, Dariusz M. Niedzwiedzki, Gregory S. Orf, Meghan C. Barnhart-Dailey, Jerilyn A. Timlin, and Robert E. Blankenship entitled "Photosynthetic Characterization of the Enigmatic Chlorophyll b Containing Aracyochloris RCC1774."

for legacy reasons). The species was isolated in the English Channel in 1975 by Dr. Jean-Claude Thomas near the biological station at Roscoff, France (personal communication, Jeremy D. King and Dr. Frédéric Partensky, Senior Scientist at Roscoff Biological Station). When it was sent from the collection to our laboratory in 2015, it had not been characterized in any way, save for sequencing of the 16S rDNA sequence to put it in the genus *Acaryochloris.* Although it was assumed at that time that the organism would have the same pigmentation as all other *Acaryochloris,* our lab found that in fact it contained Chl *b* and *a*, but no Chl *d* (Jeremy D. King, unpublished observations).

Because the enzyme(s) responsible for the catalysis of the conversion of Chl *a* to Chl *d* are not known, this strain is of particular interest. Chls *b* and *d* both contain a formyl group that shifts their absorption spectrum (see Chapter 1), though Chl *b* is blue shifted with a weak Q_y band and Chl *d* is red-shifted with a strong Q_y absorption (Chen and Blankenship 2011). This makes the substitution in R61 particularly interesting. Examination of this species has the potential to yield insights into the process of Chl *d* biosynthesis. We have found that this strain contains around 20% Chl *b*, with the remaining being Chl *a*. This is a significant deviation from the other *Acaryochloris* species; indeed, Chl *d* makes up over 95% of the total chlorophylls in *Acaryochloris marina* (Miyashita et al. 1996; Loughlin et al. 2013). To understand what causes this significant difference in pigmentation, we investigated the antenna system and spectral characteristics of this species.

In 2018, a paper detailing this species was published by the same group that sent the culture to our lab in 2015 detailing the presence of Chl *b* in an *Acaryochloris* species (Partensky et al. 2018). Although we were unaware of their interest in the strain, we have also characterized aspects of the organism that they did not present, including preparation and spectroscopy of the reaction centers, hyperspectral imaging of the species grown under varied light conditions showing localization of

the two chlorophylls and the phycobilisomes, and time-resolved fluorescence on the phycobilisomes. Presented here are these data in addition to our whole cell spectra and whole-cell pigment extract data, which are in agreement with the later-published report.

Chl *b* is rarely found in cyanobacteria, although it is ubiquitous in higher plants and green algae. It is, however, found in three genera of cyanobacteria, which form a polyphyletic group referred to as the prochlorophytes (Urbach et al. 1992; La Roche et al. 1996). Three genera are known: *Prochloron, Prochlorothrix, and Prochlorococcus* (Urbach et al. 1992). The Chl *a/b* binding proteins of all three of these cyanobacterial genera are related to several chlorophyll binding proteins, including IsiA and an antenna protein found in PSII, CP43 (La Roche et al. 1996). Although most prochlorophytes do not contain phycobiliproteins, *Prochlorococcus marinus* CCMP 1375 contains Chl *a*, Chl *b*, and phycobiliproteins (Hess et al. 1996).

Phylogenetic analysis and the presence of phycobiliproteins in one prochlorophyte suggest that Chl *b* biosynthesis and Chl *a/b* binding proteins evolved from a common ancestor with other cyanobacteria containing only Chl *a* and phycobilisomes (Urbach et al. 1992; Hess et al. 1996). It is suggested that they evolved separately from those same genes in green algae and higher plants (Palenik and Haselkorn 1992; Urbach et al. 1992; La Roche et al. 1996). Additionally, because the prochlorophytes form a polyphyletic group, Chl *b* utilization and biosynthesis appears to have arisen at least four times, either through convergent evolution or horizontal gene transfer (Palenik and Haselkorn 1992; Urbach et al. 1992; Tomitani et al. 1999).

7.2.2 Spectroscopy and Pigmentation

Compared to the type strain of *Acaryochloris*, *A. marina*, the whole cell absorption and fluorescence emission spectra of R61 show a significant blue shift. The Q_y band on the absorption is found to be at 683 nm in R61 but at 716 nm in its close relative *A. marina* (Figure 7.3A). The fluorescence shows a similar trend, with the room temperature emission maximum of R61 at 680 nm and the maximum of *A. marina* at 722 nm (Figure 7.3B). For these comparisons, both cultures were grown under white light. R61 is not capable of growth under far-red light.

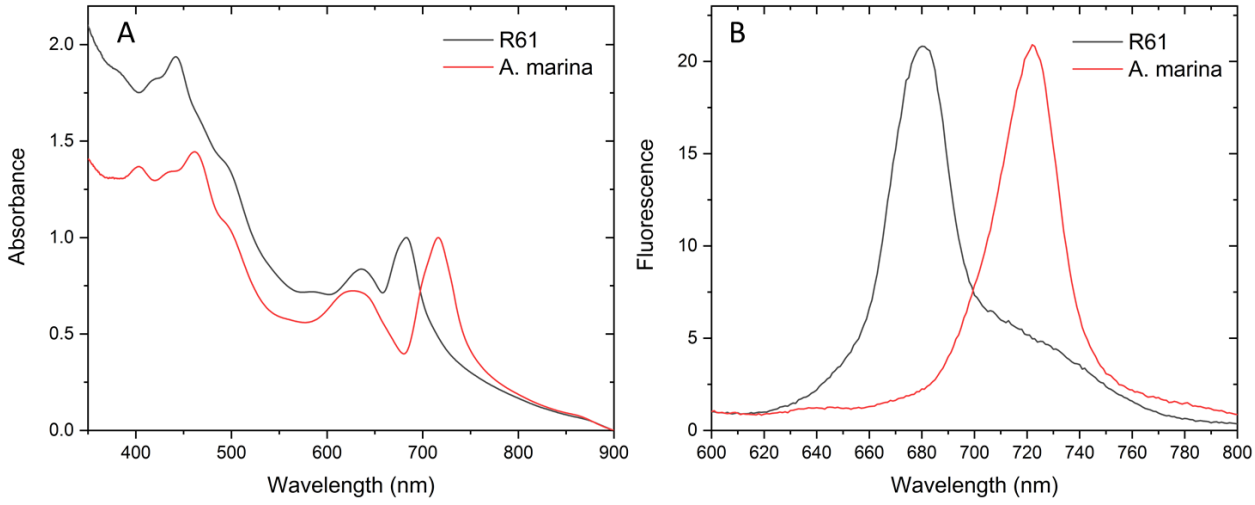

Figure 7.3: Absorbance and fluorescence spectroscopy on whole cells of *Acaryochloris* R61. A) Absorption spectrum of whole cells of R61 and the Chl *d* containing *A. marina*. Normalized to unity at the Q_y peak. B) Fluorescence emission spectrum with 435 nm excitation of both species. Spectra normalized to unity.

Through HPLC of extracted pigments, it is clear that R61 contains Chl *b* in addition to Chl *a*, but is entirely devoid of Chl *d* (Figure 7.4). A notable feature of HPLC chromatograms of Chls *d* and *b* is that they look quite similar; in fact, the retention times are almost identical. However, these two pigments are easily distinguishable spectrally, making their determination quite straightforward (Figure 7.4B). However, this could be of concern if a species was to be isolated

that contained both of these pigments. Based on HPLC chromatogram peak integrated areas, Chl *b* makes up approximately 20% of the total chlorophyll in R61 cells, whereas in the type strain *A. marina*, Chl *d* constitutes up to 95% of the total chlorophyll (Miyashita et al. 1996, 1997).

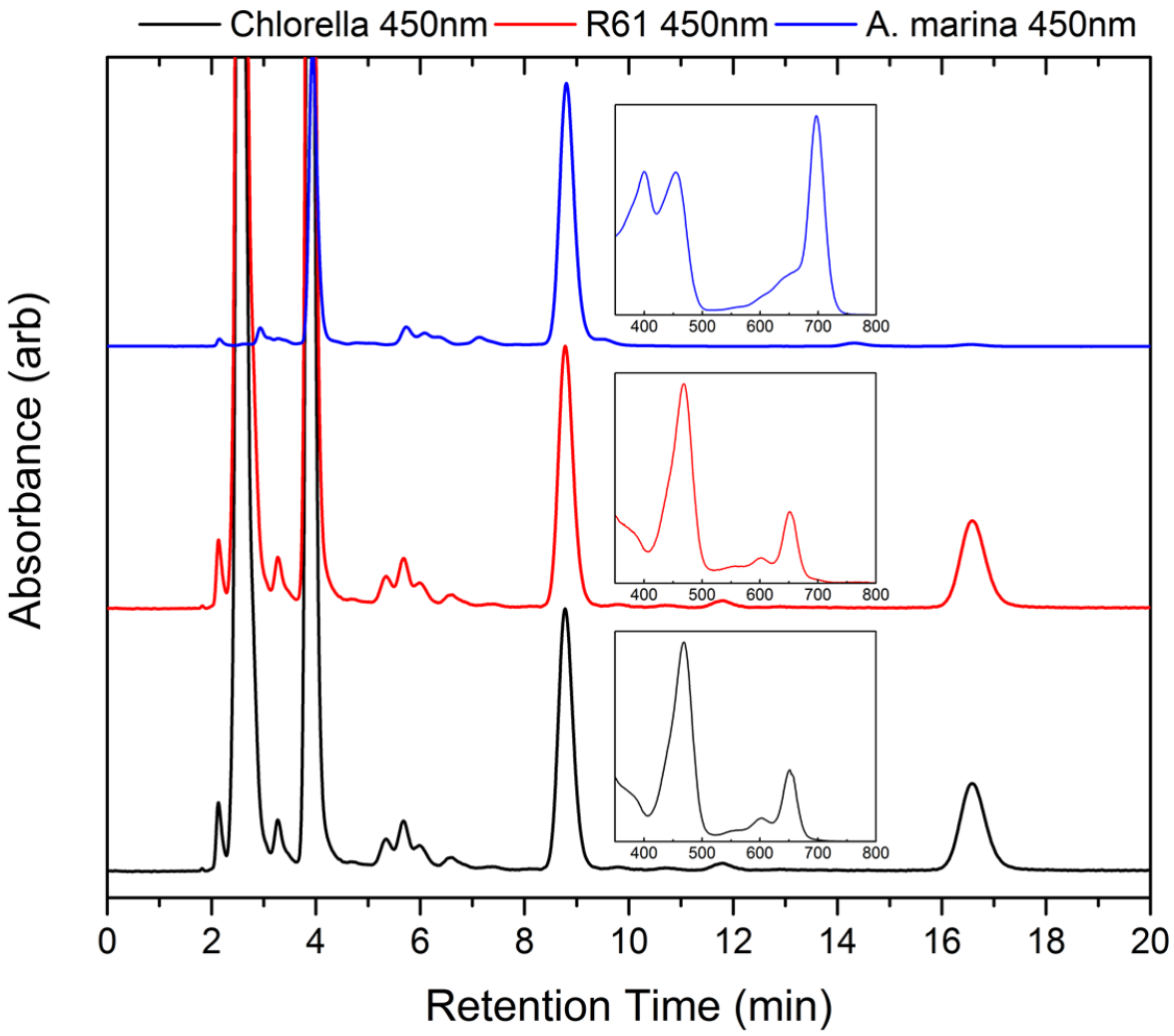

Figure 7.4: HPLC chromatogram and pigment absorption spectra of R61 run in pure methanol, isocratic flow. Chromatograms of R61, *A. marina*, and a Chl *b*-containing control *Chlorella vulgaris*, a green alga. Insets show the absorption spectrum at 8.5 minutes for each trace.

7.2.3 Biochemical Analysis of Membrane Proteins

We have separated the solubilized membrane proteins of R61 into several bands using sucrose gradient centrifugation and analyzed the pigment composition of each band using HPLC (Figure 7.5). The HPLC data clearly indicate that the highest ratio of Chl *b* to Chl *a* is found in the topmost band (Figure 7.5). These results were obtained using the areas under the Chl *b* and Chl *a* peaks on the chromatogram and using the appropriate extinction coefficients to normalize these values to one another. One unanswered question in these results is the identity of an unknown peak with the same absorbance spectrum of Chl *a* but eluting between Chl *b* and *a* (Figure 7.5).

While in most cyanobacteria, these phycobiliproteins are assembled into large complexes known as phycobilisomes, in *A. marina* there are only simple rod structures present (Marquardt et al. 1997). These rods are made up of the two typical rod proteins in phycobilisomes, phycocyanin and allophycocyanin, but the remaining structure of a phycobilisome is not present (Marquardt et al. 1997; Chen et al. 2009).

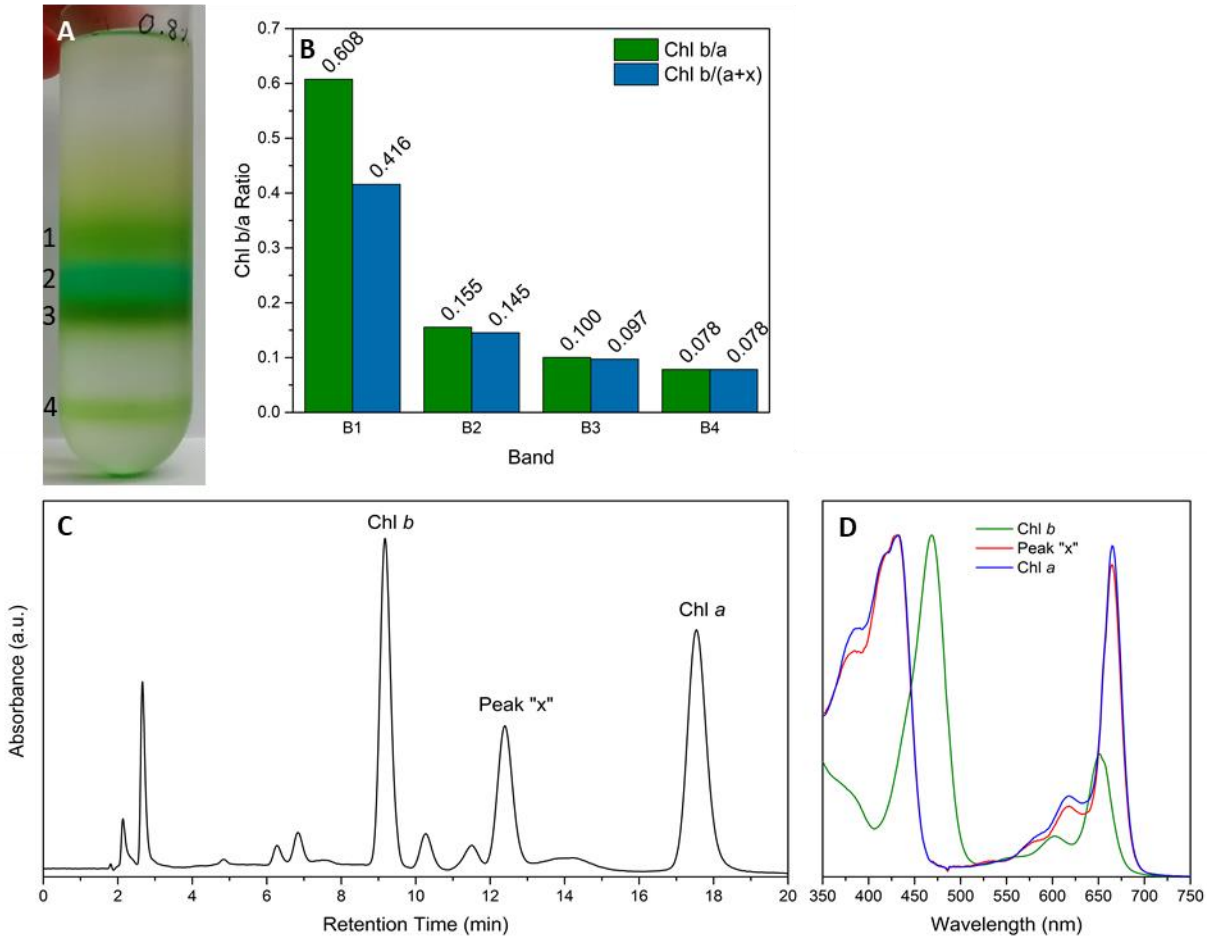

Figure 7.5: Sucrose gradient separation of solubilized membranes from R61 and characterization of bands through HPLC. A) Sucrose gradient. B) Ratios of Chls in sucrose gradient bands. C) HPLC chromatograms with peaks labeled for the top band. D) Absorption spectra of labeled peaks.

7.2.4 Separation and Analysis of Phycobiliproteins

Acaryochloris R61 contains phycobilisomes in addition to its Chl *b*-containing antennas. While in most cyanobacteria, these phycobiliproteins are assembled into large complexes known as phycobilisomes, in *A. marina* there are only simple rod structures present (Marquardt et al. 1997). These rods are made up of the two typical rod proteins in phycobilisomes, phycocyanin and

allophycocyanin, but the remaining structure of a phycobilisome is not present (Marquardt et al. 1997).

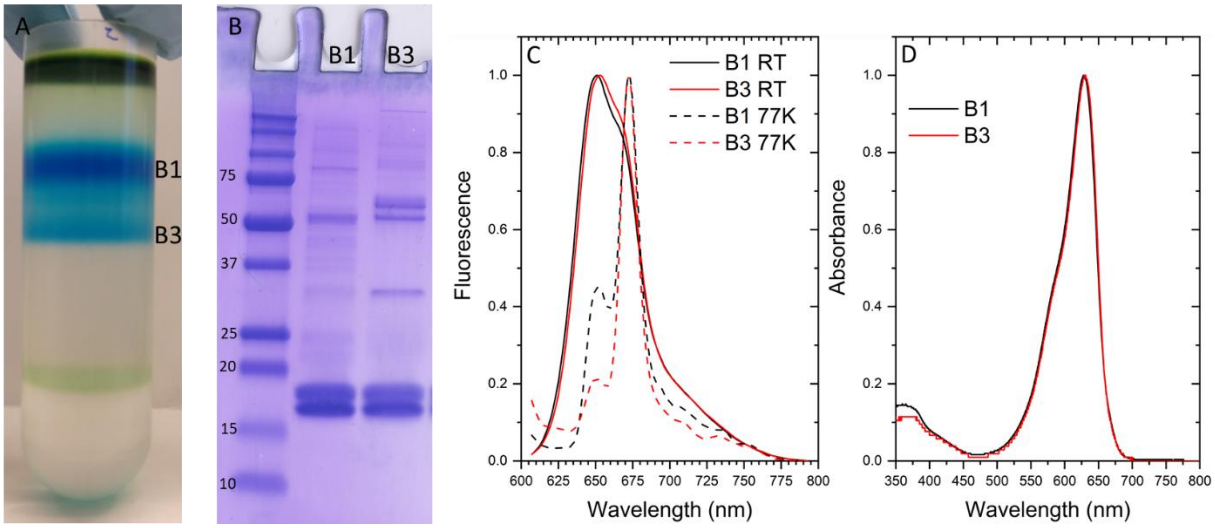

Figure 7.6: Phycobiliproteins isolated from R61 and separated using a sucrose gradient. A) Sucrose gradient image with bands labeled. B) SDS PAGE gel to separate proteins from each of the two bands. C) Fluorescence emission spectrum with excitation at 580 nm at both RT and 77K. D) Absorption spectra of bands.

An initial characterization of the phycobilisome of shows the 16.2 and 17.4 kDa components expected for an *Acaryochloris* system (Figure 7.6B), but rather than a single band as in *A. marina*, R61 has both a dense and lighter band (Figure 7.6A) (Marquardt et al. 1997). In addition, several higher molecular weight bands are observed in R61, especially the denser Band 3.

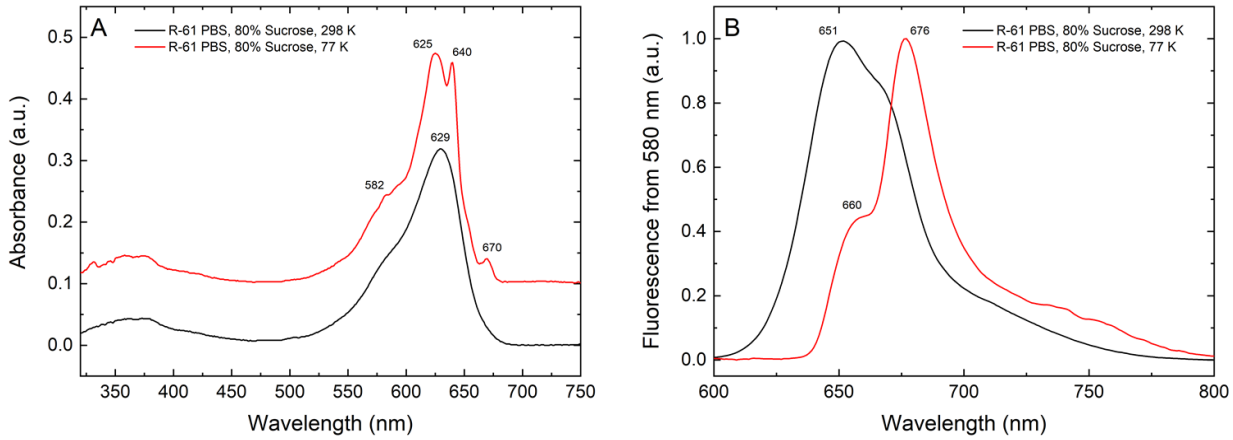

Figure 7.7: Low temperature spectral analysis of Band 1 Phycobiliproteins from the sucrose gradient in Figure 7.6. Spectra were taken in high percentage sucrose. A) Absorption spectrum at room temperature and 77K. B) Fluorescence emission spectrum with excitation at 580 nm at RT and 77K.

Phycobilisomes are sensitive to breakdown when cryoprotectants are added to take low temperature spectra, but the more abundant and lower density upper band with smaller phycobiliproteins could be successfully frozen to 77K in 80%+ sucrose, showing absorption bands at 582, 625, 640, and 670 nm (Figure 7.7A). This indicates the presence of four spectrally-distinct bilins in the upper band. At 77K, most of the energy absorbed from the 580 nm excitation light was emitted at 676 nm (Figure 7.7B), which may correspond to emission from the long wavelength 670 nm component. The fluorescence emission of Band 1 and Band 2 are very similar at both room temperature and 77K (Figure 7.6C). 676 nm is 6 nm red-shifted compared to the published low temperature emission of *A. marina* phycobiliproteins (Marquardt et al. 1997). From these experiments, it seems that the phycobiliproteins of R61 are at least somewhat more complex than those of *A. marina.*

7.2.5 Hyperspectral Imaging

Hyperspectral Confocal Fluorescence Microscopy (HCFM) was used to determine the localization of Chl *b* in living cells of R61. Chl *b* was shown to colocalize with Chl *a* within the cell periphery of R61 cells, in what appears to be the thylakoids. This suggests that Chl *b*, like Chl *a*, is associated with transmembrane proteins involved in photosynthetic energy transfer and/or collection. One interesting phenomenon noticed was that as cells aged under low-light conditions, the Chl *b* tended to localize to the poles of the cells.

Based on images collected from the two light conditions, the multivariate curve resolution (MCR) algorithm (see methods) output three spectral components present in the cells (Figure 7.8). Double peaks indicate co-variance of the two spectral signatures. The separation of Chl *a* and Chl *b* indicates that they are indeed varying separately within the images.

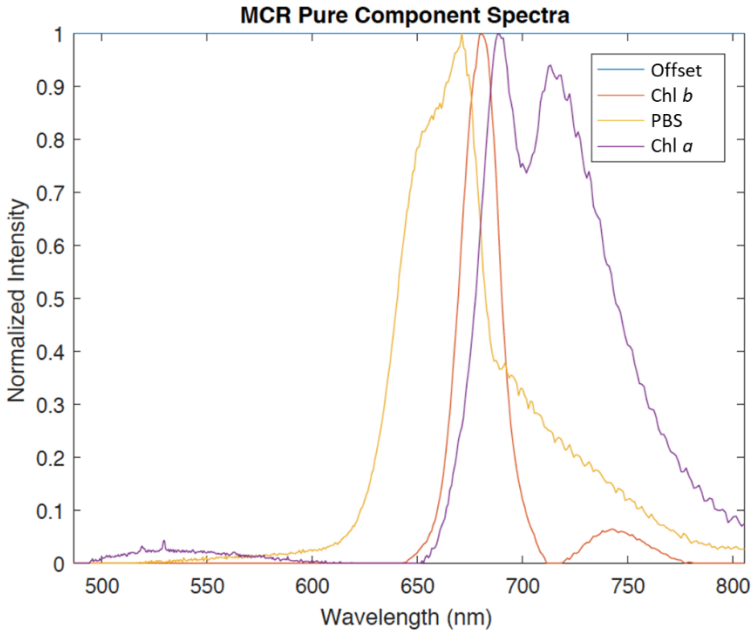

Figure 7.8: MCR spectral output for the three distinct spectral components, showing Chl *b*, Chl *a*, and Phycobiliproteins.

The three components are shown separately in Figure 7.9. Here you can see that all three photosynthetic components are most intense on the margins of the cells, corresponding to the thylakoids. However, in these images it is difficult to discern any enriched pockets of each component, though it is clear that older cells have some significant variability, especially under low light conditions (particularly in Figure 7.9A).

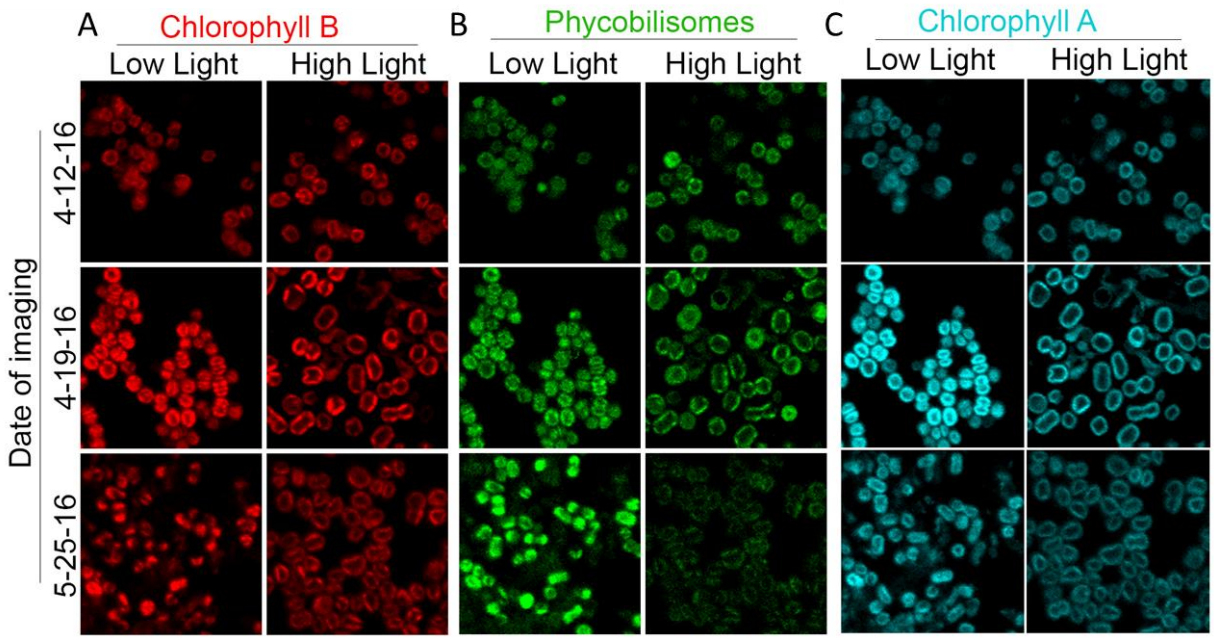

Figure 7.9: Hyperspectral confocal images of R61 cells grown under low and high light conditions and imaged several different times. Cultures were maintained in their respective condition until imaging was performed. A) Chlorophyll *b*, B) Phycobiliproteins, C) Chlorophyll *a*.

The overlay of the Chl *a* and Chl *b* signals shows some interesting localization differences, especially under low light (Figure 7.10). In general, the two chlorophylls colocalize fairly well in the thylakoid space. However, in the older cells, especially when grown under low light, there is an interesting separation of the pigments (Figure 7.10). However, the explanation for this is not fully understood at this point.

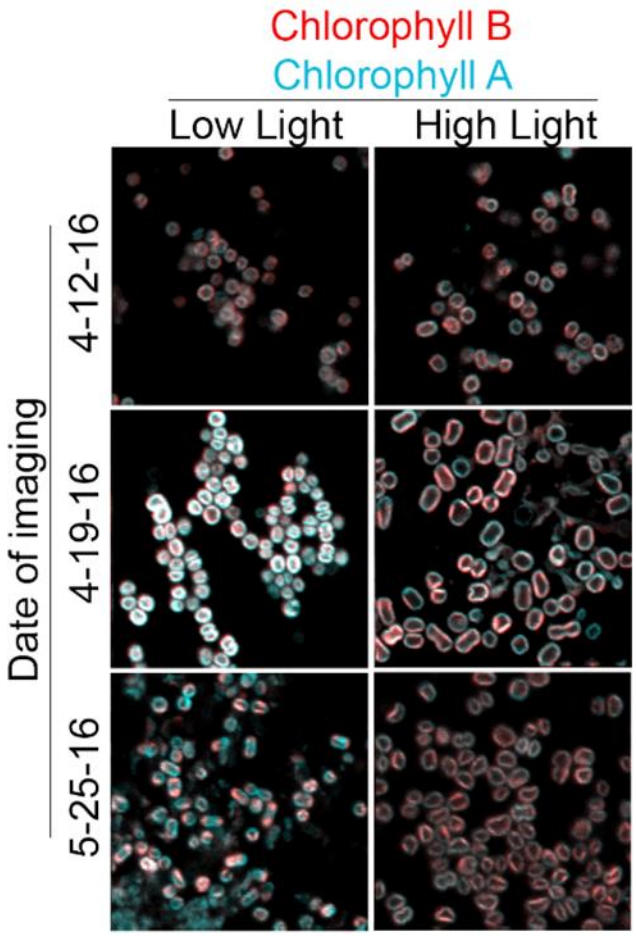

Figure 7.10: Overlays of Chlorophyll *a* and *b* signals as shown in Figure 7.9.

7.3 Conclusions

The enzyme(s) responsible for the biosynthesis of Chl *d* have not been identified, but the discovery of an *Acaryochloris* species with no Chl *d* opens the door to comparative studies with the type strain *A. marina* to establish potential knockout or mutation targets to get at the root of this process. The R61 genome has been sequenced previously (unpublished data, Jeremy D. King), but with low coverage. A second attempt at this sequencing has been made by our collaborators, and will be available soon. This will allow the photosynthetic proteins of this organism to by identified with some confidence by mass spectrometry. Currently, R61 protein hits can be compared to the

database for *A. marina,* but in this way it is impossible to identify proteins that may only be found in R61, such as the Chl *b* synthase. This makes a good, well-annotated genome key to the further characterization of this organism.

Chapter 8: Experimental Methods

8.1 Environmental Sampling and Culturing

Water samples were collected in spring in a circulating water system in Forest Park, St. Louis, MO. The sample from which *Eustigmatophyceae* sp. FP5 was cultured originated as a water sample from one of the system's partially shaded, slow-moving sections. Glass tubes containing 10 mL of BG-11 growth medium were inoculated with a small amount of each sample. Inoculum size was determined based on the sample's apparent turbidity. The tubes were placed into a growth chamber dimly illuminated using far-red (740 nm) LEDs (Fig S1) and maintained at room temperature. When green growth appeared, the organisms within were analyzed by fluorescence and absorption spectroscopy, and shaking flasks were inoculated from the tubes and maintained under FRL.

To purify the culture and obtain a clonal culture, FP5 was streaked on 0.4% Agarose BG-11 plates and grown under FRL (Shirai et al. 1989; Ferris and Hirsch 1991), and streaked again onto a similar plate to obtain single colonies. Wells of a 12-well culture plate containing BG-11 were each inoculated with a single colony, and these were grown under FRL until a dense green growth appeared, at which time some wells were used to inoculate larger cultures. The resulting clonal culture was scaled up in large (1–2 liter) flasks, and light was provided by 740 nm LEDs at a power of 2.3 mW cm^{-2}. Light intensity was measured using a Thorlabs PM200 power meter with a S120VC Si-UV Photodiode sensor. Flasks were either gently shaken on an orbital shaker or stirred using a stir bar and bubbled with air sterilized using a Whatman Hepa-Vent filter. Cultures were regularly monitored spectrally and by microscopy to ascertain their quality. Although FP5 is capable of growth under white light, we have focused on the properties of the organism when

grown under the far-red light condition described above to ascertain its far-red light absorbing characteristics.

8.2 Pigment Analysis

For chlorophylls, pigment analysis was performed using an Agilent 1100 HPLC with a C18 resin as the stationary phase and pure methanol as the mobile phase. Absorption was measured using an in-line diode array detector. The flow rate was 1.5 mL/min and 100 µL sample injections were used. The cell walls of FP5 are recalcitrant, presumably due to the presence of algaenan found in other Eustigmatophytes (Scholz et al. 2014), and resist the extraction of pigments using methanol treatment, so the cells were disrupted prior to extraction of pigment. 1 mL of a culture started from a single colony and grown under FRL was rinsed with and exchanged into Buffer A (50 mM MES, 2 mM KCl, pH 6.5), and 1.4 mm stainless steel beads were added to the culture in a screw-top vial to half the culture volume. The cells were then disrupted by five passes on a Biospec Mini Bead-Beater running at full speed for 20 seconds. Cells were cooled between runs using an ice bath.

The broken cells were then subjected to pigment extraction: 0.5 mL broken cell suspension, 2 mL 7:2 acetone/methanol, 200 µL 4M NaCl, and 3 mL petroleum ether were mixed vigorously and allowed to separate. The ether layer was removed and dried using an Eppendorf Vacufuge vacuum centrifuge, then resuspended in HPLC grade methanol immediately prior to injection on the HPLC.

8.3 Taxonomic Classification

The 18S ribosomal DNA sequence of FP5 was amplified using polymerase chain reaction (PCR). Whole cells provided template for the reaction: 1 µL of a thick cell suspension was pipetted into the PCR reaction containing GoTaq Green master mix. A 5 min 94 °C denaturation at the beginning of the PCR reaction was used to disrupt cells. The forward primer was an algal-specific

primer (5'-CGGTAATTCCAGCTCC-3') and the reverse was a universal primer (5'-GGGCGGTGTGTACAARGRG-3'). For sequencing, forward and reverse sequences were generated and aligned to produce a longer sequence. The amplicon was sequenced through the commercial vendor GeneWiz, and compared with other algal 18S rDNA sequences using the NCBI Basic Local Alignment Search Tool (BLAST) (Altschul et al. 1990). Sequences were aligned using MUSCLE in MEGA6 (Tamura et al. 2013), and excess base pairs that were longer than the FP5 sequence were removed. Using these sequences, a neighbor-joining phylogenetic tree was created using MEGA6 with 500 bootstrap replicates (Tamura et al. 2013).

8.4 Microscopy

Phase contrast light microscopy images were taken on a Nikon Labophot 2 light microscope using an oil-immersion 100X objective or on a Wild Heerbrugg light microscope using a 40X objective with a 3X adjustable second lens. Scale bars were added using a stage micrometer and ImageJ software (Schindelin et al. 2015). Confocal images were taken using a PerkinElmer Ultraview Vox spinning disc confocal system on a Zeiss Observer Z1 microscope using a Zeiss Plan Apo 100X 1.46 oil-immersion objective. 0.1 uM Z-slices were flattened and images processed using FIJI software (Schindelin et al. 2012). For deep-etch freeze-fracture cryogenic electron microscopy, samples were prepared and imaged as described previously (Weiss et al. 2012), with the following modification: FRL-grown cells were first pelleted and 5 µL of this material was applied to a cushioning material before flash freezing.

8.5 LHC Purification

The clonal FP5 culture was frozen by free air convection at -80 °C in Buffer A, which is composed of 50 mM MES, 2 mM KCl, pH 6.5. The light-harvesting complex was purified as follows, modified from previously described methods (Tichy et al. 2013; Bína et al. 2014; Kotabová et al.

2014; Pazdernik 2015). FP5 was grown under FRL at room temperature and harvested by centrifugation. The cell pellet was washed once in Buffer A. Approximately 1–2 g of the wet cell pellet were resuspended in 30 mL of Buffer A and either frozen at -80 °C or used immediately. Following thawing of cells, if frozen, and addition of DNAse (Sigma-Aldrich), cells were disrupted via three passes through a French Press Pressure Cell at 20,000 PSI. Unbroken cells and cellular debris were separated by centrifugation at 1,000 × *g* for 5 minutes in a Thermo Scientific Legend RT+ centrifuge with a Thermo- Heraeus 75006445 swinging-bucket rotor. The supernatant was then subjected to centrifugation at 45,000 × *g* for 2 hours at 4 °C in a Beckman Coulter Optima L-80 XP Ultracentrifuge using a Type 45 Ti fixed-angle rotor.

The membrane pellet was gently resuspended in 1–2 mL of Buffer A using a paint brush and the Chl *a* concentration was measured. For this, 10 µL of the cell suspension was added to 990 µL pure methanol. These were mixed and the insoluble portions were separated using an Eppendorf 5415 D benchtop centrifuge at full speed for 1 minute. The Chl *a* concentration, in mg/mL, was calculated from the Abs_{665} value. The suspension was diluted to a Chl *a* concentration of 0.5 mg/mL using Buffer A. At this point, membranes were either frozen at -80 °C or solubilized immediately. The material was solubilized by adding a stock of 10% (w/v) n-Dodecyl β-D-maltoside (DDM) to a final concentration of 1%. After one hour on ice while shaking in the dark, insoluble material was immediately removed by centrifugation at 30,000 × *g* for 20 minutes at 4 °C in a Sorvall Evolution or RC5 centrifuge using a SS34 rotor, and the supernatant stored until subjected to gel filtration. Sample storage was optimal at 4 °C in 25–50% glycerol (Fig S2), but storage overnight at 4 °C without glycerol was also used with very little sample degradation.

8.6 Gel Filtration Chromatography

Gel filtration was performed at 4 °C under dim green light using Sephacryl S-300 resin (GE Healthcare Life Sciences) at a 1 mL/min flow rate using Buffer A with 0.02% DDM. The column was 30 cm long with a 1.5 cm internal diameter. One mL fractions were collected and fluorescence spectra were recorded using a Varian Cary Eclipse fluorimeter. For analysis through CN-PAGE, all fractions containing significant FR-LHC were pooled and concentrated using a 30 kDa MWCO Millipore centrifugal filter unit.

8.7 Clear Native Polyacrylamide Gel Electrophoresis

For initial studies on FP5 grown only under far-red light, preparative CN-PAGE gels were cast using the Sturdier setup (Hoefer) with a 1.5 mm thickness, and analytical gels for 2D electrophoresis were cast using a Bio-Rad mini-gel system. The gel and buffer compositions were modified from Schägger and von Jagow (Schägger and von Jagow 1991). Coomassie was omitted from the cathode buffer and instead 0.05% sodium deoxycholate was added (Litvín et al. 2016). To increase the separation of the protein complexes of interest, the density of the gel was 9% to 16% polyacrylamide. Gradients were made using an acrylic gradient maker and a Dynamax peristaltic pump running at 5mL/min for the Sturdier setup or 1 mL/min for the Bio-Rad system. The preparative gel was run at 80 V overnight at 4 °C in the dark, and the analytical was run for 3 hours under the same conditions. For imaging, the gel was placed between two transparent sheets of plastic and was imaged using a visible light Epson Perfection V30 scanner and a Syngene PXi fluorescence imager. A blue LED excitation and a 705 nm emission filter were used to observe far-red fluorescence of the bands. When required, a Novex Nativemark native protein standard was included in the gel and was stained using 0.2% Coomassie G-250 in 40% methanol and 7% acetic acid.

For comparative studies of FP5 under blue and far-red light, The clear native polyacrylamide gel electrophoresis was performed as previously described with modifications (Wolf et al. 2018). Prior to solubilization, far-red grown membranes were adjusted to 0.5 mg mL^{-1} Chl *a* (as measured in pure methanol). The UV absorption at 280 nm was also recorded, and blue light samples were adjusted to this protein absorption band. This accounts for the lower ratio of protein to Chl *a* within blue-light grown membrane samples. Whole cell membranes were solubilized for 1 hour on ice using 1% n-dodecyl-β-D-maltopyranoside (DDM) (Anatrace). Unsolubilized material was separated by centrifugation at 30,000 xg for 20 minutes in a tabletop Beckman-Coulter ultracentrifuge using 200 uL tubes. Supernatant was prepared for gel loading by adding 0.1% Sodium Deoxycholate final concentration to charge the sample and 5% glycerol final concentration to allow it to sink into the wells.

The gel itself was a 9-16% polyacrylamide native gel in the Hoefer Sturdier setup and was a modification of previously described methods for native PAGE (Wittig et al. 2006, 2007). In this method, Coomassie die was omitted and was replaced with 0.05% Sodium Deoxycholate in the cathode buffer. In addition, 0.02% DDM was added. The cathode and anode buffers were as described previously, and contained imidazole in the place of Bis-Tris to reduce effects on protein staining (Wittig et al. 2006, 2007). The gel was run overnight at 4C and 80-100V in the dark.

The gel was imaged and the bands were cut out and spectroscopy performed as previously described (Wolf et al. 2018). In brief, gel slices were placed onto the inside walls of cuvettes for absorption. Care was taken to cover the entire beam path. For fluorescence, FP5 Buffer was added to allow the slices to sit diagonally, such that the 435 nm excitation could be absorbed and emission recorded.

8.8 2D Polyacrylamide Gel Electrophoresis (2D PAGE)

A 12% SDS-PAGE gel was poured in the Bio-Rad system using the pre-mixed Protogel (National Diagnostics) reagent set. A modified comb allowing one large well for a CN-PAGE gel slice and one small well for the ladder was used to form the stacking gel. The desired lane was carefully excised from the CN-PAGE gel and denatured in a solution of 1% β-mercaptoethanol (βME) and 1% Sodium dodecyl sulfate (SDS) for 1 hour (Wittig et al. 2006). The gel slice was then inserted into the large well on the SDS-PAGE gel. The gel was silver stained using a Pierce Sliver Stain Kit (Thermo Scientific) and imaged as described above.

8.9 Elution of Native Proteins from Native Gel

Native proteins were extracted through simple diffusion using a modification of a previously described method (Wittig et al. 2006). Bands were cut from the gel and diced using a razor blade into fragments approximately one cubic mm in size. The fragments were placed into a 1 Dram glass vial and enough Buffer A with 25% glycerol (v/v) and 0.02% DDM was added to double the volume of the gel slices. The tubes were wrapped in foil and placed on a rotator at 4 °C for 2 days. The green eluent was pipetted off and centrifuged at 4 °C in an Eppendorf 5415 D benchtop centrifuge at full speed for 5 minutes to remove gel debris. The supernatant was used for subsequent spectroscopic analysis.

8.10 Fluorescence and Absorption Spectroscopy

Absorption measurements were taken using a Shimadzu UV1800 spectrophotometer, which was equipped with a Janis Research Company VNF-100 optical liquid nitrogen cryostat for 77 K measurements. Fluorescence emission spectra were taken using a Shimadzu RF-6000 or Varian Cary Eclipse fluorimeter. For 77 K fluorescence measurements, an optical dewar filled with liquid

nitrogen was used. For all 77 K spectroscopic analysis, sample material was mixed with glycerol to a concentration of ~60% (v/v).

For spectral analysis of native gel bands, bands were cut from the gel using a razor blade. For absorption measurements, each slice was placed on the side of the cuvette such that it did not move before placing the cuvette in the instrument. An area of the gel within an unused lane was cut out and used as a blank. For fluorescence measurements, gel slices were placed in a 1 cm square plastic cuvette with Buffer A containing 0.02% DDM. The slices were placed diagonally in the fluorimeter cuvette such that the edge of the gel faced the excitation light and the wide edge faced the detector. Fluorescence spectra were taken using an excitation wavelength of 435 nm with excitation and emission slit widths of 5 nm.

Eluted pigment-protein complexes were subject to room temperature and 77 K measurements of absorption and fluorescence with excitation at 435 nm and excitation and emission bandwidths of 5.0 nm. Additionally, thermally activated energy transfer was analyzed using fluorescence excitation at 750 nm with an excitation bandwidth of 1.5 nm and an emission bandwidth of 5.0 nm. For fluorescence measurements of eluted proteins, the OD was maintained below 0.1. For 77 K and thermal activation fluorimetry, a blank sample was subtracted from the raw data to correct for dewar effects and excitation light scattering, respectively.

Spectra were analyzed using Origin 2016 software. Spectra were normalized to a range of 0 to 1 for uniformity. Prior to calculation of the second derivative, spectra were normalized to unity at the maximum within the region shown and a Savitzky-Golay smoothing algorithm was applied. The same normalization was applied to spectra before the difference was calculated. This

algorithm was also applied to smooth 77 K absorption and thermally activated energy transfer spectra.

Whole cell spectroscopy was performed using a culture grown under 740 nm LED light under stirred, aerated conditions. To disrupt cell clumps, 1 mL of culture was resuspended by shaking and was then subjected to 10 seconds of sonication using a Fischer Sonic Dismembranator Model 300 fitted with a micro probe at 35% power. To reduce scattering of light, the cell suspension was diluted with a sucrose solution to a final concentration of approximately 60% sucrose for room temperature measurements of absorption and fluorescence. For fluorescence, an excitation wavelength of 435 nm was used with excitation and emission slit widths at 5.0 nm. For 77 K fluorescence measurements, the cell suspension was diluted with a glycerol solution to a final concentration of approximately 60% glycerol and frozen using an optical dewar containing liquid nitrogen. Absorption measurements were taken using a Shimadzu UV1800 and fluorescence measurements were taken using a Varian Cary Eclipse fluorimeter.

8.11 Culturing FP5 for Imaging

FP5 cells for imaging were grown under three light conditions: white (fluorescent) (data in supplement), far-red (740 nm), and blue (450 nm). Prior to imaging at Sandia National Laboratories, FP5 was grown in 500 mL Erlenmeyer flasks on oscillatory shakers containing 200 mL of BG-11 growth medium with vitamins (see supplemental information) and several glass beads to prevent biofilm formation. Lights were set to approximately 70 $\mu E\ m^{-2}s^{-1}$. Visible light was measured with a Li-COR LI-250A light meter using a quantum sensor. Far-red light was measured using a Thor Labs S120VC sensor set to 740 nm. Under each light condition, three replicate flasks were grown. Chambers were either liquid cooled or ventilated with room air such that growth temperature was maintained at approximately 25°C.

A week prior to imaging, aliquots of each culture were shipped overnight to Sandia National Laboratories. Blue and far-red cultures were transferred directly to flasks without dilution to avoid changes in growth phase. One week was left between shipment and imaging to allow cells to recover from being in the dark for 24 hours due to shipping. At Sandia National Laboratories, far-red and blue cultures were grown using 730 nm and 450 nm SST-10 series LEDs from Luminus Devices Inc. White light cultures were maintained under fluorescent light at approximately 100 μE $m^{-2}s^{-1}$. The intensity of the blue light was initially quite high, approximately 400 μE $m^{-2}s^{-1}$, to make up for any change that may have occurred in the dark during shipping and to fully acclimate the cells. FP5 tends to self-shade strongly, so a very intense light is needed to overcome this. However, to ensure physiological similarity for imaging, the light intensity was turned down to ~100 μE $m^{-2}s^{-1}$ two days before imaging. Prior to spectroscopy and/or HCFM, cultures were sonicated for 5 x 0.5 second pulses at 30% power using a microtip probe sonicator. White light cultures were imaged later (data in supplement), but the acclimation effects of FP5 are not nearly as apparent under white light as under blue. These cultures were diluted to ensure their longevity.

8.12 Spectroscopy

Fluorescence spectroscopy of gel bands and whole cells taken prior to shipment were taken using a Varian Cary Eclipse spectrometer. Absorption spectra were taken using a Shimadzu UV-1800 UV-Vis spectrometer. Fluorescence and absorption spectra at Sandia National Laboratories were taken of each culture to determine the level of far-red antenna present using a Synergy™ H4 plate reader from BioTek® (Part Number 8031000). Spectra are shown in the supplemental data (Figure S1).

8.13 Hyperspectral Confocal Fluorescence Microscopy

Cells were imaged live on agar-coated slides sealed using nail polish. Slides were kept in the dark prior to microscopy and all microscopy was done within an hour of slide preparation. Microscopy was accomplished using a custom hyperspectral confocal fluorescence microscope (HCFM) (Sinclair et al. 2006). Fluorescence was excited with 1.1 μW from 488 nm laser (Sapphire, Coherent, Inc.) focused to a diffraction-limited spot on the sample through a 60x oil objective (Nikon Plan Apochromat, NA 1.4). Fluorescence emission is then collected back through the excitation objective, dispersed by a custom designed prism spectrometer, and focused onto the focal plane of an electron-multiplied CCD array (iXon DU897U, Andor Technologies, Inc.). The spectral range is ~ 500–800 nm with a spectral resolution ranging from ~1 nm in the green and ~3 nm in the red regions of the spectrum. Images are formed by raster scanning the beam over the sample in one direction, while simultaneously scanning the sample in the other. The step size is 0.12 μm. This generates images with diffraction limited lateral spatial resolution (250 nm) and axial resolution ~600 nm. The per pixel dwell time was 240 μs. In some experiments, a cyan colored glass bandpass filter (BG38 Schott, Inc., Elmsford, NY) was used to attenuate the Chl *a* emission and allow for more subtle spectral signatures in the 500-640 nm spectral range to be detected (Collins et al. 2014). Otherwise these features are not detectable without detector saturation from the bright Chl *a* emission. Three biological replicates of every light condition were imaged with a minimum of 20 images/replicate/condition. All images were of a 25 μm x 25 μm field of view. Representative z-stacks of 0.3 μm slices, 6 μm total thickness were obtained for FP5 cells grown under far red and blue light with the cyan filter in place.

8.14 Spectral Image Analysis

The HCFM data were pre-processed to remove dark current contribution and cosmic rays, and to calibrate the spectral axis. Pre-processing methods are described in detail previously (Jones et al. 2012). Images taken with the cyan filter in place were analyzed separately from images taken without the filter. For cyan filter images, a composite image set was created that contained a total of 30 hyperspectral images. Principal component analysis of this data determined there were 5 underlying components. Multivariate curve resolution (MCR) analysis with non-negativity constraints was performed on the cyan filter data to develop a 6-component spectral model (5 independently varying FP5 pigment components plus a linear offset arising from the detector). The MCR analysis was described in detail previously (Jones et al. 2012). The 6-component model identified was then fit using classical least squares (CLS) to the remaining hyperspectral image data to determine the relative abundance of each spectral component in each image pixel. For the images taken without the cyan filter in place, a 4-component spectral model was developed (3 independently varying FP5 pigment components plus linear offset from detector) from 60 hyperspectral images. Following these spectral analyses, each hyperspectral image is now represented by 6 (+ cyan filter) or 4 (- cyan filter) individual images corresponding to the relative abundance of each spectral component. These are written as TIFF files and subjected to traditional image processing for qualitative and quantitative analysis.

To allow accurate visual comparison of images, the maximum signal intensity of each component for each image within the comparison was recorded. All were then set to the same maximum intensity, using the maximum intensity of all images present in that comparison. All of these normalization steps were accomplished using ImageJ software (Schindelin et al. 2015). In this

way, the relative intensities between two image files of the same component were made to be comparable. Overlays were also done using ImageJ software.

8.15 Large-Scale Culturing of FP5

Self-shading is a major obstacle to acclimation of large cultures of FP5 to blue light. However, large-scale cultures are required to generate the biomass needed for LHC protein isolation. To address this problem, we fabricated a specialized blue light irradiation chamber for FP5. The chamber consists of three banks of high-intensity blue LEDs. As these LEDs are placed on three sides of the flask in close proximity, it is more useful to present overall light emitted rather than intensity in a single direction. One bank uses three 450 nm SST-10 LEDs from Luminus Devices Inc. operating at approximately 3.3 watts and emitting approximately 1.65 watts of light energy. This is equivalent to approximately 6.2 μE s^{-1} calculated using information provided in the datasheet. The remaining two banks can be dimmed, and each consists of three CREE XP-E2 475 nm blue LEDs operating at a maximum of 9 watts, which is equivalent to approximately 10.2 μE s^{-1} calculated using the information provided in the datasheet. Using all three LED banks, total photon output can thus be varied from 6.2 to 16.4 μE s^{-1} provided along 3 points surrounding the flask. For simplicity, photon emission calculations presented here assume monochromaticity, though LED emission peaks are slightly wider. The LED spectra are available in the corresponding datasheets.

A culture of FP5 was inoculated from a continuous culture and illuminated primarily by the Luminus Devices LED bank for the first three days, allowing it to enter the active growth phase without photobleaching. At 3 days, after the culture had reached an OD750 of 0.3, the CREE LED banks were turned to full power. At this time, cultures were primarily blue-shifted, with a fluorescence maximum of 700 nm.

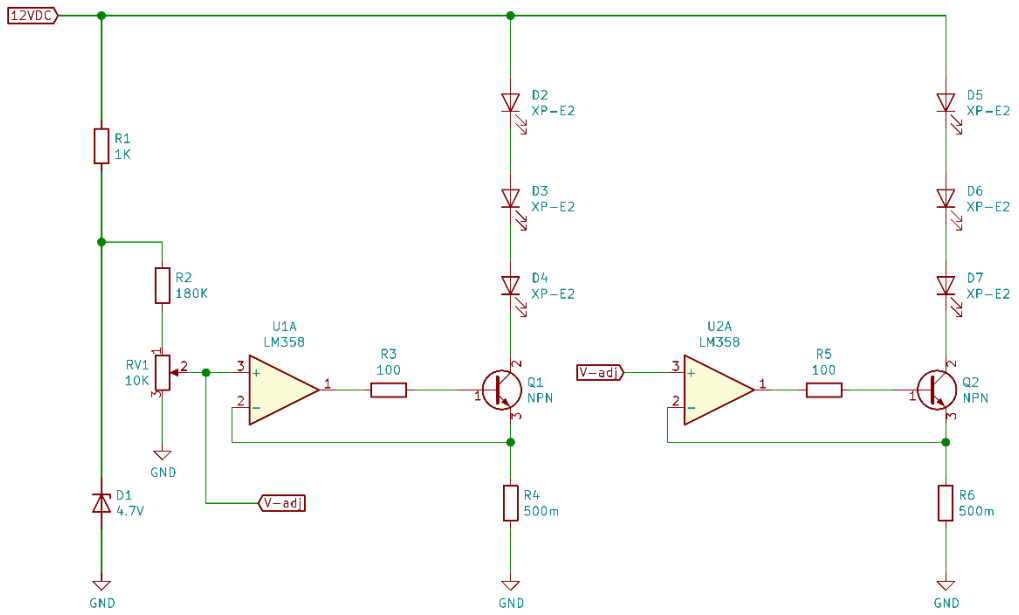

Figure 8.1: Circuit used to produce 481 nm blue light in combination with the USB-driven 450 nm light source (not diagrammed). 481 nm light penetrates the culture further than 450 nm light. The circuit is a double low-side sense constant current linear LED driver. Each independent string of CREE XP-E2 LEDs (D2-D7) is driven through its own NPN transistor (Q1 and Q2), which is maintained in its active mode using the output of the operation amplifiers U1A and U2A. A constant 4.7 volt reference is generated by the Zener diode D1. This reference is used to drive a resistor divider composed of R2 and RV1; RV1 is used to adjust the final output current of the circuit through the V_{adj} voltage, indicated. The operational amplifiers are arranged in a negative feedback loop maintaining the voltage at the inverting input (-) equal to the non-inverting input (+), which maintains a constant voltage drop across the sense resistors (R4 and R6). Although base current is passed through the sense resistor, this makes up less than 1% of the overall current flow and therefore represents a negligible error.

8.16 Preparation of Photosynthetic Membrane Proteins From FP5

Following growth of large-scale culture for 1-2 weeks, cultures were checked for acclimation using fluorescence and absorption spectroscopy. Cells were then harvested by centrifugation at 7000 rpm for 10 minutes in a FiberLite 6X250LE rotor at room temperature. Spent medium was

decanted, and cells were washed in a smaller volume of buffer (50 mM MES, 2 mM KCl, pH 6.5) (Pazdernik 2015; Wolf et al. 2018). This buffer will be referred to henceforth as FP5 Buffer. The wash consisted of a 5 minute centrifugation at 1000 xg in a swinging bucket rotor to avoid pelleting of unwanted low-density debris. The cells were then resuspended in FP5 Buffer and frozen at -80°C. Freezing was accomplished by free-air convection inside the freezer.

Membrane preparation was performed as previously described with several minor modifications (Wolf et al. 2018). In brief, samples were thawed using room temperature water and a Pierce EDTA-free protease inhibitor tablet was ground and added. The tablet was split between two tubes. Additionally, DNase was added to the cell suspension. Following this, the cells were disrupted using 3X passes on a French Press at 20,000 psi, and centrifuged for 5 minutes at 1000 xg in a swinging bucket to remove unbroken cells and cell wall debris. The supernatant was then centrifuged at 45k rpm in a Type 45Ti rotor in Beckman-Coulter Optima ultracentrifuge for 2 hours at 4°C. The membrane pellet was resuspended using FP5 Buffer containing a small amount of described protease inhibitor and brought to 0.5 mg mL^{-1} Chl *a* concentration. If not used immediately, membranes were frozen for up to several months at -80°C without any noticeable degradation of the far-red antenna complexes.

8.17 Single-Cell Analysis

Single cell analysis was performed on images at Sandia National Laboratories to report mean signal intensities for individual cells. Cells were segmented in an automated fashion based on total fluorescence signal of the RC-LHC spectral component using in-house written cell segmentation software employing a modified marker watershed algorithm. The automated cell segmentation results were verified and adjusted manually for cells that did not segment well. Out of focus cells and cells touching the edges of an image frame were excluded from single cell analysis. A variety

of parameters were calculated for the segmented cells for each component using the segmentation done in the RC-LHC component as a mask for cell location. Measurements included the mean intensity signal for each of the spectral components, and these were exported into an excel spreadsheet. Mean intensities were plotted using Origin 2018 software.

8.18 Culturing LSP65

LSP65 is a filamentous cyanobacterium isolated from a scraping of the bottom of a lily pad in Hamlin Lake, Ludington State Park, MI. LSP65 has been streaked on plates to produce a unialgal culture. The organism grows well in BG-11 medium under far-red (740 nm) illumination, and under these conditions, it produces chlorophyll *f*. As a filamentous cyanobacterium, it tends to form tough biofilms. When these biofilms are disturbed, the cultures tend to become unhealthy and die rather quickly. However, this mode of growth limits the amount of biomass that can be obtained for biochemical work.

In an attempt to grow these filaments in a suspended fashion, a bubbled flask with a pointed bottom was used. The bubbling straw was inserted to the tip of the bottom of the flask, where the bubbles released caused good circulation of the medium. The flask held 1 liter, and was illuminated with two 5 watt 740 nm LEDs, illuminating from opposing sides. After <3 weeks, this culture had grown to a high density. Pigment analysis revealed a considerable amount of Chl *f*. It is likely that this method was successful because LSP65 was never allowed to form a biofilm. It appears that the agitation of bubbling continuously prevents biofilm formation and keeps the filaments in suspension. Filaments tend to break as they get too long, and a nominal filament length appears to be maintained when observed under a microscope.

Previously, small-scale cultures of LSP65 grown under far-red and white light were imaged using hyperspectral confocal fluorescence microscopy (Jerilyn Timlin and Meghan Barnhart-Dailey; Sandia National Labs). Significant differences were observed between the pigmentation of these samples. Grown under far-red light, LSP65 had two strong fluorescence peaks in the far-red, while under white light, LSP65 filaments appeared to lose all of their far-red fluorescence.

Based on these observations, biochemical and spectroscopic investigation is warranted. This requires growing large cultures of LSP65 under white and far-red light. Because the lab has only one working flask as described above for LSP65 growth, we turned to Roux flasks with bubbling. By using flexible tubing with a glass tube at the end, we were able to concentrate bubbling in the corner of the flask, thereby creating a strong current flowing around the inside to keep the filaments in suspension.

Flasks are illuminated on one side using LEDs. For the far-red flask, a single 5 watt 740 nm LED is used. The light intensity at the flask is, at maximum, approximately 160 µmol m^{-2} s^{-1} (measured using ThorLabs laser power meter). This high intensity is not damaging to the cells due to the relatively low absorption of far-red light compared to visible. The white light flask is illuminated using a rail containing 5 Bridgelux Vero 10 cool white LEDs. Only a single LED is directly in front of the flask due to spacing. Initially, the light intensity was set to approximately 70 µmol m^{-2} s^{-1}. (measured using Li-250A with quantum sensor) to prevent photobleaching by the highly absorbed white light. As the culture increases in density, the intensity will be increased up to 160 µmol m^{-2} s^{-1} to prevent self-shading effects.

8.19 Reaction Center Preparation from cyanobacteria

LSP65 was grown under FRL in a bubbled container in BG-11 at 25°C and harvested by centrifugation with a 1X wash with RB Buffer (50 mM MES, 10mM $MgCl_2$, 5mM $CaCl_2$, 25% Glycerol, pH 6.5 with NaOH). 1.5 g of cells were saved in 30 mL RB, then frozen at -80°C by free air convection. Following thawing of cells in cold water, cells were broken using a French Press, with three passes at 1,100 gauge PSI on the high ratio (corresponds to approximately 20,000 PSI cell pressure). Following cellular disruption, a 10k rcf spin in a 50 mL conical tube for 10 min to remove cell debris and unbroken cells was performed. The supernatant was then collected and centrifuged at 45k rpm in a Ti45 rotor (Beckman-Coulter). The supernatant was discarded, and the membrane pellet resuspended in RB to 0.5 mg/mL Chl *a* concentration. The membranes were then either used immediately or frozen at -80°C by free-air convection.

8.20 Sucrose Gradients

Membranes prepared as described above were solubilized for 1hr on ice in 0.8% ß-dodecyl maltoside (DDM) for cyanobacteria, or 1% in the case of FP5. The sample was then diluted 4X with RB without glycerol (glycerol will be 6.25%) for cyanobacterial reaction centers of FP5 Buffer for FP5. The samples were then centrifuged at 30,000 rcf for 20 min to remove any insoluble material and loaded onto a continuous 8-30% gradient, which was poured using a gradient maker and peristaltic pump. Percentages were adjusted as described in the text. The gradient precursor stocks were made as follows: a stock of 4X buffer without glycerol and 50% sucrose were mixed together to either 8% or 30% and brought to volume with ddH2O. To each stock, a stock of 10% DDM was added to a final concentration of 0.02%. The gradient maker was then used to create reproducible gradients using the high and low density stocks. The gradients were then centrifuged at 32,000 rpm in Sw32 overnight at 4°C with the acceleration

and deceleration parameters set to 3 to prevent disturbing the gradients upon starting and stopping. Bands were then harvested with a blunt tipped chromatography probe and fluorescence and absorption spectra were measured. The bands were then frozen for future analysis at -20°C or used immediately.

8.21 SDS-PAGE

To precipitate and desalt proteins, 1 mL ice cold acetone was added to 250 µL of raw sample from gradient and mixed tube by vortex or vigorous inversion. The tube was then either incubated at -80°C for 1 hr or at -20°C for 2+ hrs. Following incubation, the tubes were centrifuged at maximum speed in a benchtop centrifuge at 4°C for 20 min. Next, acetone was decanted and the pellet was either dried in a rotary vacuum drier at the lowest temperature setting or allowed to dry covered on the bench. Some residual water may remain after acetone evaporates. The pellet was resuspended in 20µL Lameli buffer containing ß-mercaptoethanol (dilute 2X stock with pure water) and the tube was scraped along a tube rack to provide agitation. Then incubate at 50°C while sonicating for 30 min. 10 µL are then loaded onto a 15-well 12% minigel.

8.22 Time-Resolved Fluorescence of Phycobilisomes

For the time-resolved experiments, a Hamamatsu streak camera was used, as previously described (Niedzwiedzki et al. 2014). Excitation pulses were at a wavelength of 580 nm and emitted at a frequency of 8 MHz, and the laser power was ~60 µW over ~1 mm on the sample. Sample OD was maintained at ~0.1 in the 1 cm cuvette, and emission was measured at a right angle from this cuvette with a 610 nm long pass filter to prevent scattered emission light from interfering with the detector. Room temperature measurements were taken with a stirring

apparatus. Low temperature measurements were taken in glycerol and frozen slowly in a plastic cuvette. A VNF-100 liquid nitrogen cryostat was used (Janis, USA).

8.23 Oxygen Evolution

Cells were grown under either white, blue, or far-red light in bubbled Roux flasks at 28°C. A stirred, water-cooled oxygen electrode cell was maintained at room temperature and baselined to water saturated with atmospheric oxygen using a continuous air pump. A halogen light source was shone into a monochromator. A short-pass filter was used to block any 2^{nd}-order diffraction in the blue wavelength range. Oxywin software was used to collect the mV measurements from the oxygen electrode. Cell material was transferred to the cuvette and pigment was extracted for later corrections based on Chl *a* content. Pigment extraction: Cells were spun down, supernatant removed, then 100% methanol was added and cells were stored in darkness at -20C. The material and methanol were transferred to crew cap vial and 0.1mm zirconium beads were added to ~20% of the total volume. Then the material was subject to pulsed disruption using mini bead beater: 10s on full power, on ice until cold, repeat four times. A fixed amount of material was removed while avoiding the beads and transferred to a new tube, which was centrifuged for one min at 10,000+ rpm in microtube rotor. The supernatant was then measured with the UV-VIS spectrophotometer. For oxygen evolution measurements, the cell was allowed to stabilize with no light for several minutes, at which point each wavelength was cycled for ~300 seconds before a dark period was initiated. In both cases, Origin 2018 software was used to measure the slope of the mV change after stabilization.

Chapter 9: Conclusions and Future Directions

Light-harvesting systems in oxygenic phototrophs are not limited to the visible spectrum of light, and the far-red light enrichment campaign that provided the isolates FP5 and LSP65 as well as a handful of others shows how ubiquitous are the adaptations to far-red light conditions. Far-red light harvesting systems have broad implications for not only the field of photosynthesis research as a whole, but also for agriculture. Photosynthetic efficiency is often regarded as the "final frontier" of agricultural improvements, as a possible driver for a second Green Revolution. Such a dramatic improvement will be required to feed the 10 billion people expected to live on this planet within this century. An understanding of how nature already captures and efficiently utilizes far-red light energy could be one key aspect of many to drive this shift in agricultural research.

The characterization we have performed on the antenna systems of FP5 and other far-red utilizing species provides a groundwork that will be essential to this potential bioengineering coup, but there is still a great deal of work to be done. Due to its eukaryotic nature, the Eustigmatophyte alga FP5 is likely the most promising candidate described in this work for a donor of a far-red utilizing antenna to transform into plants. However, the time of this writing, a full genomic sequence of FP5 has not been obtained, though some initial legwork has been done regarding this by our collaborator in the Czech Republic, Prof. Marek Elias. When a genomic sequence has been obtained, a much greater wealth of opportunity will be attained. Genomic sequencing will allow less expensive and more successful assembly of RNA sequencing reads to create a eukaryotic proteome database, which will allow for more effective mass spectrometric analysis for a start, and later provide genetic information required for cloning.

One of the most promising far-red light absorbing antenna systems to use in agricultural improvement is the red-shifted LHC-type systems found in some diatoms, *Chromera velia,* and FP5. As it is still not known specifically how these antenna systems red-shift the absorption spectrum of Chl *a*, a directed mutational approach may be utilized to determine specific properties of these LHC systems leading to red shifting. This approach has been successful in the far-red light harvesting system of PSI in plants (Wientjes et al. 2012). The recent crystallization and structural determination of a Fucoxanthin Chlorophyll *a/c* binding Protein (FCP) in the diatom *Phaeodactylum tricornutum* (Wang et al. 2019) serves as an important step to facilitating this research. *P. tricornutum* has been shown in other studies to absorb far-red light when grown under a red-enriched spectrum through a specific FCP-type protein (Herbstová et al. 2015). A genetic system has been established in *P. tricornutum* (Zaslavskaia et al. 2000; Zhang and Hu 2014), opening the door to mutational modification of the far-red LHC system.

Of the 16 LHC-type genes in *P. tricornutum, lhcf15* has been implicated as the gene coding a far-red absorbing LHC (Herbstová et al. 2015), while the highly homologous *lhcf4* gene product was the blue-shifted LHC that was recently crystallized (Wang et al. 2019). Several pigment-coordinating ligands were shown to be different between Lhcf4 and Lhcf15, and subsequent modeling may identify additional binding pocket residues to target. Through the mutation of these particular residues in both Lhcf4 and Lhcf15, it should be possible to determine those that are key for the far-red absorbing characteristics of Lhcf4 but are clearly absent in blue-shifted Lhcf15 through subsequent fluorescence and absorption spectroscopy of whole cells or extracted membranes of mutants.

In plants, LHCs interacting with PSI have been shown to absorb far-red light, and the nature of this interaction has been characterized to some degree. The properties of coordinating amino acids

have been shown to play a key role in this red-shifting (Morosinotto et al. 2003), as well as pigment-pigment interactions (Morosinotto et al. 2005). Mutational analysis has shown that a single asparagine residue binding chlorophyll in Lhca4 is necessary for red-shifting of that pigment-protein (Wientjes and Croce 2011), suggesting that the proposed point mutational method in the *Phaeodactylum tricornutum* system could indeed be found to be workable. Using the results from such an experiment, the homologous *lhcb* genes encoding the light-harvesting complexes of PSII in plants and green algae could possibly be modified to absorb further into the far-red region.

In the Eustigmatophyte alga FP5, the far-red LHC system is expressed constitutively under white and far-red light conditions. This antenna has several advantages compared to the *Phaeodactylum tricornutum* system: it has a very strong far-red absorption spectrum, it does not bind chlorophyll *c* as the FCP antennas of diatoms do, and it has been shown to support photosynthesis using entirely far-red wavelengths. Particularly, the elimination of the need to introduce Chl *c* into a plant makes this system highly advantageous.

An alternative approach to the red shifting of the absorption spectra of plants is to introduce one of the two identified far-red chlorophylls, Chls *f* and *d.* Although these have a distinct advantage in their ability to absorb wavelengths spanning much further into the far-red region than any of the red-shifted Chl *a* LHC systems, integration of the biosynthetic pathway would also require the ability of these systems to efficiently insert the far-red absorbing pigment molecule into the light harvesting systems of plants. In addition, in organisms containing Chl *d* and in far-red adapted Chl *f*-containing species, the reaction centers of PSI and PSII were shown to contain far-red pigments (Tomo et al. 2007; Nürnberg et al. 2018). In Chl *f*-containing species, a significant reorganization of the reaction centers occurs (Ho et al. 2016b, c), which suggests that successful transformation of a plant with all of the necessary genes to make a Chl *f*-synthesis and binding system in a plant

could be prohibitively difficult. By contrast, LHC-type systems are already present in plants and it may be possible to simply make small modifications to existing proteins or chimeras of existing LHCs and far-red ones.

Several steps will be required before the FP5 antenna system can be transformed into plants. First, a biochemical purification of the FP5 far-red antenna without any contaminating red antennas should be devised. This has proven difficult, mainly because identification of the far-red component requires that the protein remain stable, even when not complexed with other proteins it would normally interact with. This is challenging, as maintaining this stability is not necessarily compatible with all chromatography techniques (Bína et al. 2014). However, if a sample containing only a small variety of antennas can be obtained, when a proteome is complete, this may be sufficient for mass spectrometric identification.

Establishment of a genetic system in FP5 will be important to further narrow the search down to a particular protein through directed point mutagenesis. Once the protein or proteins of interest can be identified, these genes can be cloned into a relative of FP5, *Nannochloropsis* using one of the established genetic systems (Kilian et al. 2011; Radakovits et al. 2012; Li et al. 2014a; Poliner et al. 2018). If far-red light utilization can be established in this algal model organism, the next step will be to attempt the same transformation in something more closely related to crops, such as the plant model *Arabidopsis thaliana.* If successful, this would be observed through a change in the leaf absorption spectrum. The transformed algae and potentially plants would be analyzed biochemically as well as spectroscopically to determine the integration of the far-red system into the light harvesting system, and oxygen evolution would be used to assess photosynthetic activity at far-red wavelengths.

Another approach is to mutationally probe the antenna in FP5 as has been done with the antennas of PSI in plants (Wientjes et al. 2012). This approach would potentially allow the identification of key residues, and crystallization or cryo-EM could be used to generate an informative structure to direct the design and analysis of these experiments. Potentially, native plant or *Nannochloropsis* LHC-type genes could be modified to introduce features found to be important in the red-shifting of Chl *a* in FP5's antenna system.

Eukaryotic far-red light harvesting systems are strong candidates for a source of genes to increase the photosynthetic action spectrum of plants, including crops. The characterization of the far-red light harvesting system of the Eustigmatophyte alga FP5 lays a groundwork for future experiments that could potentially lead to this becoming a reality.

References

Airs RL, Temperton B, Sambles C, et al (2014) Chlorophyll f and chlorophyll d are produced in the cyanobacterium Chlorogloeopsis fritschii when cultured under natural light and near-infrared radiation. FEBS Lett 588:3770–3777. doi: 10.1016/j.febslet.2014.08.026

Allakhverdiev SI, Tomo T, Shimada Y, et al (2010) Redox potential of pheophytin a in photosystem II of two cyanobacteria having the different special pair chlorophylls. Proc Natl Acad Sci 107:3924–3929. doi: 10.1073/pnas.0913460107

Altschul SF, Gish W, Miller W, et al (1990) Basic local alignment search tool. J Mol Biol 215:403–10. doi: 10.1016/S0022-2836(05)80360-2

Anagnostidis K, Komárek J (1988) Modern approach to the classification system of cyanophytes. 3. Oscillatoriales. In: Archiv für Hydrobiologie. pp 327–472

Basso S, Simionato D, Gerotto C, et al (2014) Characterization of the photosynthetic apparatus of the Eustigmatophycean Nannochloropsis gaditana: Evidence of convergent evolution in the supramolecular organization of photosystem i. Biochim Biophys Acta - Bioenerg 1837:306–314. doi: 10.1016/j.bbabio.2013.11.019

Behrendt L, Brejnrod A, Schliep M, et al (2015) Chlorophyll f-driven photosynthesis in a cavernous cyanobacterium. ISME J 9:2108–2111. doi: 10.1038/ismej.2015.14

Behrendt L, Larkum AWD, Norman A, et al (2011) Endolithic chlorophyll d-containing phototrophs. ISME J 5:1072–1076. doi: 10.1038/ismej.2010.195

Bína D, Bouda K, Litvín R (2017) A two-component nonphotochemical fluorescence quenching in eustigmatophyte algae. Photosynth Res 131:65–77. doi: 10.1007/s11120-016-0299-x

Bína D, Durchan M, Kuznetsova V, Litvín R (2019) Energy transfer dynamics in a red-shifted violaxanthin-chlorophyll a light- harvesting complex. BBA - Bioenerg 1860:111–120. doi: 10.1016/j.bbabio.2018.11.006

Bína D, Gardian Z, Herbstová M, et al (2014) Novel type of red-shifted chlorophyll a antenna complex from Chromera velia: II. Biochemistry and spectroscopy. Biochim Biophys Acta - Bioenerg 1837:802–810. doi: 10.1016/j.bbabio.2014.01.011

Blankenship RE (2014) Molecular mechanisms of photosynthesis, 2nd edn. John Wiley & Sons, West Sussex

Blankenship RE, Chen M (2013) Spectral expansion and antenna reduction can enhance photosynthesis for energy production. Curr Opin Chem Biol 17:457–461. doi: 10.1016/j.cbpa.2013.03.031

Blankenship RE, Chen M, Willows R (2013) Gene Constructs Comprising Nucleic Acids that Modulate Chlorophyll Biosynthesis and Uses Thereof

Büchel C (2015) Evolution and function of light harvesting proteins. J Plant Physiol 172:62–75. doi: 10.1016/j.jplph.2014.04.018

Büchel C (2003) Fucoxanthin-Chlorophyll Proteins in Diatoms: 18 and 19 kDa Subunits Assemble into Different Oligomeric States. Biochemistry 42:13027–13034. doi: 10.1021/bi0349468

Carbonera D, Agostini A, Di Valentin M, et al (2014) Photoprotective sites in the violaxanthin-chlorophyll a binding Protein (VCP) from Nannochloropsis gaditana. Biochim Biophys Acta - Bioenerg 1837:1235–1246. doi: 10.1016/j.bbabio.2014.03.014

Chen M (2014) Chlorophyll modifications and their spectral extension in oxygenic photosynthesis. Annu Rev Biochem 83:317–40. doi: 10.1146/annurev-biochem-072711-162943

Chen M, Blankenship RE (2011) Expanding the solar spectrum used by photosynthesis. Trends Plant Sci 16:427–431. doi: 10.1016/j.tplants.2011.03.011

Chen M, Floetenmeyer M, Bibby TS (2009) Supramolecular organization of phycobiliproteins in the chlorophyll d-containing cyanobacterium Acaryochloris marina. FEBS Lett 583:2535–2539. doi: 10.1016/j.febslet.2009.07.012

Chen M, Li Y, Birch D, Willows RD (2012) A cyanobacterium that contains chlorophyll f - A red-absorbing photopigment. FEBS Lett 586:3249–3254. doi: 10.1016/j.febslet.2012.06.045

Chen M, Schliep M, Willows RD, et al (2010) A red-shifted chlorophyll. Science 329:1318–1319. doi: 10.1126/science.1191127

Chen M, Telfer A, Lin S, et al (2005) The nature of the photosystem II reaction centre in the chlorophyll d-containing prokaryote, Acaryochloris marina. Photochem Photobiol Sci 4:1060–1064. doi: 10.1039/b507057k

Collins AM, Jones HDT, McBride RC, et al (2014) Host cell pigmentation in Scenedesmus dimorphus as a beacon for nascent parasite infection. Biotechnol Bioeng 111:1748–1757. doi: 10.1002/bit.25235

Collins AM, Liberton M, Jones HDT, et al (2012) Photosynthetic Pigment Localization and Thylakoid Membrane Morphology Are Altered in Synechocystis 6803 Phycobilisome Mutants. Plant Physiol 158:1600–1609. doi: 10.1104/pp.111.192849

Croce R, Zucchelli G, Garlaschi FM, et al (1996) Excited state equilibration in the photosystem I-light-harvesting I complex: P700 is almost isoenergetic with its antenna. Biochemistry 35:8572–8579. doi: 10.1021/bi960214m

Davis RW, Jones HDT, Collins AM, et al (2013) Label-free measurement of algal triacylglyceride production using fluorescence hyperspectral imaging. Algal Res 5:181–189. doi: 10.1016/j.algal.2013.11.010

De PK (1938) The role of blue-green algae in nitrogen fixation in rice-fields. In: Proceedings of the Royal Society of London. Series B - Biological Sciences. pp 121–139

Durnford DG, Aebersold R, Green BR (1996) The fucoxanthin-chlorophyll proteins from a chromophyte alga are part of a large multigene family: structural and evolutionary relationships to other light harvesting antennae. Mol Gen Genet 253:377–386. doi: 10.1007/s004380050334

Eliáš M, Amaral R, Fawley KP, et al (2017) Handbook of the Protists. Springer International Publishing

Ferris MJ, Hirsch CF (1991) Method for isolation and purification of cyanobacteria. Appl Environ Microbiol 57:1448–1452. doi: 10.1007/978-3-662-13187-9_8

Fork DC, Larkum a. WD (1989) Light harvesting in the green alga Ostreobium sp., a coral symbiont adapted to extreme shade. Mar Biol 103:381–385. doi: 10.1007/BF00397273

Furuya M, Schäfer E (1996) Photoperception and signalling of induction reactions by different phytochromes. Trends Plant Sci 1:301–307. doi: 10.1016/1360-1385(96)88176-3

Gan F, Bryant DA (2015) Adaptive and acclimative responses of cyanobacteria to far-red light. Environ Microbiol 17:3450–3465. doi: 10.1111/1462-2920.12992

Gan F, Shen G, Bryant D (2014a) Occurrence of Far-Red Light Photoacclimation (FaRLiP) in Diverse Cyanobacteria. Life 5:4–24. doi: 10.3390/life5010004

Gan F, Zhang S, Rockwell NC, et al (2014b) Extensive remodeling of a cyanobacterial photosynthetic apparatus in far-red light. Science (80-) 345:1–11. doi: 10.1126/science.1256963

Gantt E (1981) Phycobilisomes. Annu Rev Plant Physiol 327–347

Gartner G, Stoyneva MP, Uzunov BA, et al (2012) Ultrastructure of vegetative cells and autospores of an aerophytic strain of Vischeria stellata (Chodat ex Poulton) Pascher (Eustigmatophyceae) from Bulgaria. Fottea, Olomouc 12:273–280. doi: 10.5507/fot.2012.019

Gilbert IR, Jarvis PG, Smith H (2001) Proximity signal and shade avoidance differences between early and late successional trees. Nature 411:792–795. doi: 10.1038/35081062

Gloag RS, Ritchie RJ, Chen M, et al (2007) Chromatic photoacclimation, photosynthetic electron transport and oxygen evolution in the Chlorophyll d-containing oxyphotobacterium Acaryochloris marina. Biochim Biophys Acta - Bioenerg 1767:127–135. doi: 10.1016/j.bbabio.2006.11.014

Gruszecki WI, Zelent B, Leblanc RM (1990) Fluorescence of zeaxanthin and violaxanthin in aggregated forms. Chem Phys Lett 171:563–568. doi: 10.1016/0009-2614(90)85264-D

Guglielmi G, Lavaud J, Rousseau B, et al (2005) The light-harvesting antenna of the diatom Phaeodactylum tricornutum: Evidence for a diadinoxanthin-binding subcomplex. FEBS J 272:4339–4348. doi: 10.1111/j.1742-4658.2005.04846.x

Gundermann K, Büchel C (2014) The Structural Basis of Biological Energy Generation. In: The

Structural Basis of Biological Energy Generation. pp 21–37

Gutu A, Kehoe DM (2012) Emerging perspectives on the mechanisms, regulation, and distribution of light color acclimation in cyanobacteria. Mol Plant 5:1–13. doi: 10.1093/mp/ssr054

Herbstová M, Bína D, Koník P, et al (2015) Molecular basis of chromatic adaptation in pennate diatom Phaeodactylum tricornutum. Biochim Biophys Acta - Bioenerg 1847:534–543. doi: 10.1016/j.bbabio.2015.02.016

Hess WR, Partensky F, van der Staay GW, et al (1996) Coexistence of phycoerythrin and a chlorophyll a/b antenna in a marine prokaryote. Proc Natl Acad Sci U S A 93:11126–11130. doi: 10.1073/pnas.93.20.11126

Hibberd DJ, Leedale GF (1972) Observations on the cytology and ultrastructure of the New Algal Class, Eustigmatophyceae. Ann Bot 36:49–71. doi: 10.1093/oxfordjournals.aob.a084577

Hibberd DJ, Leedale GF (1971) A New Algal Class: The Eustigmatophyceae. Taxon 20:523–525

Ho M, Shen G, Canniffe DP, et al (2016a) Light-dependent chlorophyll f synthase is a highly divergent paralog of PsbA of photosystem II. 9178:. doi: 10.1126/science.aaf9178

Ho MY, Gan F, Shen G, et al (2016b) Far-red light photoacclimation (FaRLiP) in Synechococcus sp. PCC 7335: I. Regulation of FaRLiP gene expression. Photosynth Res 131:1–14. doi: 10.1007/s11120-016-0309-z

Ho MY, Gan F, Shen G, Bryant DA (2016c) Far-red light photoacclimation (FaRLiP) in Synechococcus sp. PCC 7335. II.Characterization of phycobiliproteins produced during acclimation to far-red light. Photosynth Res 131:1–16. doi: 10.1007/s11120-016-0303-5

Holt AS, Morley H V. (1959) A Proposed Structure for Chlorophyll d. Can J Chem 37:507–514

Hou HJM, Allakhverdiev SI, Najafpour MM (2014) Plant Physiology Current challenges in photosynthesis : From natural to artificial Current challenges in photosynthesis : From natural to artificial. Front Plant Sci 5:232. doi: 10.3389/fpls.2014.00232

Hu Q, Miyashita H, Iwasaki I, et al (1998) A photosystem I reaction center driven by chlorophyll d in oxygenic photosynthesis. Proc Natl Acad Sci U S A 95:13319–13323. doi: 10.1073/pnas.95.22.13319

Itoh S, Mino H, Itoh K, et al (2007) Function of chlorophyll d in reaction centers of photosystems I and II of the oxygenic photosynthesis of Acaryochloris marina. Biochemistry 46:12473–12481. doi: 10.1021/bi7008085

Janouškovec J, Horák A, Oborník M, et al (2010) A common red algal origin of the apicomplexan, dinoflagellate, and heterokont plastids. PNAS 107:10949–10954. doi: 10.1073/pnas.1003335107

Jennings RC, Zucchelli G, Croce R, Garlaschi FM (2003) The photochemical trapping rate from

red spectral states in PSI–LHCI is determined by thermal activation of energy transfer to bulk chlorophylls. Biochim Biophys Acta - Bioenerg 1557:91–98. doi: 10.1016/S0005-2728(02)00399-7

Jones HDT, Haaland DM, Sinclair MB, et al (2012) Preprocessing strategies to improve MCR analyses of hyperspectral images. Chemom Intell Lab Syst 117:149–158. doi: 10.1016/J.CHEMOLAB.2012.01.011

Kasperbauer MJ (1987) Far-Red Light Reflection from Green Leaves and Effects on Phytochrome-Mediated Assimilate Partitioning under Field Conditions. Plant Physiol 85:350–354. doi: 10.1104/pp.85.2.350

Kilcrease J, Collins AM, Richins RD, et al (2013) Multiple microscopic approaches demonstrate linkage between chromoplast architecture and carotenoid composition in diverse Capsicum annuum fruit. Plant J 76:1074–1083. doi: 10.1111/tpj.12351

Kilian O, Benemann CSE, Niyogi KK, Vick B (2011) High-efficiency homologous recombination in the oil-producing alga Nannochloropsis sp. Proc Natl Acad Sci 108:21265–21269. doi: 10.1073/pnas.1105861108

Koehne B, Elli G, Jennings RC, et al (1999) Spectroscopic and molecular characterization of a long wavelength absorbing antenna of Ostreobium sp. Biochim Biophys Acta - Bioenerg 1412:94–107. doi: 10.1016/S0005-2728(99)00061-4

Kotabová E, Jarešová J, Kaňa R, et al (2014) Novel type of red-shifted chlorophyll a antenna complex from Chromera velia. I. Physiological relevance and functional connection to photosystems. Biochim Biophys Acta - Bioenerg 1837:734–743. doi: 10.1016/j.bbabio.2014.01.012

Kühl M, Chen M, Ralph PJ, et al (2005) A niche for cyanobacteria containing chlorophyll d. Nature 433:2005–2005. doi: 10.1038/433820a

La Roche J, van der Staay GW, Partensky F, et al (1996) Independent evolution of the prochlorophyte and green plant chlorophyll a/b light-harvesting proteins. Proc Natl Acad Sci U S A 93:15244–15248. doi: 10.1073/pnas.93.26.15244

Larkum a. WD, Kühl M (2005) Chlorophyll d: The puzzle resolved. Trends Plant Sci 10:355–357. doi: 10.1016/j.tplants.2005.06.005

Li F, Gao D, Hu H (2014a) High-efficiency nuclear transformation of the oleaginous marine Nannochloropsis species using PCR product. Biosci Biotechnol Biochem 78:812–817. doi: 10.1080/09168451.2014.905184

Li Y, Cai ZL, Chen M (2013) Spectroscopic properties of chlorophyll f. J Phys Chem B 117:11309–11317. doi: 10.1021/jp402413d

Li Y, Lin Y, Garvey CJ, et al (2016) Characterization of red-shifted phycobilisomes isolated from the chlorophyll f-containing cyanobacterium Halomicronema hongdechloris. Biochim Biophys Acta - Bioenerg 1857:107–114. doi: 10.1016/j.bbabio.2015.10.009

Li Y, Lin Y, Loughlin PC, Chen M (2014b) Optimization and effects of different culture conditions on growth of Halomicronema hongdechloris - a filamentous cyanobacterium containing chlorophyll f. Front Plant Sci 5:67. doi: 10.3389/fpls.2014.00067

Li Y, Scales N, Blankenship RE, et al (2012) Extinction coefficient for red-shifted chlorophylls: Chlorophyll d and chlorophyll f. Biochim Biophys Acta - Bioenerg 1817:1292–1298. doi: 10.1016/j.bbabio.2012.02.026

Litvín R, Bína D, Herbstová M, Gardian Z (2016) Architecture of the light-harvesting apparatus of the eustigmatophyte alga Nannochloropsis oceanica. Photosynth Res. doi: 10.1007/s11120-016-0234-1

Liu Z, Yan H, Wang K, et al (2004) Crystal structure of spinach major light-harvesting complex at 2.72 A resolution. Nature 428:287–292. doi: 10.1038/nature02373

Llansola-Portoles MJ, Uragami C, Pascal AA, et al (2016) Pigment structure in the FCP-like light-harvesting complex from Chromera velia. Biochim Biophys Acta - Bioenerg 1857:1759–1765. doi: 10.1016/j.bbabio.2016.08.006

Loughlin P, Lin Y, Chen M (2013) Chlorophyll d and Acaryochloris marina: Current status. Photosynth Res 116:277–293. doi: 10.1007/s11120-013-9829-y

Majumder ELW, Wolf BM, Liu H, et al (2017) Subcellular pigment distribution is altered under far-red light acclimation in cyanobacteria that contain chlorophyll f. Photosynth Res 134:183–192. doi: 10.1007/s11120-017-0428-1

Manning WM, Strain HH (1943) Chlorophyll d, a green pigment of red algae. J Biol Chem 1–19

Marquardt J, Senger H, Miyashita H, et al (1997) Isolation and characterization of biliprotein aggregates from Acaryochloris marina, a Prochloron-like prokaryote containing mainly chlorophyll d. FEBS Lett 410:428–432. doi: 10.1016/S0014-5793(97)00631-5

Miyashita H, Adachi K, Kurano N, et al (1997) Pigment composition of a novel oxygenic photosynthetic prokaryote containing chlorophyll d as the major chlorophyll. Plant Cell Physiol 38:274–281. doi: 10.1093/oxfordjournals.pcp.a029163

Miyashita H, Ikemoto H, Kurano N, et al (1996) Chlorophyll d as a major pigment. Nature 383:402–402

Miyashita H, Ikemoto H, Kurano N, et al (2003) Acaryochloris marina gen. et sp. nov. (Cyanobacteria), an oxygenic photosynthetic prokaryote containing chl d as a major pigment. J Phycol 39:1247–1253. doi: 10.1111/j.0022-3646.2003.03-158.x

Moore RB, Oborník M, Janouškovec J, et al (2008) A photosynthetic alveolate closely related to apicomplexan parasites. Nature 451:959–963. doi: 10.1038/nature06635

Morosinotto T, Breton J, Bassi R, Croce R (2003) The nature of a chlorophyll ligand in Lhca proteins determines the far red fluorescence emission typical of photosystem I. J Biol Chem 278:49223–49229. doi: 10.1074/jbc.M309203200

Morosinotto T, Mozzo M, Bassi R, Croce R (2005) Pigment-pigment interactions in Lhca4 antenna complex of higher plants photosystem I. J Biol Chem 280:20612–20619. doi: 10.1074/jbc.M500705200

Murakami A, Miyashita H, Iseki M, et al (2004a) Chlorophyll d in an epiphytic cyanobacterium of red algae. Science 303:1633. doi: 10.1126/science.1095459

Murakami A, Miyashita H, Iseki M, et al (2004b) Chlorophyll d in an Epiphytic Cyanobacterium of Red Algae. Science (80-) 303:1633

Nagy F, Schäfer E (2002) Phytochromes Control Photomorphogenesis by Differentially Regulated, Interacting Signalling Pathways in Higher Plants. Annu Rev Plant Biol 53:329–355. doi: 10.1146/annurev.arplant.53.100301.135302

Niedzwiedzki DM, Orf GS, Tank M, et al (2014) Photophysical properties of the excited states of bacteriochlorophyll f in solvents and in chlorosomes. J Phys Chem B 118:2295–2305. doi: 10.1021/jp409495m

Niedzwiedzki DM, Wolf BM, Blankenship RE (2019) Excitation energy transfer in the far-red absorbing violaxanthin / vaucheriaxanthin chlorophyll a complex from the eustigmatophyte alga FP5. Photosynth Res 0:0. doi: 10.1007/s11120-019-00615-y

Nilsson H, Krupnik T, Kargul J, Messinger J (2014) Substrate water exchange in photosystem II core complexes of the extremophilic red alga Cyanidioschyzon merolae. Biochim Biophys Acta - Bioenerg 1837:1257–1262. doi: 10.1016/j.bbabio.2014.04.001

Nürnberg DJ, Morton J, Santabarbara S, et al (2018) Photochemistry beyond the red limit in chlorophyll f – containing photosystems. Science (80-) 1210–1213

Ohashi S, Miyashita H, Okada N, et al (2008) Unique photosystems in Acaryochloris marina. Photosynth Res 98:141–149. doi: 10.1007/s11120-008-9383-1

Ort DR, Merchant SS, Alric J, et al (2015) Redesigning photosynthesis to sustainably meet global food and bioenergy demand. Proc Natl Acad Sci 112:1–8. doi: 10.1073/pnas.1424031112

Oster U, Tanaka R, Tanaka A, Rudiger W (2000) Cloning and functional expression of the gene encoding the key enzyme for chlorophyll b biosynthesis (CAO) from Arabidopsis thaliana. Plant J 21:305-310.

Palenik B, Haselkorn R (1992) Multiple evolutionary origins of prochlorophytes, the chlorophyll b-containing prokaryotes. Nature 355:265–267. doi: 10.1038/355265a0

Pan H, Šlapeta J, Carter D, Chen M (2012) Phylogenetic analysis of the light-harvesting system in Chromera velia. Photosynth Res 111:19–28. doi: 10.1007/s11120-011-9710-9

Partensky F, Six C, Ratin M, et al (2018) A novel species of the marine cyanobacterium Acaryochloris with a unique pigment content and lifestyle. Sci Rep in press:1–13. doi: 10.1038/s41598-018-27542-7

Pazdernik M (2015) Light harvesting complexes and chromatic adaptation of Eustigmatophyte alga Trachydiscus minutus. Master's Thesis, Univ South Bohemia

Pettai H, Oja V, Freiberg A, Laisk A (2005a) The long-wavelength limit of plant photosynthesis. FEBS Lett 579:4017–4019. doi: 10.1016/j.febslet.2005.04.088

Pettai H, Oja V, Freiberg A, Laisk A (2005b) Photosynthetic activity of far-red light in green plants. Biochim Biophys Acta - Bioenerg 1708:311–321. doi: 10.1016/j.bbabio.2005.05.005

Poliner E, Takeuchi T, Du ZY, et al (2018) Nontransgenic Marker-Free Gene Disruption by an Episomal CRISPR System in the Oleaginous Microalga, Nannochloropsis oceanica CCMP1779. ACS Synth Biol 7:962–968. doi: 10.1021/acssynbio.7b00362

Porra RJ, Schäfer W, Cmiel E, et al (1994) The derivation of the formyl-group oxygen of chlorophyll b in higher plants from molecular oxygen. Achievement of high enrichment of the 7-formyl-group oxygen from 18O2 in greening maize leaves. Eur J Biochem 219:671–679

Quigg A, Kotabová E, Jarešová J, et al (2012) Photosynthesis in Chromera velia Represents a Simple System with High Efficiency. PLoS One 7:. doi: 10.1371/journal.pone.0047036

Radakovits R, Jinkerson RE, Fuerstenberg SI, et al (2012) Draft genome sequence and genetic transformation of the oleaginous alga Nannochloropis gaditana. Nat Commun 3:610–686. doi: 10.1038/ncomms1688

Raymond J, Swingley WD (2008) Phototroph genomics ten years on. Photosynth Res 97:5–19

Reed JW, Nagatani A, Elich TD, et al (1994) Phytochrome A and phytochrome B have overlapping but distinct functions in Arabidopsis development. Plant Physiol 104:1139–1149. doi: 104/4/1139 [pii]

Renger T, Schlodder E (2008) The primary electron donor of photosystem II of the cyanobacterium acaryochloris marina is a chlorophyll d and the water oxidation is driven by a chlorophyll a/chlorophyll d heterodimer. J Phys Chem B 112:7351–7354. doi: 10.1021/jp801900e

Rivadossi A, Zucchelli G, Garlaschi FM, Jennings RC (1999) The importance of PS I chlorophyll red forms in light-harvesting by leaves. Photosynth Res 209–215. doi: 10.1023/A:1006236829711

Rochaix J-D (2014) Regulation and Dynamics of the Light-Harvesting System. Annu Rev Plant Biol 65:287–309. doi: 10.1146/annurev-arplant-050213-040226

Santos LMA (1996) The Eustigmatophyceae: actual knowledge and research perspectives. Nov Hedwigia Beih 112:391–406. doi: 0078-2238/96/0112-0391

Schagger H, von Jagow G (1991) Blue Native Electrophoresis for Isolation of Membrane Protein Complexes in Enzymatically Active Form. Anal Biochem 199:223–231. doi: 10.1016/0003-2697(91)90094-A

Schindelin J, Arganda-Carreras I, Frise E, et al (2012) Fiji: an open-source platform for biological-image analysis. Nat Methods 9:676–682. doi: 10.1038/nmeth.2019

Schindelin J, Rueden CT, Hiner MC, Eliceiri KW (2015) The ImageJ ecosystem: An open platform for biomedical image analysis. Mol Reprod Dev 82:518–529. doi: 10.1002/mrd.22489

Schliep M, Crossett B, Willows RD, Chen M (2010) 18O labeling of chlorophyll d in Acaryochloris marina reveals that chlorophyll a and molecular oxygen are precursors. J Biol Chem 285:28450–28456. doi: 10.1074/jbc.M110.146753

Schlodder E, Çetin M, Eckert HJ, et al (2007) Both chlorophylls a and d are essential for the photochemistry in photosystem II of the cyanobacteria, Acaryochloris marina. Biochim Biophys Acta - Bioenerg 1767:589–595. doi: 10.1016/j.bbabio.2007.02.018

Scholz MJ, Weiss TL, Jinkerson RE, et al (2014) Ultrastructure and composition of the Nannochloropsis gaditana cell wall. Eukaryot Cell 13:1450–1464. doi: 10.1128/EC.00183-14.

Schreiber U (2004) Pulse-Amplitude-Modulation (PAM) Fluorometry and Saturation Pulse Method: An Overview. In: Papageorgiou GC, Govindjee (eds) Chlorophyll a Fluorescence: A Signature of Photosynthesis. Springer Netherlands, Dordrecht, pp 279–319

Searle NE (1965) Physiology of Flowering. Annu Rev Plant Physiol 16:97–118

Shirai M, Matumaru K, Ohotake a, et al (1989) Development of a solid medium for growth and isolation of axenic microcystis strains (cyanobacteria). Appl Environ Microbiol 55:2569–2571

Sinclair MB, Haaland DM, Timlin JA, Jones HDT (2006) Hyperspectral confocal microscope. Appl Opt 45:6283. doi: 10.1364/AO.45.006283

Stomp M, Huisman J, Stal LJ, Matthijs HCP (2007) Colorful niches of phototrophic microorganisms shaped by vibrations of the water molecule. ISME J 1:271–282. doi: 10.1038/ismej.2007.59

Strand DD, Fisher N, Kramer DM (2017) The higher plant plastid NAD(P)H dehydrogenase-like complex (NDH) is a high efficiency proton pump that increases ATP production by cyclic electron flow. J Biol Chem 292:11850–11860. doi: 10.1074/jbc.M116.770792

Sukenik A, Livne A, Apt KE, Grossman AR (2000) Characterization of a Gene Encoding the Light-Harvesting Violaxanthin- Chlorophyll Protein of Nannochloropsis Sp . (Eustigmatophyceae). J Phycol 36:563–570. doi: 10.1046/j.1529-8817.2000.99115.x

Tamura K, Stecher G, Peterson D, et al (2013) MEGA6: Molecular evolutionary genetics analysis version 6.0. Mol Biol Evol 30:2725–2729. doi: 10.1093/molbev/mst197

Tichy J, Gardian Z, Bina D, et al (2013) Light harvesting complexes of Chromera velia, photosynthetic relative of apicomplexan parasites. Biochim Biophys Acta - Bioenerg 1827:723–729. doi: 10.1016/j.bbabio.2013.02.002

Tomitani a, Okada K, Miyashita H, et al (1999) Chlorophyll b and phycobilins in the common ancestor of cyanobacteria and chloroplasts. Nature 400:159–162. doi: 10.1038/22101

Tomo T, Okubo T, Akimoto S, et al (2007) Identification of the special pair of photosystem II in a chlorophyll d-dominated cyanobacterium. Proc Natl Acad Sci U S A 104:7283–7288. doi: 10.1073/pnas.0701847104

Trissl HW (1993) Long-wavelength absorbing antenna pigments and heterogeneous absorption bands concentrate excitons and increase absorption cross section. Photosynth Res 35:247–263. doi: 10.1007/BF00016556

Urbach E, Robertson DL, Chisholm SW (1992) Multiple evolutionary origins of prochlorophytes within the cyanobacterial radiation. Nature 355:267–270. doi: 10.1038/355267a0

Vermaas WFJ, Timlin JA, Jones HDT, et al (2008) In vivo hyperspectral confocal fluorescence imaging to determine pigment localization and distribution in cyanobacterial cells. Proc Natl Acad Sci 105:4050–4055. doi: 10.1073/pnas.0708090105

Wang C, Berg CJ, Hsu CC, et al (2012) Characterization of carotenoid aggregates by steady-state optical spectroscopy. J Phys Chem B 116:10617–10630. doi: 10.1021/jp3069514

Wang W, Yu L-J, Xu C, et al (2019) Structural basis for blue-green light harvesting and energy dissipation in diatoms. Science (80-) 363:1–8. doi: 10.1126/science.aav0365

Weatherby K, Carter D (2013) Chromera velia. The missing link in the evolution of parasitism, 1st edn. Elsevier Inc.

Weiss TL, Roth R, Goodson C, et al (2012) Colony organization in the green alga Botryococcus braunii (Race B) is specified by a complex extracellular matrix. Eukaryot Cell 11:1424–1440. doi: 10.1128/EC.00184-12

Wientjes E, Croce R (2011) The light-harvesting complexes of higher-plant Photosystem I: Lhca1/4 and Lhca2/3 form two red-emitting heterodimers. Biochem J 433:477–485. doi: 10.1042/BJ20101538

Wientjes E, Roest G, Croce R (2012) From red to blue to far-red in Lhca4: How does the protein modulate the spectral properties of the pigments? Biochim Biophys Acta - Bioenerg 1817:711–717. doi: 10.1016/j.bbabio.2012.02.030

Wilhelm C, Jakob T (2006a) Uphill energy transfer from long-wavelength absorbing chlorophylls to PS II in Ostreobium sp. is functional in carbon assimilation. Photosynth Res 87:323–329. doi: 10.1007/s11120-005-9002-3

Wilhelm C, Jakob T (2006b) Uphill energy transfer from long-wavelength absorbing chlorophylls to PS II in Ostreobium sp. is functional in carbon assimilation. Photosynth Res 87:323–329. doi: 10.1007/s11120-005-9002-3

Willows RD, Li Y, Scheer H, Chen M (2013) Structure of chlorophyll f. Org Lett 15:1588–1590. doi: 10.1021/ol400327j

Wittig I, Braun H-P, Schägger H (2006) Blue native PAGE. Nat Protoc 1:418–428. doi: 10.1038/nprot.2006.62

Wittig I, Karas M, Schägger H (2007) High Resolution Clear Native Electrophoresis for In-gel Functional Assays and Fluorescence Studies of Membrane Protein Complexes. Mol Cell Proteomics 6:1215–1225. doi: 10.1074/mcp.M700076-MCP200

Wolf BM, Niedzwiedzki DM, Magdaong NCM, et al (2018) Characterization of a newly isolated freshwater Eustigmatophyte alga capable of utilizing far-red light as its sole light source. Photosynth Res 135:177–189. doi: 10.1007/s11120-017-0401-z

Xu M, Kinoshita Y, Tamiaki H (2014) Synthesis of chlorophyll-f analogs possessing the 2-formyl group by modifying chlorophyll-a. Bioorganic Med Chem Lett 24:3997–4000. doi: 10.1016/j.bmcl.2014.06.022

Zaslavskaia LA, Casey Lippmeier J, Kroth PG, et al (2000) Transformation of the diatom Phaeodactylum tricornutum (Bacillariophyceae) with a variety of selectable marker and reporter genes. J Phycol 36:379–386. doi: 10.1046/j.1529-8817.2000.99164.x

Zhang C, Hu H (2014) High-efficiency nuclear transformation of the diatom Phaeodactylum tricornutum by electroporation. Mar Genomics 16:63–66. doi: 10.1016/j.margen.2013.10.003

Zhao C, Gan F, Shen G, Bryant DA (2015) RfpA, RfpB, and RfpC are the Master Control Elements of Far-Red Light Photoacclimation (FaRLiP). Front Microbiol 6:1–13. doi: 10.3389/fmicb.2015.01303